Contents — C

Water and Hematite: On the Spectral Properties and Possible Origins of Aram, Meridiani, and Candor
W. M. Calvin, A. Fallacaro, and A. Baldridge 3075

MGS-MOC Observations of Martian Dust Storm Activity
B. A. Cantor 3166

Enigmatic Landforms in Cydonia: Geospatial Anisotropies, Bilateral Symmetries, and Their Correlations
M. J. Carlotto 3208

A Case for Hydrothermal Gray Hematite in Aram Chaos
D. C. Catling and J. M. Moore 3245

Mars Mission Optimization Based on Collocation of Resources
G. E. Chamitoff, G. H. James, D. C. Barker, and A. L. Dershowitz 3054

The Mars Express Mission and Its Beagle-2 Lander
A. F. Chicarro and the Science Team 3049

Global Dispersion of Dust Following Impact Cratering Events on Mars
J. Y-K. Cho and S. T. Stewart 3232

Water on Mars: Evidence from Minerals and Morphology
P. R. Christensen 3126

Vertical Distributions of Dust Optical Depth During the 2001 Planet Encircling Storm from a Spherical Radiative Transfer Analysis of MOC Limb Images
R. T. Clancy, M. J. Wolff, B. A. Whitney, and B. A. Cantor 3205

Acid Snowbank as Source, Sink and Abode
B. C. Clark 3106

From Global Reconnaissance to Sample Return: A Proposal for a Post-2009 Strategy to Follow the Water on Mars
S. M. Clifford, J. A. George, C. R. Stoker, and G. Briggs 3269

Post Impact Mars Climate Simulations Using a GCM
A. Colaprete, R. M. Haberle, T. L. Segura, O. B. Toon, and K. Zahnle 3281

High Channels on Mars Indicate Hesperian Recharge at Low Latitudes
N. M. Coleman, C. L. Dinwiddie, and K. Casteel 3071

Development and Testing of Laser-induced Breakdown Spectroscopy for the Mars Rover Program: Elemental Analyses at Stand-Off Distances
D. A. Cremers, R. C. Wiens, Z. A. Arp, R. D. Harris, and S. Maurice 3107

Factors Controlling the Position of the Martian Magnetic Pileup Boundary
D. H. Crider, M. Acuña, D. Vignes, A. Krymskii, T. Breus, and N. Ness 3103

Development of a Surface-to-Exosphere Mars Atmosphere Model
G. Crowley, M. A. Bullock, C. Freitas, S. Chocron, C. Hackert, D. Boice, L. Young, D. H. Grinspoon, R. Gladstone, W. Huebner, G. Wene, and M. Westerhoff 3284

Physical Characteristics, Geologic Setting, and Possible Formation Processes of Spring Deposits on Mars Based on Terrestrial Analogs
L. S. Crumpler 3228

WATER AND HEMATITE: ON THE SPECTRAL PROPERTIES AND POSSIBLE ORIGINS OF ARAM, MERIDIANI, AND CANDOR. W. M. Calvin[1], A. Fallacaro[1] and A. Baldridge[2], [1]Dept of Geological Sciences, University of Nevada, Reno, NV 89503 (wcalvin@unr.edu), [2]Dept. of Geological Sciences, Arizona State University, Tempe, AZ 85287

INTRODUCTION

The Terra Meridiani hematite area was recently selected as one of two final landing sites for the Mars Exploration Rovers. This selection was based in part on the spectral signature from the Mars Global Surveyor Thermal Emission Spectrometer experiment (MGS-TES) that shows a strong signature of bulk grey hematite in the region [1,2]. Both aqueous and non-aqueous processes have been used to account for the presence of this material [2,3,4,5]. Calvin [6,7,8] has long argued for the presence of alteration minerals in medium to low albedo regions and we have recently demonstrated the correlation between the TES hematite locations and those spectra from the Mariner 6 and 7 Infrared Spectrometer (IRS) that suggest increased water of hydration [9]. As the bulk hematite does not include hydration features it suggests the presence of other, associated hydrated minerals at the site and supports and aqueous formation mechanism. We here summarize the Mariner IRS evidence for increased water, explore the observations by the French Imaging Spectrometer for Mars (ISM) over these regions and consider possible scenarios for the concurrent deposition of bulk hematite and hydrated minerals.

TES HEMATITE REGIONS

Christensen et al. (2001) [2] found three regions of Mars that contained the spectral signature of bulk grey hematite.[1] The largest of the three deposits is in Meridiani exposed as a flat, layered deposit underlying etched and eroded terrain. The second largest deposit is in Aram Chaos, a large collapse zone at the source of the Ares outflow channel. The third region encompasses a number of small outcrops distributed primarily in East and West Candor Chasmae in the Valles Marineris, and the largest of these is approximately 50km wide at the base of a mesa in East Candor. There are number of other small outcrops in northern Melas, Coprates and Capri Chasmae. Christensen et al. [2] noted all occurrences are in association with layered sedimentary units and they favored an aqueous origin via chemical precipitation at either ambient or hydrothermal conditions.

Much of the ensuing discussion has focused on the largest Meridiani site. The even elevation and moderate surface roughness make it a possible landing site where the rugged terrain excludes both Aram Chaos and East Candor. Recent articles have studied in detail the morphology of the hematite outcrop and the surrounding terrain [3,10] noting that volcanic ash fall or volcanic material interacting with groundwater are possible sources of the deposit.

Our preference is to consider the spectral signatures in conjunction with each other, and as the identification is unique and spatially isolated the origins are probably related and must be consistent with the diverse morphologies of the sites. Even before the TES hematite identification, Calvin [6] noted that Aram Chaos appeared to have a spectral signature suggestive of more water in surface materials. This lead to the postulation of dark alteration analogs for Mars [7] and this scenario is consistent with the subsequent identification of bulk hematite.

MARINER 6/7 AND WATER

Calvin's [6] study focused on the region of overlap between IRS and ISM in Eos Chasma [11]. So, while the Mariner instruments covered the Meridiani site, they were not included in the original study. Baldridge and Calvin [9] revisited the analysis including a larger portion of the Mariner 6 ground track and previously unanalyzed Mariner 7 data. Figure 1 shows the locations of the Mariner and ISM data from Capri Chasma across Meridiani. Both Mariner 6 and 7 observed the TES Meridiani hematite region, Mariner 6 observed Aram Chaos and the ISM "Arabia" track just misses the northern most edge of small hematite outliers shown by Christensen et al. [2].

[1] We prefer to use the term "bulk" as opposed to crystalline or specular hematite as the latter can imply a high pressure or high temperature metamorphic regime considered unlikely for the surface of Mars. As we will show, bulk grey hematite can form as a chemical precipitate without either large crystals or specular nature.

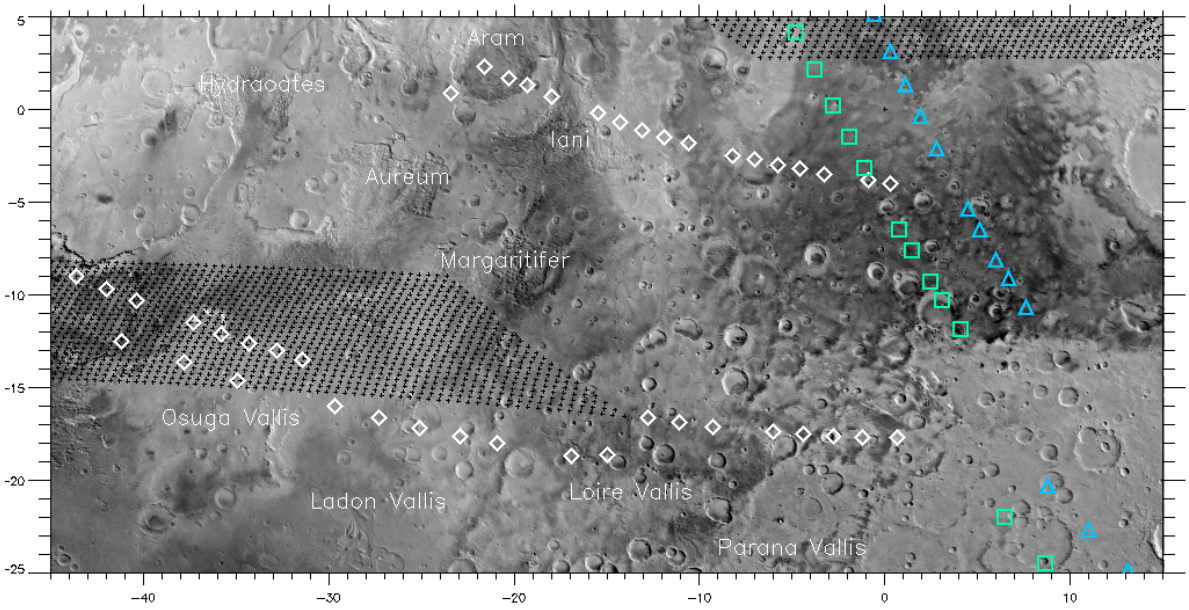

Figure 1: Location of Mariner 6/7 IRS and Phobos ISM spectral observations. White diamonds are Mariner 6, green squares are Mariner 7 short wavelength (2-6 μm), blue triangles are Mariner 7 long wavelength (5 to 15 μm). Small black points are ISM points of the Aurora and Arabia swaths.

Baldridge and Calvin [9] found there is a marked correlation between the Mariner spectra that have an increased integrated band depth for the entire water of hydration feature with regions identified by TES containing bulk hematite. Both Mariner 6 and 7 show increased water over Meridiani and Mariner 6 shows increased water in the spectra that correspond with the Aram Chaos hematite outcrop, consistent with the earlier study [6,9].

There are very few studies that quantify the amount of water in a sample and the reflectance shape of the 3-μm absorption feature. Yen et al. (1998) [12] used apparent absorbance to study water content. For soils of well characterized grain sizes, the apparent absorbance shows a near-linear trend with water content as determined by thermal gravimetry. However this band can be grain size dependent, and they also note that exceptionally fine-grained hydrated materials coating larger grains can lead to similar absorbance values with as little at 0.5% H_2O. More recently, Milliken and Mustard [13] have modeled dehydration of water adsorbed on montmorillonites using the optical constants of water relative to a dry sample.

The spatial footprint of the Mariner IRS instrument is quite large, ~ 100 x 200km. The viewing geometry is not strongly varying over the duration of the observations. The intermediate to low thermal inertia of the Meridiani site [3,10] suggests loose, sand size material. This and the albedo suggest there is not a strong component of fine-grained material. The integrated band depth is normalized so that the albedo of the surface is removed. Hence we have argued that the Mariner data are not likely sensitive to small scale variations in surface physical properties but are in fact recording a parameter sensitive to the hydration state of surface materials. Based on the apparent absorbance model, the Mariner data indicate an increase of water of 1 to 2 wt%. As the average soil is inferred to have only 1 to 2wt % water this is a significant local enhancement in hydrated minerals.

The marked spatial correlation of the two spectral properties suggests a genetic link, not just a coincidence, particularly given that both properties are atypical for the Martian surface. As the bulk oxide hematite is not hydrated, there must be an additional hydrated phase on the surface in these regions. Identification of the phase based strictly on the 3-μm absorption feature is unlikely.

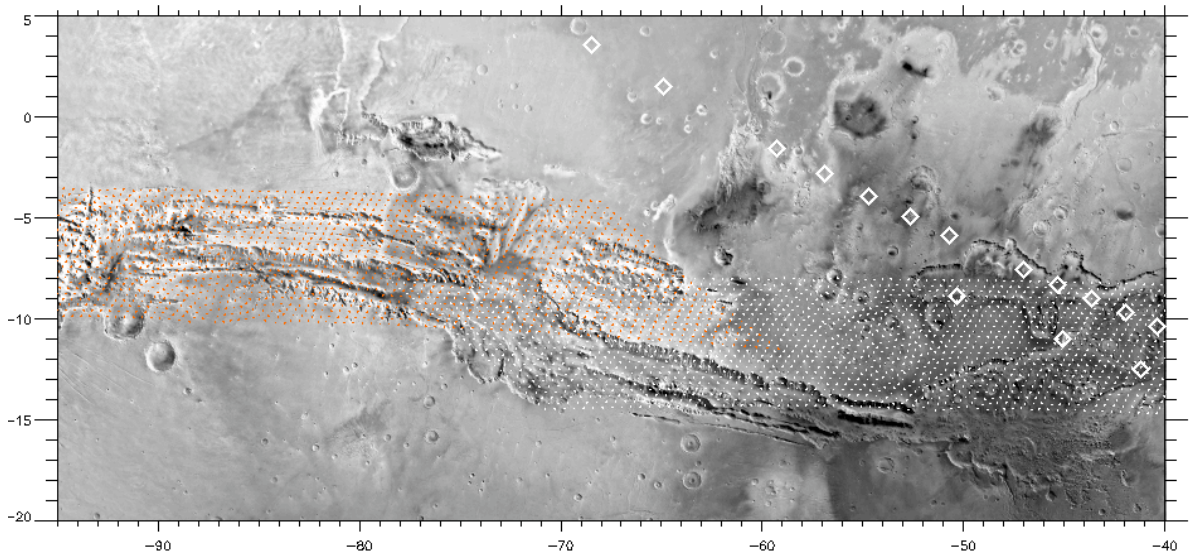

Figure 2: Locations of the VMC (Valles Marineris Center) and AUR (Aurora) swaths for ISM are shown as small points, red and white respectively. Mariner 6 IRS footprints overlapping AUR in Ganges and EOS Chasmae are shown as white diamonds.

ISM AND WATER

Only two orbiting spectrometers have observed Mars in the region sensitive to water of hydration. While many minerals have absorptions near 1.4 and 1.9 μm in addition to 3-μm, the shorter wavelengths are difficult to observe through abundant atmospheric absorptions and scattering. The Phobos ISM spectrometer also observed similar wavelengths to IRS, but at markedly reduced spectral sampling due to problems of calibration of the even and odd detectors [e.g. 14]. ISM also only observed to 3.1 μm, so that most analysis of that data set uses a simple ratio to albedo at shorter wavelengths to determine a 3-μm "band depth" [14,15]. The disadvantage of this approach relative to the integrated value determined by IRS is the strong correlation of the ratio method to albedo. Hence only among material of similar albedo can a 2.5/3.1 ratio appropriately be considered to reflect possible variations in surface hydration. Murchie et al. [15] recently summarized the ISM results noting increased hydration in intermediate albedo dark red soils and in layered terrains in the Valles Marineris.

Given the exciting correlation between integrated 3-μm band depth and the TES hematite regions we here revisit the ISM data set. Erard and Calvin [11] note good agreement between the IRS and ISM instruments overall and strong agreement in absolute value of 3-μm reflectance in low albedo regions. Also, while IRS did not observe the hematite sites in Candor in the Valles Marineris the ISM has three swaths over this region: VMC, HEB and AUR, for Valles Marineris Center, Hebes Chasma and Aurora Planum as shown in Figure 2.

In their summary paper, Murchie et al. [15] performed spatial averaging to smooth out calibration and other noise sources. We are looking for spatial properties that are 1 to 2 ISM pixels in Candor and hope to derive a method that is less sensitive to the overall albedo correlation. Figure 3 shows the apparent absorbance (-ln(r)) using a single wavelength channel for the calibrated data available on the ISM web page [14]. The apparent absorbance still has a strong correlation to albedo which makes this property somewhat suspect in determining hydration state. We are currently examining atmospherically corrected data as well as averaging a few channels for apparent absorbance. Figure 3 has been thresholded to map only the most extreme values of the 3-μm apparent absorbance. We are exploring various methods to remove the linear component of the hydration vs albedo fit in order to examine variations in band strength that deviate from the linear trend. Comparison to IRS values will be presented at the meeting.

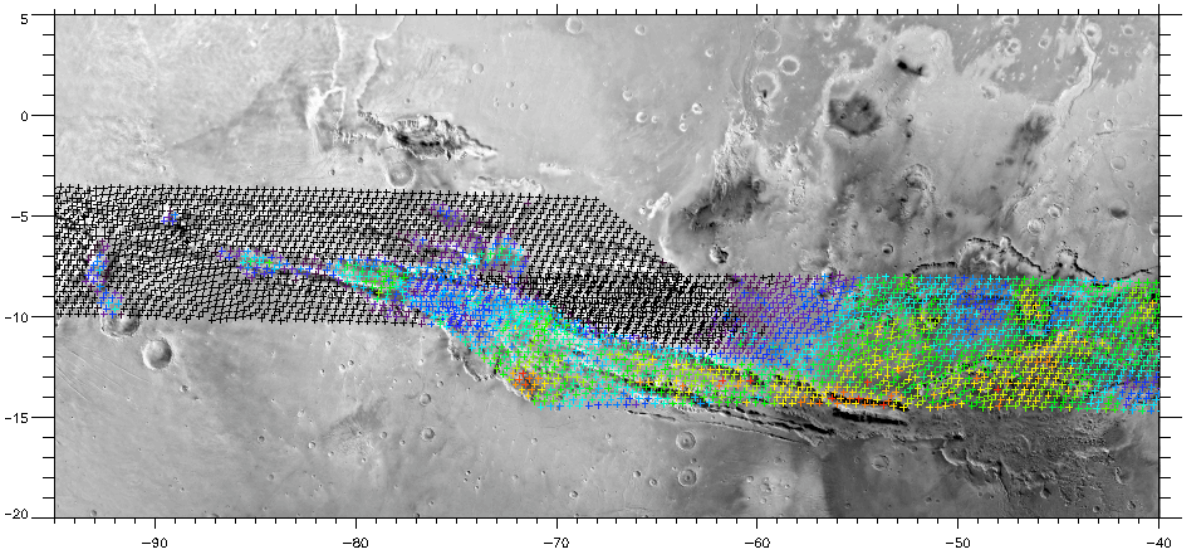

Figure 3: Apparent absorbance of ISM values at ~3.1 μm. Red indicates a higher strength due to the spectral features of water. The image has been thresholded so that brighter surfaces (albedos at 2.3 μm > ~ 0.25 have been set to zero.

POSSIBLE ORIGINS

The hydrated component of the hematite regions could be associated with carbonate, silicate or sulfate materials [9]. There are only a few natural environments where bulk oxides and hydrated minerals appear concurrently. These include terrestrial Archean iron formations and carbonaceous chondrites. An additional property is that both these environments lack abundant oxygen, similar to the present and inferred past state of the Martian atmosphere. A general similarity is seen between the alteration products in Archean Iron Formation (IF) and carbonaceous chondrites [8] and, in addition, both these assemblages are associated with organic materials or possible biological precipitation in the case of IF. Fallacaro and Calvin [16] describe spectral and chemical studies of Lake Superior Banded Iron Formation (BIF) associated with shallow sea precipitation. Previous work [7,8,17] has explored the silicate facies minerals similar in some detail. Here we expand on the work of Calvin [7] by considering the amount of silicate BIF spectral signatures that can be included in a mixture with oxides and still be compatible with TES observations in the 10-μm region. We will present linear mixtures models for thermal wavelengths at the conference.

2004: MER

The rovers carry a suite of chemical and mineralogical instrumentation for determining the detailed nature of surface materials, including Moessbauer, APXS, thermal IR spectroscopy as well as color, panchromatic, and microscopic imagery. We look forward to the data returned by that mission and its ability to resolve the origins of the deposits and the nature of accessory minerals at the Meridiani site.

References: [1]Christensen et al. *JGR*, **105**, 9623, 2000. [2]Christensen et al. *JGR*, **106**, 23873, 2001. [3]Hynek et al. *JGR*, **107**, 5088, 2002. [4]Lane et al. *JGR*, **107**, 5126, 2002. [5]Kirkland et al. *LPSC XXXIV* abs 1944, 2003. [6]Calvin, *JGR*, **102**, 9097, 1997. [7]Calvin, *GRL*, **25**, 1597, 1998. [8]Calvin et al. LPSC XXXIII, abs 1154, 2002. [9]Baldridge and Calvin JGR submitted. [10]Arvidson et al JGR submitted. [11]Erard and Calvin *Icarus*, **130**, 449, 1997. [12]Yen et al. *JGR*, **103**, 11125, 1998. [13]Milliken and Mustard *LPSC XXXIV* abs 1345, 2003) [14]Erard et al. *Proc. Lun Planet. Sci.* **21**, 437, 1991, http://www.ias.fr [15]Murchie et al. *Icarus*, **147**, 444, 2000. [16]Fallacaro and Calvin, this conference. [17]Calvin and King, *Meteorit. Planet. Sci*., **32**, 693, 1997.

MGS-MOC OBSERVATIONS OF MARTIAN DUST STORM ACTIVITY. B. A. Cantor[1], [1]Malin Space Science, San Diego, CA.,USA (cantor@msss.com).

Introduction: The Mars Observer Camera (MOC) completed its second consecutive Martian year of monitoring on December 12, 2002, since entering its mapping orbit on March 9, 1999. During this time the narrow-angle (NA) camera has been taking snapshots of the surface at a resolution of 3-40 m/pixel, while the two wide-angle (WA) cameras, which cover two wavelength bands spanning from the blue (400-450 nm) to the red (575-625 nm), have been continuously mapping the dayside of Mars at a constant resolution of 7.5 km/pixel. Because the WA cameras have a 140° FOV, which allows for limb-to-limb views of the planet, the local time across these low-resolution images ranges from 12:17 to 15:43 at the equator. Some overlap exists between images taken on consecutive orbits, allowing for complete global coverage of the planet to be obtained in two colors in only 12 to 13 orbital passes or about once per a sol.

The MGS-MOC experiment has provided an unique opportunity to study Martian weather phenomena, ranging from dust devils and dust storms to condensate clouds to the seasonal behavior of the Martian polar caps, all on time scales ranging from semi-diurnally to interannually. We present here a brief description of the dust activity observed by MOC during the past 2 Mars years in terms of the interannual invariability/variability of these events.

MOC has observed dust events across much of the planet from the depths of Hellas basin to the summit of Arsia Mons. These events range in size from dust devils to planet encircling dust veils.

Dust Devils: Martian dust devils range in size from a few to 10s of meters across to 100s of meters across and over 6 km high. Though dust devils occur throughout most of the Martian year, each hemisphere has a "dust devil season" that generally follows the subsolar latitude and appears to be repeatable from year-to-year. An exception is NW Amazonis, which has frequent, large dust devils throughout northern spring and summer.

MOC observations show no evidence that dust devils cause or lead to dust storms, however, observations do suggest that dust storms can initiate dust devil activity (i.e., Dust devils sometimes do occur near small, localized storms). One specific relation occurred during the onset of the planet encircling dust event of 2001, when slightly elevated levels of atmospheric dust, associated with the developing planet encircling dust veil, triggered a very short period of dust devil activity in NW Amazonis in early northern autumn. The redistribution of dust by the initial onset of the 2001 planet-encircling dust activity may have also affected subsequent spring and summer dust devil activity in Hellas, where considerably fewer dust devils occurred in 2001-2002 than 1999-2000. In SW Syria, frequent, large dust devils occurred after the 2001 global activity and persisted through southern summer. While dust devils have no specific relation to dust storms, they might play a role in maintaining the low background dust opacity of the Martian atmosphere, as well as, the seasonal "wave of darkening" at middle and high latitudes by removing or disrupting thin veneers of dust.

Dust devils are also important in terms of the shadows they cast, which can provide a snapshot view of the afternoon vertical structure of the lower several kilometers. A northern Amazonis, summertime dust devil, shown in Figure 1, has a distinct shadow that shows the fine vertical structure of the vortex and plume. The bending of the vortex by 45° to the northwest is indicative of a wind-shear layer about 0.6 km high, which extend from 0.64 km to 1.24 km above the surface. The direction of the prevailing winds in this layer are to the northwest. The point where the vortex and plume interface, defines another boundary layer, which occurs at an altitude of 1.68 km above the surface.

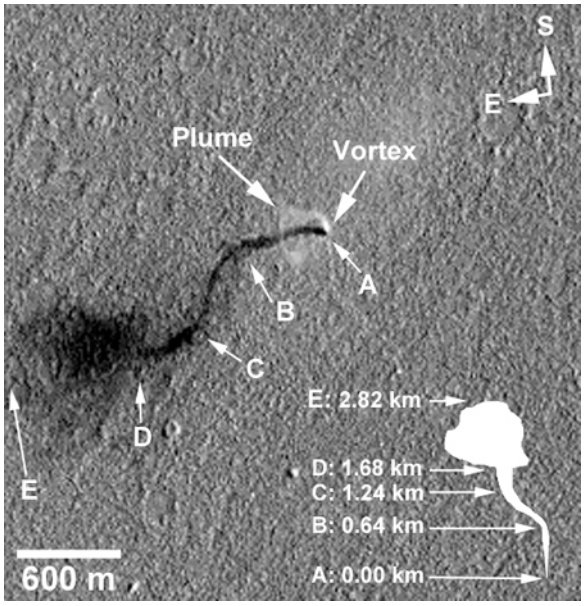

Figure 1. MOC-NA image of an Amazonis dust devil.

Dust Storms: Global maps are important for monitoring all but the smallest scale dust activity on Mars. MGS global observations have shown that storms occur almost daily with few exceptions, with thousands occurring each year in the present Martian environment, dispelling the notion of a "Classical Dust Storm Season". However, there does appear to be an annual dust storm cycle, with storms developing in specific locations during certain seasons; see Figure 2. MOC observations taken during the past 2 Martian years, suggest that this dust cycle was in general, repeatable from year-to-year. The majority of storms develop near the receding seasonal polar cap edge or along the corresponding polar hood boundaries in there respective hemispheres, suggesting that large thermal gradients and the surface winds they generate are the triggering mechanism for some of the dust activity. Because of MGS's polar orbit, some of these high-latitude local dust storms have been monitored with sufficient temporal sampling density (every 2 hours) to observe their semi-diurnal evolution; see Figure 3. These observations showed that most high-latitude storms formed in the early to late morning hours when boundary layer instabilities would be greatest and would expand rapidly, covering a large area in a matter of just 4-6 hours.

In the northern plains, spiral dust events tend to be seen in the spring and summer seasons and resemble terrestrial polar lows "cold fronts". Those seen during late northern summer tend to resemble terrestrial baroclinic fronts and are accompanied by condensate clouds, traveling eastward at about 12-15 m/s for several days before dissipating. Still other storms develop in the low laying regions where atmospheric conditions are optimized for dust lifting (e.g., plains on the windward side of Olympus and Elysium Mons and Alba Patera, in Hellas and Argyre Basins, in Chryse Planitia, ect…).

Dust storms such as the cross-equatorial events that form in Acidalia/Chryse and travel southward following the low-lying topography into Valles Marineris, also tend to follow a seasonal trend occurring in two periods from about L_s = 208°-224° and L_s = 315°-333°; see Figure 4. They appear to be associated with the strengthening of the Hadley circulation during the southern spring and summer seasons. These storms are part of a class of large dust events referred to in the scientific literature as "Regional" dust storms because of their great extent and duration (> 3 sols). Though limited in number with a few 10s of regional storms occurring per Martian year, their size, duration, and unrestricted seasonality make them ideal tracers of atmospheric circulation for global mapping investigations. MOC has used this capability to observe for the first time the north-to-south cross-equatorial circulation associated with the lower-branch Hadley circulation in the Chryse/Valles Marineris region (as noted above), as well as, the general circulation at high latitudes in both hemispheres. At present our understanding of regional storms is fairly limited. Analysis of the historical records suggested that regional dust storms occur in all seasons, but are absent during two periods of the year L_s = 130°-160° and L_s = 330°-20°. Recent MOC observations suggest that this later time period may be even shorter (L_s = 0°-20°). As for why some local storms become regional is unclear, but WA images suggest that about half of the larger regional storms may form from the merge of two or more active local storms.

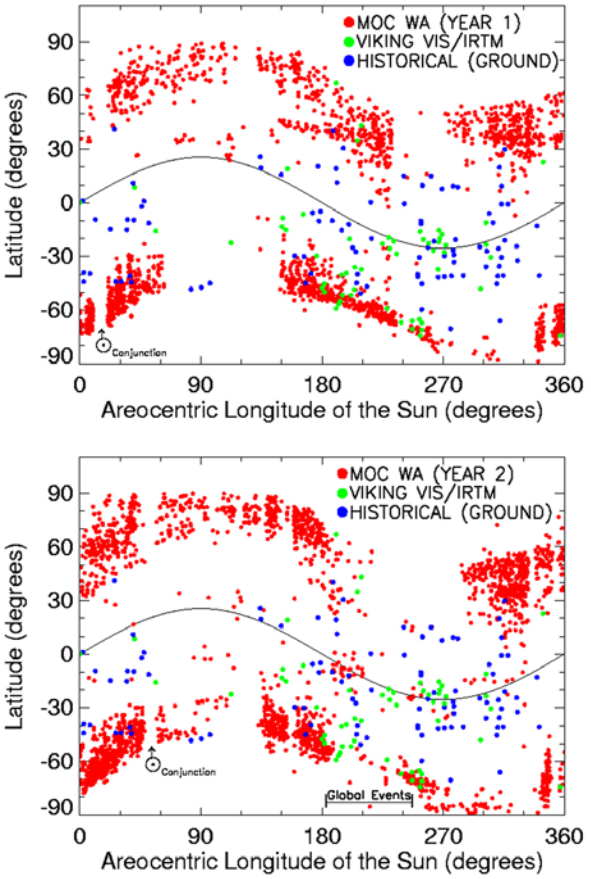

Figure 2. Latitudinal distribution of dust storms as a function of L_s. Comparison of the MOC wide-angle red filter observations taken during the first Mars year (top) [1] and the second Mars year (bottom) with Viking Orbiters' infrared and visible observations [2, 3] and historical ground-based observations [4]. Solid line corresponds to the subsolar latitude.

Figure 3. Semi-diurnal evolution of summertime, local dust events in the southern hemisphere.

Figure 4. Cross-equatorial dust storm observed during northern winter.

The largest and rarest of dust phenomena on Mars are referred to as the "Great Storms" or "Global Storms". These dust events can encircle the planet in specific latitude bands, such as the southern subtropics ("planet encircling" storm) or on occasion have been observed to enshroud the planet ("global" storm). These dust events are quite rare, with only 6 confirmed events on record, 4 planet-encircling and 2 global [5]. The MGS MOC global imaging investigation has provided the first comprehensive planet-wide views of almost the entire development of the 2001 global "planet enshrouding" dust event. Such global mapping has led to new insights into the initiation and evolution of these global atmospheric phenomena, as well as place constraints on model predictions. With MOC we have observed that global dust events are not individual storms but are composed of a number of local and regional storms (sources). The storms that created the planet-encircling dust veil lasted from a few days to a few months, as in the case of the Syria-Claritas regional storm, which lasted for over 3 months in the same location. It was the dust raised into the upper atmosphere by the larger, longer-lasting storms that appears to have stimulated further storm activity across the planet, possibly due of diabatic heating of atmospheric dust, and are also responsible for the planet-encircling dust veil. MOC also observed that the storms responsible for the initiation of the start of the "planet-encircling dust activity" did not form in the southern subtropics, but developed in the mid-latitudes adjacent to the receding south polar cap. These storms then traveled northward into the subtropics, which is consistent with the class of global storm generating mechanism models that emphasize enhancement of the planetary scale circulation [6]. The effects of the planet-encircling dust activity on the Martian climate are at best minimal, in fact, dust storm and condensate cloud activity returned to their normal predictable seasonal behavior within a few months of the ending of the planet-encircling event.

Though dust storms occur throughout the Martian year and across most of the planet, there are regions and times where dust activity was at a minimum or non-existent; see Figure 2. One region where MOC has observed no dust activity over the past 3 Martian years is Arabia Terra. In the Northern Hemisphere, the period of minimum dust activity occurs during northern fall between about L_s = 235°-270°. In the southern hemisphere, there appears to be three periods of minimum dust activity, the most significant occurs while the seasonal south polar cap is forming between about L_s = 65°-130°. The other two occur during southern summer between about L_s = 275°-290° and L_s = 313°-340°. Because of the lingering effects of the planet-encircling dust veil of 2001, MOC was not able to confirm whether the period of minimum dust activity in the Northern Hemisphere was repeatable from year-to-year. The periods of minimum dust activity in the Southern Hemisphere have been fairly repeatable, with the exception that the southern fall/winter minimum was of shorter duration (by about two months) in 2002. Possibly the result of the redistribution of surface dust caused by the long-lived (90-sol duration) dust storm in the Syria-Claritas region, part of the planet-encircling dust activity of 2001.

In summary, MOC has observed that dust events follow general seasonal cycles that are reproducible from one year to the next and that global dust events do not signify climatic changes, but are only short-term perturbations to the interannual repeatable dust and condensate cloud cycles of Mars.

References: [1] Cantor, B. A. et al. (2001) *JGR, 106,* 23653–23687. [2] Peterfruend A. R. (1985) *Ph.D. thesis*, Ariz. *State Univ.*, 246. [3] Briggs, B. A. et al. (1979) *JGR, 84,* 2795-2820. [4] Wells, R. A. (1979) *Geophysics of Mars*, *Elsevier Sci.*, 678. [5] Zurek, R. W. and Martin, L. J. (1993) *JGR, 98,* 3247–3259. [6] Leovy, C. B. et al. (1973) *J. Atmos. Sci.*, *30*, 749-762.

ENIGMATIC LANDFORMS IN CYDONIA: GEOSPATIAL ANISOTROPIES, BILATERAL SYMMETRIES, AND THEIR CORRELATIONS. M. J. Carlotto, Veridian Systems Division, 705 Broughton Dr., Beverly MA 01915 (mark.carlotto@veridian.com)

Introduction: Geospatial terrain statistics and object symmetries of enigmatic landforms in Cydonia are examined and correlations identified. Analysis of Viking image-derived MDIM data (1/256 deg./pixel) over Cydonia (37.5-42.5° N and 4.5-15.5° W) shows directional anisotropies in the spatial autocorrelation (variogram) at medium to long wavelengths (10-100 km.). One is in the direction of the crustal dichotomy in this part of Mars (~ 64.6°, or ~25.4° north of east), along with two others at 103.7° and 164.2°. Anisotropies in similar directions at shorter wavelengths (down to tens of meters) are evident in the variograms of Viking, THEMIS, and MGS images within this area. The spatial autocorrelation structure of selected regions in Viking images show indications of rectilinear geometry (directional anisotropies approximately 90 deg. apart) similar to that of highly eroded terrestrial archaeological ruins. Previous analyses of THEMIS and MGS imagery reveal a high degree of bilateral symmetry in several landforms. We show the axes of symmetry are roughly in line with the directional anisotropy at 164.2° noted above.

Geospatial Statistics: Variograms describe correlations in spatial data. The variogram of an image $i(x,y)$ is:

$$\begin{aligned} 2\gamma(u,v) &= Var\left[i(x,y) - i(x+u,y+v)\right] \\ &= E\left\{\left[i(x,y) - i(x+u,y+v)\right]^2\right\} - \\ &\quad \left\{E\left[i(x,y) - i(x+u,y+v)\right]\right\}^2 \\ &= E\left\{\left[i(x,y) - i(x+u,y+v)\right]^2\right\} \end{aligned}$$

for stationary random processes. The variogram and the autocorrelation function are related

$$\begin{aligned} 2\gamma(u,v) &= E\left\{\left[i(x,y) - i(x+u,y+v)\right]^2\right\} \\ \gamma(u,v) &= R(0,0) - R(u,v) \end{aligned}$$

where $R(u,v) = E\left[i(x,y)i(x+u,y+v)\right]$. For efficiency the autocorrelation function is computed using the Fast Fourier Transform (FFT):

$$\begin{aligned} R(u,v) &= i(x,y) * i(-x,-y) \\ &= \Im^{-1}\left\{\Im[i(x,y)]\Im^*[i(x,y)]\right\} \end{aligned}$$

The image formation model [1] relates the spatial statistics of an image to its underlying terrain surface. We are interested in the correlation structure of the terrain, specifically in its directional anisotropy. The autocorrelation function in polar coordinates is $R(r,\theta)$ where $r = \sqrt{u^2 + v^2}$ and $\theta = \tan^{-1}(v/u)$. The polar distribution function

$$F(\theta | r_1, r_2) = \int_{r_1}^{r_2} R(r,\theta)dr$$

expresses directional correlations in spatial data over a given scale range. Peaks in the angular distribution indicate directions along which correlations exist in the terrain.

Mars Crustal Dichotomy: MDIM data provide the appropriate spatial scale to illustrate long term directional trends in the terrain (Fig. 1a). The MDIM autocorrelation function is shown in Fig. 1b with a polar plot showing directional anisotropies for $9 < r < 115$ km. Three peaks occur at 64.7±2.5°, 103.2±3.9°, and 164.0±0.9°. The first (direction A) corresponds to the direction of the crustal dichotomy in this part of Mars [2]. The other two directions (B and C) are referenced later in the paper.

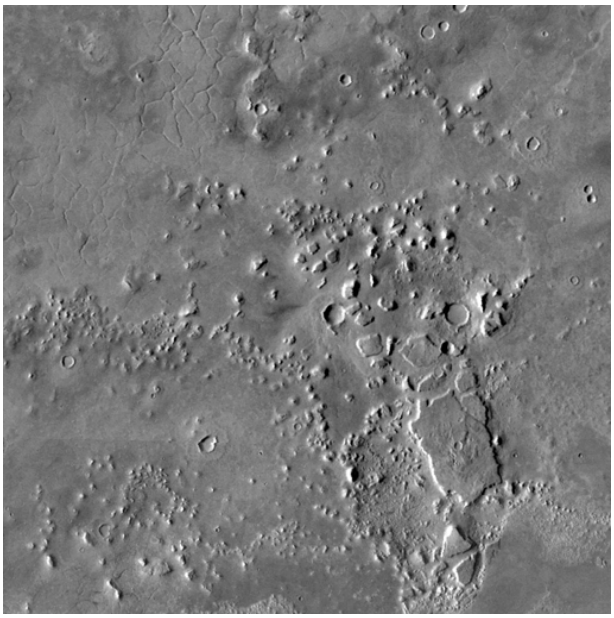

Fig. 1a Mosaic of two MDIM images at 1/256 degrees/pixel (231 m/pixel) in sinusoidal equal-area projection.

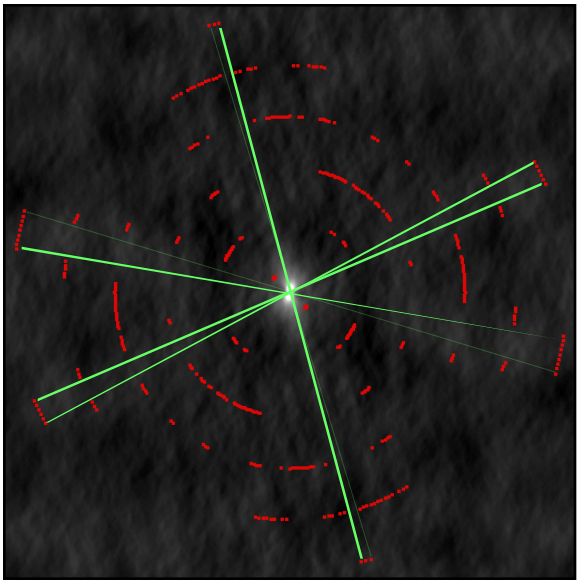

Fig. 1b Polar plot of MDIM autocorrelation function computed over distances of 9-115 km.

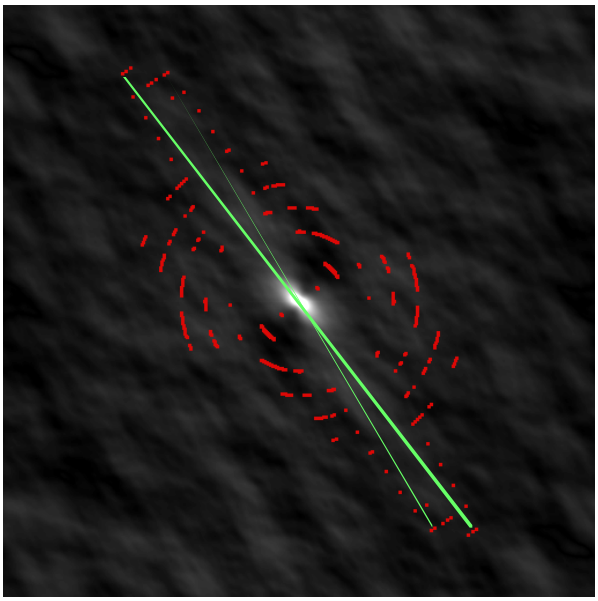

Fig. 2b Polar plot showing directional anisotropies in THEMIS image over distances of 2-25 km.

Shorter Scale Correlations: Anisotropies in similar directions at shorter wavelengths (down to tens of meters) can be found in the autocorrelation functions of THEMIS, Viking, and MGS images within this area. Fig. 2a shows two sections of a THEMIS image strip. This area is toward the northeast corner of the MDIM image in Fig. 1. A directional anisotropy exists in the autocorrelation at 153.5±3.7° over distances of 2-25 km (Fig. 2b). This is approximately 90° away from the direction of the Mars crustal dichotomy (direction A).

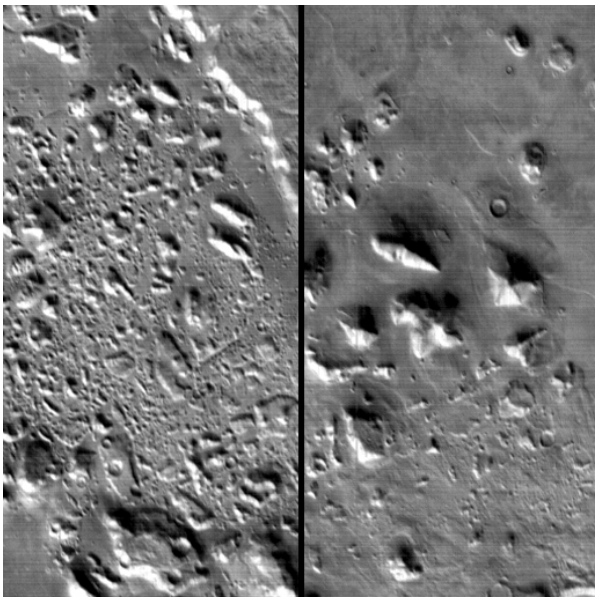

Fig. 2a Two sections of THEMIS image 20020413a over Cydonia

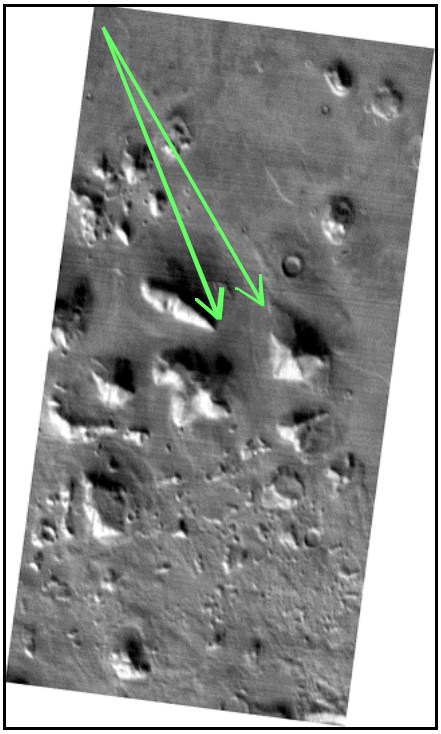

Fig. 2c Directions 149.8° and 157.2° (153.5±3.7°) overlaid on portion of THEMIS image

In Fig. 2c the directional interval 153.5±3.7° is represented by the two arrows overlaid on the portion of the THEMIS image strip which includes the two enigmatic landforms known as the D&M Pyramid and Face [3]. Both of these objects possess a high degree of bilateral

symmetry (Fig. 3) with their axes of symmetry closely lined up with the 153.5±3.7° anisotropy.

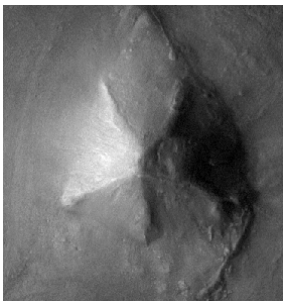

"D&M Pyramid" from THEMIS image 20020413a

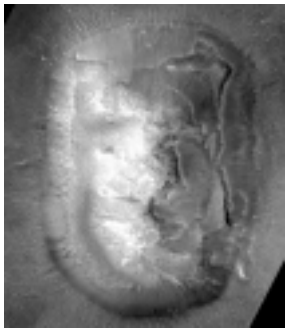

"Face" from MGS image E1701041

Fig. 3 Enigmatic landforms rotated so that their axes of symmetry are in the vertical direction

Analysis of Viking orbiter imagery (Fig. 4) reveals spatial correlations at 48° and 167.7±2.5° between 2.5-10 km. that coincide roughly with those seen in MDIM and THEMIS images.

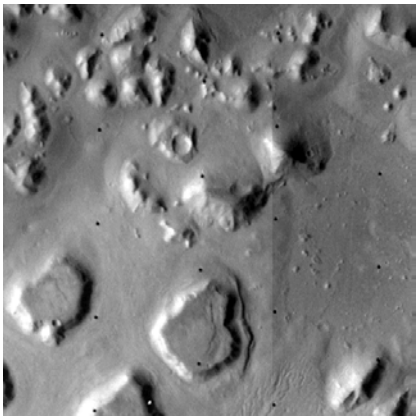

Fig 4a Mosaic of map projected Viking frames from orbit 35 over an area showing evidence of rectilinear organization

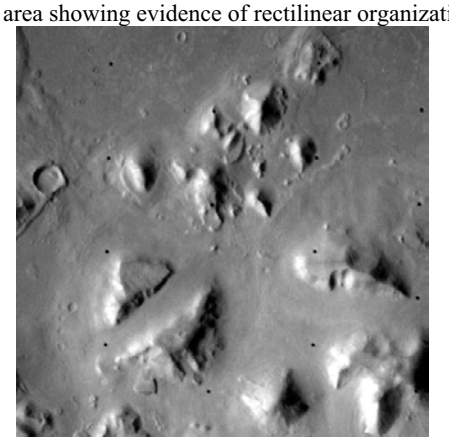

Fig. 4b. Portion of map projected Viking frame 35A72 showing the enigmatic landform known as the "City"

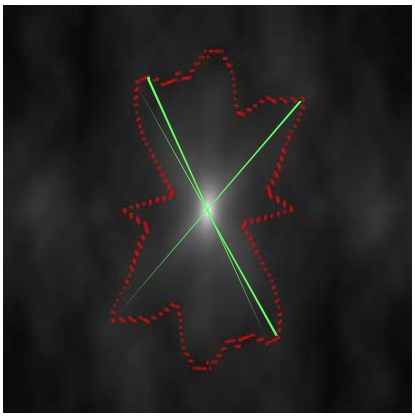

Fig. 4c Polar plot showing directional anisotropies in Viking images over distances of 2.5-10 km. (Peaks at 0° and 90° are edge artifacts that are a result of FFT processing.)

Finally in Fig. 5 we show a portion of an MGS image near 39.95° N 14.8° W containing small bumps oriented at 52.7±6.7° over scales of 150-580 meters. This area is about 250 km. away from the Cydonia landforms, in the southwest corner of the MDIM image in Fig. 1.

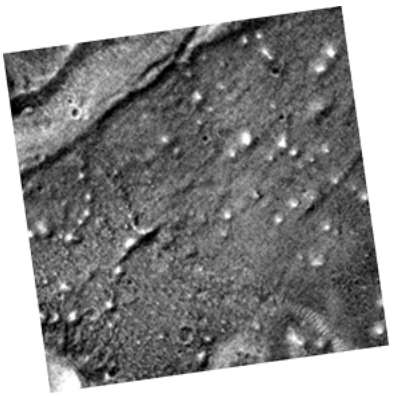

Fig. 5a Portion of MGS image SP249604 (area shown in about 1.4 sq. km.)

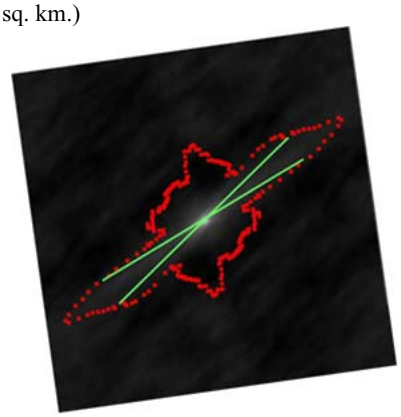

Fig. 5b Peak in polar plot of MGS autocorrelation function at 52.4±6.7°

Discussion: The results presented here lead naturally to three questions:
1) Why do directional anisotropies exist over such a wide range of spatial scale?
2) Why are some of them about 90° apart?
3) Why do their directions coincide roughly with the axes of symmetry of several enigmatic landforms in Cydonia?
While the Null Hypothesis -- that these correlations have a natural (geological) interpretation -- is to be preferred over others, we offer the hypothesis that this collection of features may represent the eroded remains of ancient archaeology on Mars. Fig. 6 shows an aerial image over an eroded site on the South coast of Peru [4]. Its rectilinear pattern of organization leads to a correlation structure with directional anisotropies 90° apart. Similar correlation signatures are observed in Cydonia.

Fig. 6a Aerial view eroded archaeological site (La Centinela, Peru)

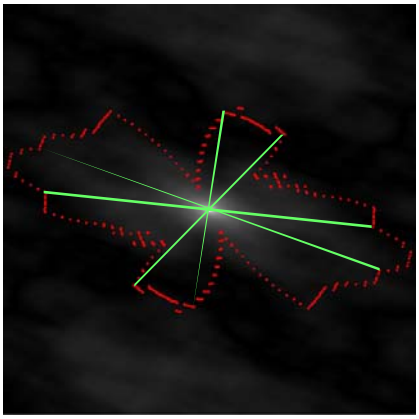

Fig. 6b Polar plot of spatial autocorrelation of La Centinela showing anisotropies about 90 degrees apart. Note angle difference differs from 90° in this image due to perspective foreshortening.

Following Sagan's criteria for detecting signs of planetary intelligence [5], deviation from fractal behavior was proposed as a measure for detecting anomalous (possibly artificial objects) in terrestrial [6] and planetary imagery. Positive detections were obtained in medium resolution Viking imagery over selected features in Cydonia [7].

The correlations described in this paper may be related to earlier fractal indications of artificiality in Cydonia. Although the alignment of the geospatial anomaly with the crustal dichotomy suggests a natural explanation, the origin of the dichotomy itself is not well understood. Furthermore, an explanation of the dichotomy would also have to explain the wide range of scales (10^2-10^5 meters) spanned by the anomaly, alignments in other directions (some about 90° apart), and their alignment with the symmetry axes of the "Face" and "D&M Pyramid".

References: [1] Pentland, A.P., and Kube, P. (1988), *IEEE Trans. PAMI 10,* 704-707. [2] Cattermole, P. (1992), *Mars - The Story of the Red Planet*, 191-193, Chapman and Hall. [3] Carlotto, M.J. (1988) *Applied Optics 27*, 1926-1933. [4] Bridges, M. (1991), *Planet Peru*, 83, Kodak/Aperture. [5] Sagan, C. (1975), *Proc. Royal Society 189*, 143-153. [6] Stein, M. C. *Proc. SPIE 845*, 293-300. [7] Carlotto, M.J. and Stein, M. C., (1990) *JBIS 43*, 209-216.

A CASE FOR HYDROTHERMAL GRAY HEMATITE IN ARAM CHAOS. D. C. Catling[1] and J. M. Moore[2], [1]Dept. Atmospheric Sciences & Astrobiology Program, Box 351640, University of Washington, Seattle, WA 98195-1640 (davidc@atmos.washginton.edu) [2]M/S 245-3, Space Science Division, NASA Ames Research Center, Moffett Field, CA 94035-1000 (jmoore@mail.arc.nasa.gov).

Introduction:

The Thermal Emission Spectrometer (TES) on Mars Global Surveyor has detected deposits of coarse-grained, gray crystalline hematite in Sinus Meridiani, Aram Chaos, and Vallis Marineris [1]. Detailed features in the hematite spectral signature of the Sinus Meridiani region show that the spectrum is consistent with emission dominated by crystal c-faces of hematite, implying that the hematite is specular [2]. Gray specular hematite (also known as "specularite") is a particular gray crystalline form that has intergrown, hexagonal plates with a silvery metallic luster. We believe that the key to the origin of specularite is that it requires crystallization at temperatures in excess of about 100°C. In reviewing the occurrence of gray hematite on Earth, we find no exceptions to this warm temperature requirement [3]. Thermal crystallization on Mars could occur (1) as diagenesis at a depth of a few kilometers of sediments originally formed in low-temperature waters, or (2) as direct precipitation from hydrothermal solution. Aram Chaos has unique chaotic terrain that offers more clues to the formation of the hematite than the relatively featureless flat terrain (as seen from orbit) of Sinus Meridiani. Aram Chaos provides the opportunity to look at a combination of TES data, Mars Orbiter Camera images, and Mars Orbiter Laser Altimeter (MOLA) topography. This combination of data suggests that high concentrations of hematite were formed in planar strata and have since been exposed by erosion of an overlying light-toned, caprock. Lesser concentrations of hematite are found adjacent to these strata at lower elevations, which we interpret as perhaps a lag deposit. The topography and the collapsed nature of the chaotic terrain favor a hydrothermally charged aquifer as the original setting where the hematite formed. An alternative sedimentary origin requires post-depositional burial to a depth of ~3-5 km to induce thermally driven recrystallization of fine-grained iron oxides to coarse-grained hematite.

How does gray hematite form on Earth?: We can consider formation in (a) igneous (b) sedimentary and (c) hydrothermal environments.

(a) *Igneou environments*. Gray hematite cannot be a directly ascended, igneous rock (a "lava") because the magmatic oxygen fugacity on Mars is unlikely to ever lie in the hematite stability field. Hematite is not plausible because the oxygen fugacity (f_{O2}) is vastly lower (~4 to 8 orders of magnitude) than the magnetite-hematite buffer, based on redox-sensitive geochemical indicators in Martian meteorites [4,5]. Where hematite occurs in so-called "igneous" environments on Earth, such as Kiruna-type ores (e.g., El Laco in Chile), fluid inclusions containing chlorides and anhydrite and field observations suggest hydrothermal alteration of the host rock [6,7]. For example, specular hematite in volcanic rocks of Pilot Knob in the St. Francois Mountains (Missouri) is clearly hydrothermal, given the occurrence of hematite veins (some as much as 3 m in width), cavity fills, and mineral like tourmaline that are indicative of warm temperatures [8]. High temperature oxidation of basalt in O_2-rich terrestrial air can produce thin coatings of gray hematite [9], but it is doubtful if the early Martian atmosphere has sufficient O_2 to make this a realistic scenario; also if atmospheric oxidation were all that were required for specular hematite, it would be ubiquitous on Earth and Mars rather than occuring in unique geological predicaments.

(b) *Sedimentary formation*. Gray hematite does not form directly from a low-temperature aqueous solution. Instead, fine reddish-colored iron oxides form, usually goethite (FeOOH). So-called "sedimentary" deposits of specularite require diagenesis where sediments have been heated at depth to greater than ~100°C., causing recrystallization of fine-grained iron oxides to coarse-grained gray hematite. For buried sediments at moderate depths, water is either bound in chemical compounds or adsorbed onto the iron oxide grains. Porosity and permeability are small and fluids "fight" their way out, which yields the approximate assumption that the pore-fluid pressure approaches the lithostatic pressure. Thus iron oxide dehydration and hematite recrystallization will occur at a depth where the geotherm intersects the dehydration line for bound water. Fig. 1 shows a thermodynamic calculation using the data of [10]. Assuming a typical megaregolith conductivity of 2.5 W m^{-1} K^{-1} and an early Mars geothermal gradient gives the depth of intersection (dashed line assumes a geothermal heat flux of 50 mW m^{-2}; solid line, assumes a geothermal heat flux of ~80 mW m^{-2}). The depth of burial is 3-5 km of overburden matieral, which is difficult to reconcile with commonly inferred Martian geological processes.

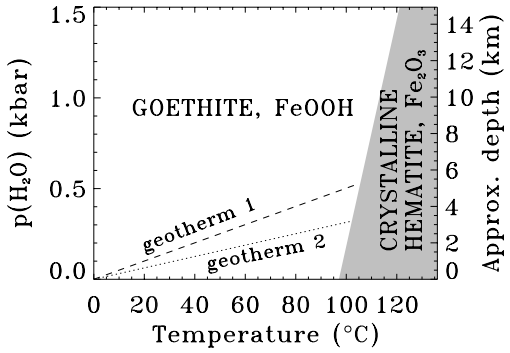

Fig. 1: Stability fields of goethite (FeOOH) and hematite (Fe_2O_3) as a function of temperature and H_2O pressure. The latter can be taken as being approximately equal to the lithostatic pressure, giving the equivalent subsurface depth. At depth, hydrous iron oxides (typified by goethite) recrystallize to coarsely crystalline hematite due to heating (see text).

That thermal transformation is needed is borne out by all terrestrial field observations [3]. As an example, specularite (with 50-100 μm-sized platy crystals) in the the Brockman Formation, part of the Hamersley Range in Western Australia, formed at temperatures ~140°C on the basis of oxygen isotopes [11]. This temperature is consistent with the estimated maximum temperature of 205-325°C from an estimate of the burial depth. If the origin of the coarsely crystalline hematite on Mars started with aqueous deposition in a standing body of water, this must have been followed by either deep burial up the geothermal gradient or some other large-scale thermal perturbation due to igneous activity.

(c) *Hydrothermal formation*.

Gray, platy hematite can form directly in hydrothermal solution. Small crystals have larger vapor pressures and greater solubility than larger crystals. Thus, the response to heating is grain growth because at higher temperatures bigger crystals are more stable. Also, when a $Fe(OH)_3$ gel is formed from aqueous oxidation at warm temperatures (i.e., closer to 100°C rather than room temperature), it is found that there tend to be more hematite nuclei present, which leads to large hematite platelets (several microns or tens of microns) in subsequent aging to coarse hematite crystals. This is borne out by several laboratory studies that show a temperatures >100°C is required, with the exact temperature depending on pH and pressure [12,13]. In the field, specularite occurs hydrothermally, around fumaroles, for example, the Valley of Ten Thousand Smokes in Alaska. Here fumaroles developed on hot ash-flow tuff that fell on top of the water and ice of preexisting rivers, lakes and glaciers. It has been suggested that specularite froms from $FeCl_3$ vapor upon contact with water vapor to form fumarolic specular hematite deposits. Ferric chloride has a high vapor pressure is readily transported in the vapor phase above 200°C where it can react with water vapor and form hematite:

$$2FeCl_3(g) + 3H_2O(g) = Fe_2O_3(s) + 6HCl(g)$$

Fig. 2 shows a summary of pathways to gray hematite.

Aram Chaos: geomorphology of thehematite

[1] report the presence of a gray hematite zone in the north-east quadrant of Aram Chaos. Aram Chaos (21°W, 2°N) is an isolated area of chaotic terrain contained completely within an eroded and largely infilled crater. It forms part of the larger occurrence of chaotic terrain to the east of Vallis Marineris between 10 to 50°W and 20°S to 10°N. Chaos regions on Mars are areas where jumbled arrays of blocks have apparently been produced by collapsed ground. Chaotic terrain (and several box canyons) serve as the source regions for large out-flow channels that generally flow northwards and converge in the northern lowlands, principally Chryse Planitia. We now examine the geology and topography of Aram Chaos in some detail.

We examined the topography of Aram Chaos from Mars Orbiter Laser Altimeter (MOLA) data. MOLA tracks across the hematite-rich region in Aram Chaos show that the crystalline hematite is typically confined between about -3000 m and -2500 m elevation relative to the Martian geoid defined by the MOLA team. The TES spectral signature is weak at elevations close to -3000 m. The maximum signal occurs around -2600 m, equivalent to topographic benches in the MOLA topography. We interpret the lesser concentrations of hematite found at elevations up to a few hundred meters below this level as most likely a lag deposit from physical weathering. The individual tracks show that hematite does not occur above about -2500 m elevation. Thus, where the topography rises above this evevation, a break occurs in the hematite signal.

Correlation of the TES gray hematite location in Aram Chaos with MOLA topographic mapping and imaging by MOC allows us to characterize the morphology and local stratigraphy of this material. Wide angle MOC images show that much of Aram Chaos' interior is surfaced by a prominent light-toned caprock.

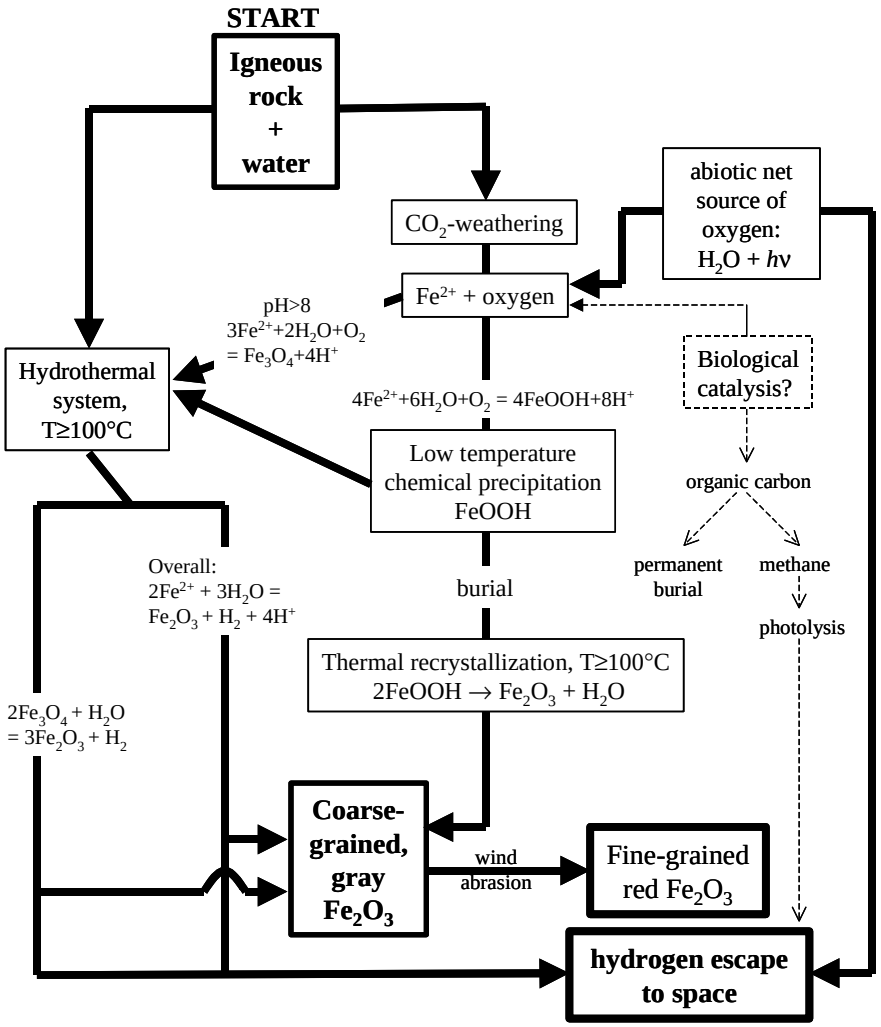

Fig. 2. Chemical pathways for the formation of gray crystalline hematite. Two main routes are shown: (1) low-temperature precipitation followed by hydrothermal processing (2) direct hydrothermal formation. Redox balance requires that the production of an oxidized species, hematite, be balanced by stoichiometric reductant, such as hydrogen. A dashed sub-pathway shows the likely effect of microbial biology, if it ever existed on early Mars.

Fig 3. shows that scarp-bounded outliers of the caprock (labeled 'C') occur to the east of a main outcrop (not shown, left of the image), which suggests that caprock was once more extensive. Bounding scarps of caprock material exhibit step benches in MOC NA images, which we interpret to be due to the differential erosion of horizontal discrete layers. Locally, the upper caprock surface immediately above the hematite deposit is relatively smooth at the scale resolvable in MOC NA images (Fig. 3). The main gray hematite-bearing material emerges from beneath the caprock. The hematite deposit itself also shows alternating benches and steps, inferred to be an erosional expression of layering. The hematite-bearing outcrops always appear to be heavily etched and pitted on decameter scales, with some fluting in MOC NA images. These outcrops generally do not extend beyond 10-15 km of the last occurrence of the caprock, from which we speculate that it is more susceptible to erosion than is the caprock. It is reasonable to infer that the hematite-bearing rock is much more extensive than its exposures, where protected by caprock. Laterally beyond and topographically below the bounding scarps of the hematite-bearing rock outcrop is a surface ubiquitously covered by duneforms (Fig. 3). There is a detectable weak presence of hematite in

this "duneform" material. If the duneform material is composed of relatively recently formed sand dunes whose sands were derived from the erosion of the hematite-bearing material, then the hematite-bearing deposit is probably not well consolidated and composed of individual sand-sized grains of predominantly basaltic composition. Presumably, the abrasion of sands in the dunes of the duneform material fairly quickly mutes or destroys the hematite signature. However, the evidence for the duneform deposit being stratigraphically superposed is not absolutely unequivocal. These "dunes," if in fact that is what they are, could be "fossils" exhumed from beneath the hematite material.

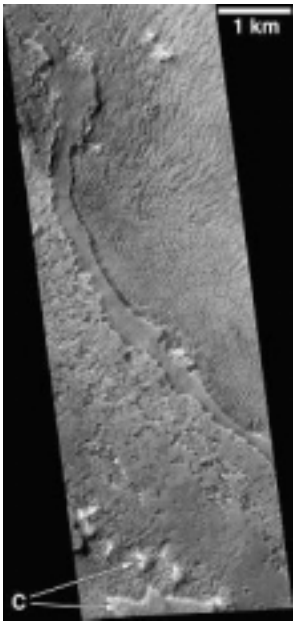

Fig. 3. Portion of MOC narrow angle image M19-01361, centered at ~3.5°N, 20.6°W.

Groundwater release and structural failure is a plausible explanation for how the apparently collapsed ground of Martian chaotic terrain formed [14]. Presumably, such release would be triggered by tectonic or geothermal activity. Thus the geology and topography of Aram Chaos is consistent with the formation of gray hematite due to the confinement and subsequent release of a hydrothermal aquifer. Possible terrestrial analogs are the Proterozoic brecciated zones in northern Yukon, Canada [15]. Here, breccia was generated by explosions of volatile-rich fluids within the crust, most probably caused by igneous intrusions at depth. Hydrothermal fluids shattered large volumes of rock. The Yukon breccia zones, collectively called Wernecke Breccia, cover an area 48,000 km^2 and are characterized by disseminated specular hematite [15]. Massive specularite zones are present in some Wernecke breccias. The gray hematite in Aram Chaos may have similarly had such a hydrothermal origin.

Conclusion: We conclude that the gray crystalline hematite in Aram Chaos most likely resulted from hydrothermal activity, given that:

(1) Thermal processing at temperatures > ~100°C is necessary to produce gray crystalline hematite based on thermodynamic calculations and bearing in mind the warm temperature constraint associated with all known occurrences of gray crystalline hematite on Earth.
(2) The chaotic terrain of Aram Chaos is thought to have formed by the geothermal melting of ground ice or the expulsion of groundwater, causing a loss of support and collapse of overlying material. Such a geological context would have been accompanied and probably preceded by hydrothermal activity.
(3) The topography of the gray hematite region in Aram Chaos indicates its occurrence in geologic strata within a specific topographic range. This is consistent with an ancient aquifer, which at one point, we postulate, was hydrothermally charged.

The observed caprock may be mechanically homogeneous and perhaps relatively impermeable, such that it confined an aquifer. Also, the erosional pitting and etching of the hematite-bearing outcrops could be the consequence of a form of cavernous weathering, in which fluids passing though such rock differentially cement (or uncement) the rock.

References: [1] Christensen, P et al.. (2001) *JGR, 106*, 23,873. [2]Lane, M. et al (2002) *JGR 107*, 9.1 [3] Catling, D.C. & Moore, J.M. *Icarus.*, submitted, 2002. [4] Herd, C. D. K., & Papike, J. J. (2000) *Meteorit. Planet. Sci. 35*, Supp., A70 [5] Wadhwa, M. (2001) *Science 291*, 1527. [6] Bookstrom A. A (1995) *Econ. Geol*. **90**, 469. [7] Sheets, S. A. et al. (1997) *GSA Ann. Meeting*, #50418 [8] Seeger, C. M. et al (1989) *"Olympic Dam-type" deposits and Geology of Middle Proterozoic Rocks in the St. Francois Mountains*, 55, Soc. Econ. Geol. [9] Minitti, M. E, et al., (2002) *LPS XXXIII*, #1674. [10] Diakonov, I. et al (1994) *Eur. J. Min. 6*, 967. [11] Becker, B. H. & Clayton R. N. (1976) *GCA 40*, 1153. [12] Schmalz, R. A. (1959) *JGR 64*, 575. [13] Vorobyeva, K. A., Y. P. Melnik (1977) *Geochem. Int. 8*, 108. [14] Sharp R. P. (1973) *JGR 78*, 4073 [15] Thorkelson, D. J. et al. (2001) *Precambrian Res. 111*, 31.

MARS MISSION OPTIMIZATION BASED ON COLLOCATION OF RESOURCES. G. E. Chamitoff[1], G. H. James[2], D. C. Barker[3], A. L. Dershowitz[4], [1]NASA Johnson Space Center (2101 NASA Rd 1, Houston, TX 77058, chamitoff@jsc.nasa.gov), [2]NASA Johnson Space Center, [3]MAXD, Inc. & United Space Alliance, [4]United Space Alliance.

Introduction: This paper presents a powerful approach for analyzing Martian data and for optimizing mission site selection based on resource collocation. This approach is implemented in a program called PROMT (Planetary Resource Optimization and Mapping Tool), which provides a wide range of analysis and display functions that can be applied to raw data or imagery. Thresholds, contours, custom algorithms, and graphical editing are some of the various methods that can be used to process data. Output maps can be created to identify surface regions on Mars that meet any specific criteria. The use of this tool for analyzing data, generating maps, and collocating features is demonstrated using data from the Mars Global Surveyor and the Odyssey spacecraft. The overall mission design objective is to maximize a combination of scientific return and self-sufficiency based on utilization of local materials. Landing site optimization involves maximizing accessibility to collocated science and resource features within a given mission radius. Mission types are categorized according to duration, energy resources, and *in-situ* resource utilization. Optimization results are shown for a number of mission scenarios.

The optimization of planetary landing sites for human exploration missions requires the integration of scientific objectives, mission requirements, in-depth understanding of local geography, and knowledge regarding the accessibility and availability of local resources. Judicious selection of landing sites for the first human missions to Mars is of preeminent importance due to the economic constraints surrounding any early missions. Collocation of indigenous resources that can be utilized on early missions will decrease initial launch mass and overall mission cost. A good example is the production of propellants (methane/oxygen) from the Martian atmosphere, which can be used as fuel for crew return vehicles, surface rovers, and auxiliary power sources. Every kilogram of material (chemical or mineral) that can be obtained from the Martian environment reduces the mass that must be delivered from Earth at substantial cost.

When the landing site for the first human mission to Mars is chosen, it will undoubtedly be based on the most recent remote sensing and surface data available. Organizing, processing, and combining all of this information in such a way that it can be used for mission design and optimization, however, is a major challenge. This problem has motivated the development of a data management and mission optimization tool, called the Planetary Resource Optimization and Mapping Tool (PROMT). This tool (shown in Figure 1) is designed to provide a common platform for managing data from all sources (including remote-sensed or theoretically derived), to process data or images using a variety of functions (built-in or user–developed), and to perform site selection optimization based on various parameters and optimization criteria. The final output from PROMT is typically a global map indicating the relative value of potential landing sites based on the union of all input data, maps, parameters and constraints.

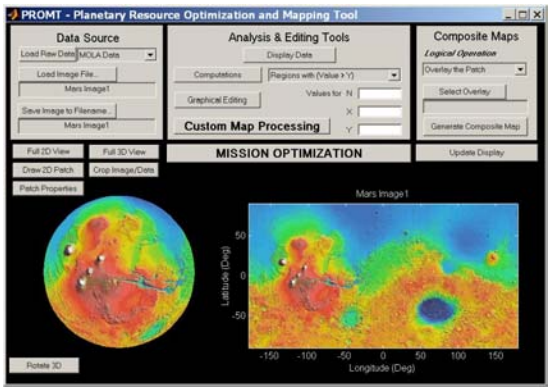

Figure 1: PROMT Main Display

Approach: The meaning of "optimality" for a human Mars mission, depends on many factors which characterize the nature of the mission. In this paper, missions to Mars are described using a three-axis matrix. Each mission scenario can be categorized according to the duration of the surface mission, the power available, and the amount of *in-situ* resource utilization that will be performed. These mission qualities affect a number of other parameters, which, in effect, determine the relative importance of different data in determining the optimal landing site. PROMT enables the user to perform site selection optimization for a wide range of mission scenarios. Some of the important Mars mission scenarios are listed in Table 1 and described further in the paper.

Category	Name	Description
000	Sprint	**Robotic, Opposition, Plant the Flag**
111	Robust NASA	High Energy, Limited Resource Utilization
112	ISRU	High Energy, Focus of Resource Utilization
113	Drilling	High Energy, Access the Subsurface
121	All-Solar	Low Energy, Limited Resource Utilization
222	Self-Sufficient	Live-off-the-Land for Power & Consumables
213	Infrastructure	Long Stay, High Energy, Serious Resource Development
223	Independence	Self Sufficient Mission with Subsurface Resources
323	Growth	Independent Mission and Committed to the Planet
333	Colony	Permanent Habitation with Sustainable Resources

Table 1: Mars Mission Scenarios

Although PROMT was initially designed to address human Mars missions, it uses a generalized approach that is equally applicable to robotic missions, or even missions to other planetary bodies for which data is available.

The overall optimization process is outlined in Figure 2. Typically, the inputs to the optimization are a composite map of local resources, a composite map of scientific sites of interest, a mission (or landing) constraint matrix, and additional parameters specific to the mission scenario (such as exploration radius). Various performance functions can be selected, and the optimization is executed. The final output is an intensity map showing the relative value of each mission site. The entire process can be customized to each mission scenario through custom map generating sequences, adjusting the relative weights for each resource or science map, and through the parameters that are used throughout the design. The challenge for the user is to understand the constraints and objectives of a particular mission, and to program the appropriate sequence, specialized functions, and parameters into PROMT.

A wide range of possible input map types are possible, including raw imagery, parametric data on a latitude/longitude grid, or highly processed data that highlights specific features of qualities of interest. For this study, a composite science map was created from the union of scientific points of interest, including regions depicting the Outflow Channels, the Valley Networks, distinct Hematite regions, and regions with "recent" channelized erosion from high resolution photography. This map is shown in Figure 3. Notice that the highest intensity regions are those encompassing the greatest number of adjacent or overlapping sites of interest.

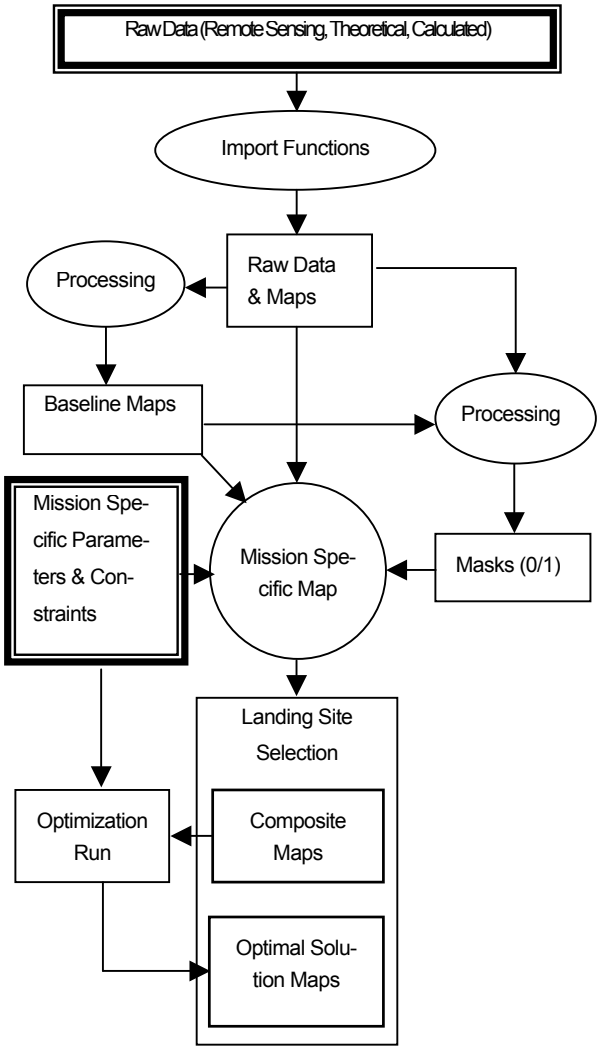

Figure 2: PROMT Optimization Flow Chart

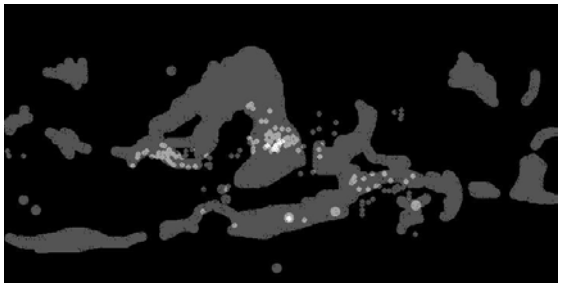

Figure 3: Science Composite Intensity Map

An example of a highly processed input map for the optimization is the Safe Landing Constraint Map as shown in Figure 4. This map is based on the con-

straint of landing on a low slope region (< 3 degrees in this case), away from the polar caps (+/- 75 degrees latitude), and accounting for a landing error uncertainty (assumed to be 100 km). The admissible landing locations, shown in white, are computed by applying the above constraints to slope data derived from planet-wide altimetry data.

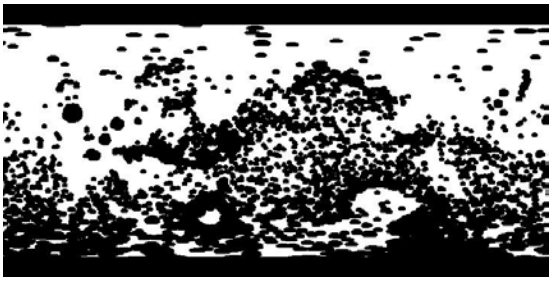

Figure 4: Safe Landing Constraint Map

Typical resource maps are show in Figures 5 and 6. The Composite Water Intensity Map indicates the collocation of indicators for the presence of accessible water on or near the surface (based on latitude and neutron emission data from the Odyssey spacecraft). The High Atmospheric Density Map indicates the potential for atmospheric mining of Oxygen, Carbon, and Argon in order to produce breathable air, and to provide oxidizer and fuel for launch vehicles, rovers, and power generators. Atmospheric processing in these regions would require the least amount of energy to extract a usable supply of these resources.

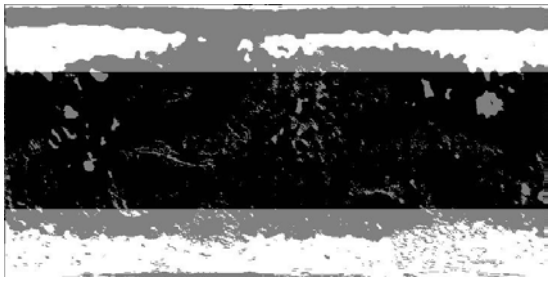

Figure 5: Composite Water Intensity Map

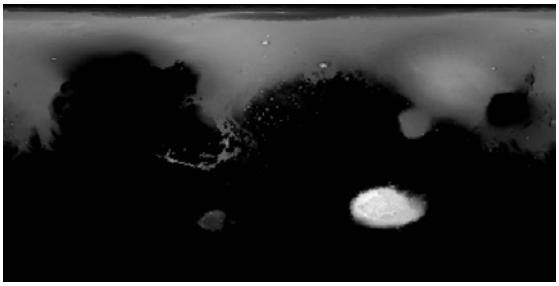

Figure 6: High Atmospheric Density

Similar constraint or intensity maps can be generated for all types of resources, including solar or surface-based energy, consumables, building material, minerals, launch-site compatibility, radiation protection, etc.

Results: Mission optimization includes an appropriate set of resources and constraints consistent with a given mission scenario (from Table 1). This is combined with scientific or mission objectives to generate a final "mission performance" map. The final step in the optimization process is to examine every admissible site on the planet surface, and determine its relative merit on the basis of mission performance (science return and resource utilization). Associated with each mission scenario is an assumed exploration radius. The optimization integrates the performance map within this given radius of every potential landing site. An example of the resulting map is shown in Figure 7.

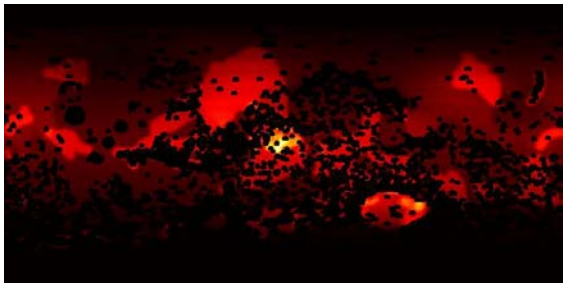

Figure 7: Landing Site Optimization for the NASA Robust Mission Scenario

The brightest points on this map correspond to the best landing sites for the parameters and input maps associated with one specific mission scenario. Similar results can be obtained for a wide range of mission scenarios, while taking into account the constraints, science objectives, and resource requirements specific to that mission. As new planetary data is obtained, and as mission parameters become better defined, this information can be readily incorporated into a new mission optimization using PROMT.

THE MARS EXPRESS MISSION AND ITS BEAGLE-2 LANDER

A.F. Chicarro and the Science Team, European Space Agency, Space Science Department, ESTEC/Code SCI-SB, Postbus 299, 2200 AG Noordwijk, The Netherlands (email: agustin.chicarro@esa.int).

The European Space Agency and the scientific community have performed concept and feasibility studies for more than ten years on potential future European missions to the red planet (*Marsnet, Intermarsnet)*, focusing on a network of surface stations complemented by an orbiter, a concept which is being implemented by the CNES-led *Netlander* mission to be launched in 2005. Before that, however, the ESA *Mars Express* mission includes an orbiter spacecraft and a small lander module named Beagle-2 in remembrance of Darwin's ship Beagle. The mission, to be launched in 2003 by a Russian Soyuz rocket, will recover some of the lost scientific objectives of both the Russian *Mars-96* mission and the ESA *Intermarsnet* study, following the recommendations of the International Mars Exploration Working Group (IMEWG) after the failure of *Mars-96*, and also the endorsement of ESA's Advisory Bodies that *Mars Express* be included in the Science Programme of the Agency.

The specific scientific objectives of the *Mars Express* orbiter are: global high-resolution imaging with 10 m resolution and imaging of selected areas at 2 m/pixel, global IR mineralogical mapping, global atmospheric circulation study and mapping of the atmospheric composition, sounding of the subsurface structure down to the permafrost, study of the interaction of the atmosphere with the surface and with the interplanetary medium as well as radio science. The goals of the Beagle-2 lander are: geology, geochemistry, meteorology and exobiology of the landing site.

The scientific payload on the *Mars Express* orbiter includes a Super/High-Resolution Stereo Colour Imager (HRSC), an IR Mineralogical Mapping Spectrometer (OMEGA), a Planetary Fourier Spectrometer (PFS), a Subsurface-Sounding Radar Altimeter (MARSIS), an Energetic Neutral Atoms Analyser (ASPERA), an UV and IR Atmospheric Spectrometer (SPICAM) and a Radio Science Experiment (MaRS). The Beagle-2 lander includes a suite of imaging instruments, organic and inorganic chemical analysis, robotic sampling devices and meteorological sensors (see **Table**).

The Mars Express mission will address the issue of astrobiology on Mars both directly and indirectly. The majority of instruments on the orbiter will look for indications of favourable conditions to the existence of life, either at present or during the planet's past, and in particular for traces of liquid, solid or gaseous water. Therefore, the HRSC camera will take pictures of ancient riverbeds, the OMEGA spectrometer will look for minerals with OH^- radicals formed in the presence of water, the MARSIS radar will look for subsurface ice and liquid water, the PFS and SPICAM spectrometers will analyse water vapour in the atmosphere, and finally ASPERA and MaRS will study neutral atom escape from the atmosphere, in particular O_2 coming from water and carbonates. The instruments on Beagle-2 will also look for the presence of water in the soil, rocks and the atmosphere, but will also try to find traces of life with direct measurements, such as presence of methane (CH_4) indicative of extanct life and a larger amount of the light C^{12} isotope compared to the heavier C^{13}, which would even indicate the existence of extinct life. Since NASA's Viking mission in 1976, it is the first time that the exhaustive search for life is so central to a space mission to Mars.

Current design estimates allow for an orbiter scientific payload of about 110 kg and 65 kg total lander mass (at launch) compatible with the approved mission scenario. The Beagle-2 lander was selected due to its innovative scientific goals and challenging payload. Beagle-2 will deploy a sophisticated robotic-sampling arm, which could manipulate different types of tools and retrieve samples to be analyzed by the geochemical instruments mounted on the lander platform. One of the tools to be deployed by the arm is a 'mole' capable of subsurface sampling to reach soil unaffected by solar-UV radiation, another is a corer/grinder to reach the rock under the weathering varnish.

A Soyuz-Fregat launcher will inject a total of about 1200 kg into Mars transfer orbit in early June 2003, which is the most favorable launch opportunity to Mars in terms of mass in the foreseeable future. The Mars Express orbiter is 3-axis stabilized and will be placed in an elliptical martian orbit (250 × 10142 km) of 86.35 degrees inclination and 6.75 hours period, which has been optimized for communications with Beagle-2, the *Netlanders*, as well as NASA landers or rovers to be launched both in 2003 and 2005. The Beagle-2 lander module will be independently targeted from separate arriving hyperbolic trajectory, enter and descend through the martian atmosphere in about 5 min, and land with an impact velocity <40 m/sec and an error landing ellipse of 100 × 20 km. A preliminary Beagle-2 landing site has been selected in the Isidis Planitia area (10.6° N, 270° W). The nominal mission lifetime of one martian year (687 days) for the orbiter investigations will be extended by another martian year for lander relay communications and to complete global coverage. The Beagle-2 lander lifetime will be of a few months.

ESA provides the launcher, the orbiter and the operations, while the Beagle-2 lander is delivered by an UK-led consortium of space organizations. The orbiter instruments are provided by scientific institutions through their own funding. In addition to relaying the data from the Beagle-2 lander to Earth, Mars Express will also service landers and rovers from other agencies during its nominal/extended lifetime. The ground segment includes the ESA station at Perth, Australia, and the mission operations centre at ESOC. The *Mars Express* mission is now in Phase-C/D, with Astrium (formerly Matra Marconi Space) in Toulouse, France, as its Prime Contractor and involving a large number of European companies.

International collaboration, either through the participation in instrument hardware or through scientific data analysis is very much valued to diversify the scope and enhance the scientific return of the mission, such as NASA's major contribution to the subsurface-sounding radar, and the use of its DSN for increased science data downloading and critical manoeuvres. Also, arriving at Mars at the very end of 2003, *Mars Express* will be followed by the Japanese *Nozomi* spacecraft a few days later. Both missions are highly complementary in terms of orbits and scientific investigations; *Nozomi* focusing on the study of the upper atmosphere of Mars as well as the interaction of the solar wind with the ionosphere from a highly elliptic equatorial orbit. Close cooperation, including scientific data exchange and analysis, is foreseen by the *Nozomi* and *Mars Express* teams within a joint ESA-ISAS programme of Mars exploration.

For more details on the *Mars Express* mission and its Beagle –2 lander:

http://sci.esa.int/marsexpress/ and **http://www.beagle2.com/**

Table: MARS EXPRESS SCIENTIFIC PAYLOAD			
Acronyms	**Instruments**	**Principal Investigators**	**Countries**
Orbiter			
HRSC	Super/High-Resolution Stereo Colour Imager	G. Neukum	D, F, RU, US, FI, I, UK
OMEGA	IR Mineralogical Mapping Spectrometer	J.P. Bibring	F, I, RU
PFS	Atmospheric Fourier Spectrometer	V. Formisano	I, RU, PL, D, F, E, US
MARSIS	Subsurface-Sounding Radar/Altimeter	G. Picardi & J. Plaut	I, US, D, CH, UK,DK
ASPERA	Energetic Neutral Atoms Analyzer	R. Lundin & S. Barabash	S, D, UK, F, FI, I, US, RU
SPICAM	UV and IR Atmospheric Spectrometer	J.L. Bertaux	F, B, RU, US
MaRS	Radio Science Experiment	M. Paetzold	D, F, US, A
Lander			
BEAGLE-2	Suite of imaging instruments, organic and inorganic chemical analysis, robotic sampling devices and meteo sensors	C. Pillinger & M. Sims	UK, D, F, HK, CH

GLOBAL DISPERSION OF DUST FOLLOWING IMPACT CRATERING EVENTS ON MARS. J. Y-K. Cho[1] and S. T. Stewart[2], [1]Carnegie Institution of Washington (Department of Terrestrial Magnetism, 5241 Broad Branch Road, N.W., Washington, D.C. 20015-1305, USA, jcho@dtm.ciw.edu), [2]Carnegie Institution of Washington (Geophysical Laboratory, 5251 Broad Branch Road, N.W., Washington, D.C. 20015-1305, USA, sstewart@gl.ciw.edu).

Introduction: Hypervelocity impacts on Mars inject dust and vapors into the upper atmosphere. If the particles (derived from the projectile or surface) are widely distributed, impact events could drive intense weather patterns and perhaps transient climate change on Mars [1]. Recent work on small impact events (< 100 m-sized projectiles) find that the mass of dust stirred into the troposphere may be equivalent to global dust storms [2]. For ~10 to ~100 km-sized impactors, dust and greenhouse vapors may be delivered to the upper troposphere and lower stratosphere, where the long residence time has the potential for regional or even global effects on the weather.

In this work, we investigate the mechanisms that control the dispersion of dust injected into the upper troposphere from large impact events, using a high-resolution global atmospheric dynamics model. The spreading rates, dispersal extent, and the potential for weather and climatological perturbations from both medium-sized (~10 km) impactors and giant (~100 km) impactors are studied. The overarching goals in this study are to identify locations of persistent concentrations of aerosols and to estimate the smallest impact which may generate transient rainfall on Mars.

Approach: We start the atmospheric simulations several minutes after the impact, when the ejecta plume is a few times larger than the final crater diameter (Fig. 1). The shock from the impact propagates radially outward from the impact site through an atmosphere initialized with balanced zonal winds, which are representative of the seasons — e.g., northern winter (L_s = 270 to 300) at ~50 km altitude (Fig. 2) [3]. The Mars Orbiter Laser Altimeter (MOLA) topography is included in the simulations. The combination of shock, nonlinearly evolving wind, and topography redistributes the initial ejecta plume. Here, we restrict out attention to the dispersal pattern of fine (micron-sized) particles and neglect radiative heating/cooling effects and chemistry in the days immediately following the impact event.

Model Description: At high altitudes on Mars, motions are predominantly horizontal, due to the strong vertical stability. Hence, features whose lateral extent is large compared to the scale height of the atmosphere (~10 km) may be modeled with the shallow-water equations (SWE) [4]. SWE are vertically integrated version of the set of primitive equations of meteorology, used in general circulation models (GCMs). SWE constitute the simplest atmospheric dynamics model which allows the effects of stratification, horizontal compressibility, topography, and differential rotation to be included and studied at high spatial resolution over long simulation times. It has been successfully used in many stratospheric modeling studies for the Earth (e.g., [5]), as well as for the upper troposphere of the giant planets in our solar system [6].

To solve the SWE, a highly-accurate pseudospectral algorithm with hyperdiffusion is used, with up to 1024×512 grid resolution to resolve small-scale features. A large number of simulations (~100) are performed to fully explore the available parameter space and to identify the robust features.

Results: Our simulations show the following generic features:

1. Both the impact shock and variable topography produce complex dispersal patterns.
2. Dispersal patterns from northern impacts are simpler compared to the southern impact, due to the topographic dichotomy on Mars, as emphasized in a recent GCM study of the tropospheric circulation [7].
3. The particles from ~100 km and smaller size impact craters are dispersed along a narrow range in latitude.
4. The particles from 100's km impact craters are dispersed hemispherically within several days. We find that the efficiency of dispersion across the latitudes increases with increasing topographic variability (Fig. 3).
5. On short timescales (smaller than radiative timescales), the equivalent of a basin-forming impact is necessary for global dispersion of the ejected particles (Fig. 4).

Discussion: From our simulations, we find that modeling of the climatological response from basin-forming impact events may assume nearly spatially homogeneous aerosol distribution. Understanding the atmospheric response to the more frequent smaller cratering events requires explicit treatment of the spatial inhomogeneities caused by atmospheric motion. Hence, 2-D or 3-D models are needed.

We seek to identify the *smallest* impact which may generate transient rainfall on Mars. Concentrations in the flow patterns in the southern hemisphere — e.g., arrow in Fig. 3C — are particularly intriguing, as pos-

sible locations for storm fronts after large impact events.

Future Work: We will include the following enhancements or extensions in our post-impact study:

- More realistic winds from GCM calculations
- Martian paleotopography
- Thermal feedback, for longer simulation times
- Closer look at shock wave and topographic perturbations on the flow stability
- Comparison (of low resolution SWE model) with GCM calculations
- More details pertaining to the impact event (secondary craters, water vapor, etc.)

References: [1] Segura, T. L. et al. (2002) *Science* 298, 1977. [2] Nemtchinov, I. V. et al. (2002) *JGR* 107(E12), 5134. [3] Forget, F. et al. (1999) *JGR* 104(E10), 24155. [4] Gill, A. E. (1982) *Atmosphere-Ocean Dynamics*, Academic Press: San Diego, p. 95-246. [5] Juckes, M. N. and McIntyre, M. E. (1987) *Nature* 328(6131), 590. [6] Cho, J. Y-K. and Polvani, L. M. (1996) *Science* 273, 335. [7] Richardson, M. I. and Wilson, R. J. (2002) *Nature* 416, 298.

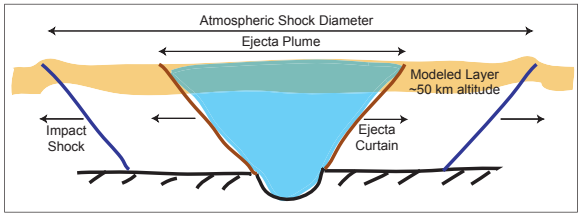

Figure 1. Schematic of initial conditions. The atmospheric dynamics model is initialized with the atmospheric shock and ejecta plume several minutes after the time of impact.

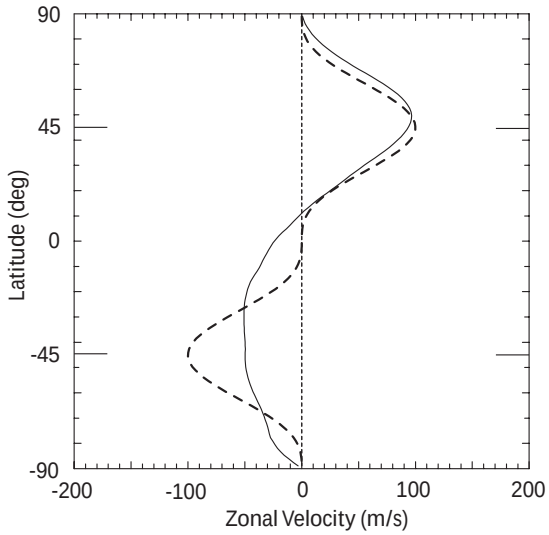

Figure 2. Example zonal wind profiles. The atmospheric dynamics model is initialized with balanced zonal winds (dashed line) which nonlinearly evolve into stable zonal winds (solid line) due to forcing.

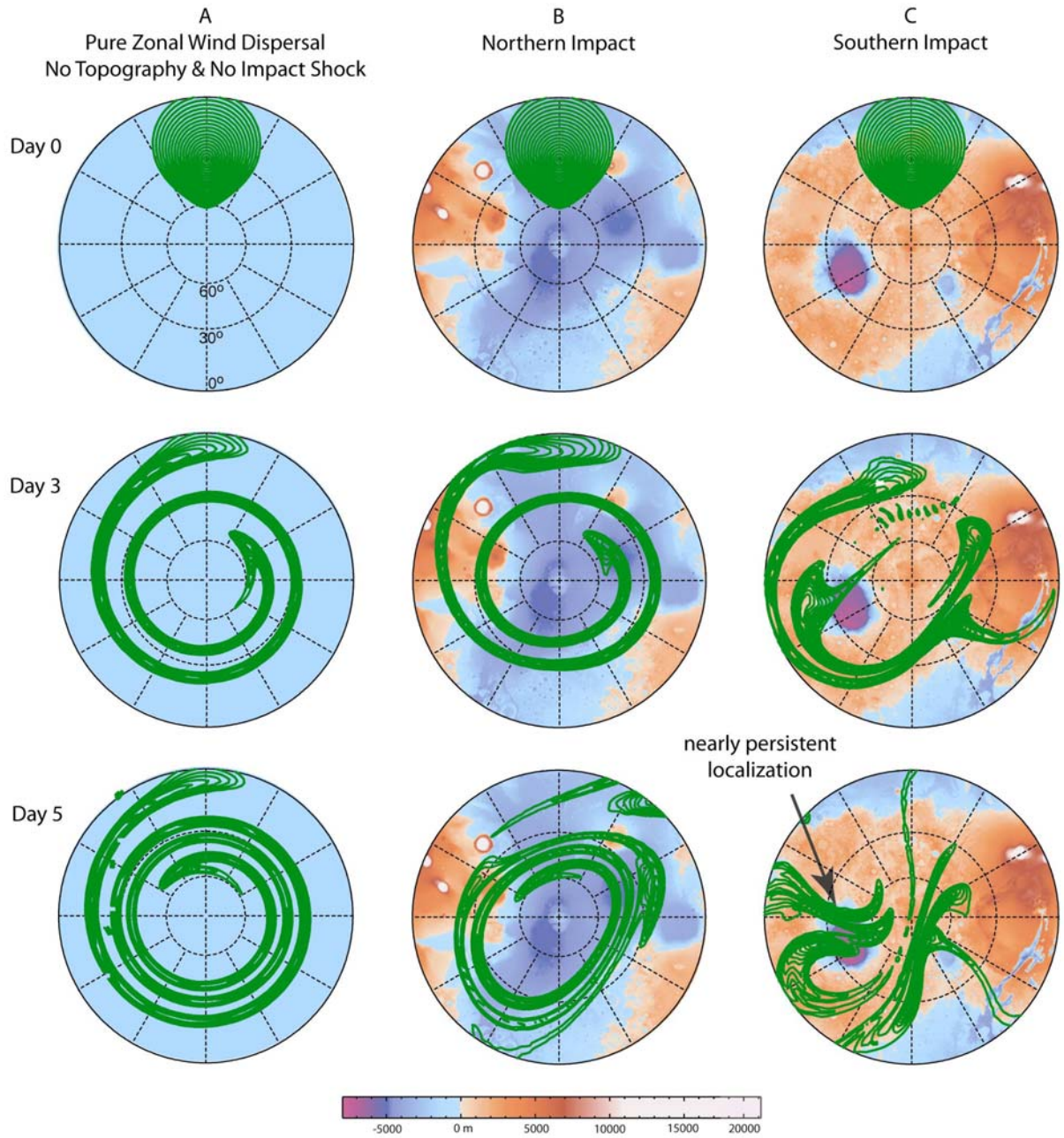

Figure 3. Topography Effects. Polar stereographic projections showing MOLA topography under tracer distribution (green contours) for an impact event creating a crater several 100 km in diameter. The initial plume radius is 2000 km and initial shock radius is 4800 km. Without topography, the dust plume is sheared into zonal spirals (A). The larger topography variations in the south (C) compared to the north (B) increases the complexity in the dispersal pattern and latitudinal range.

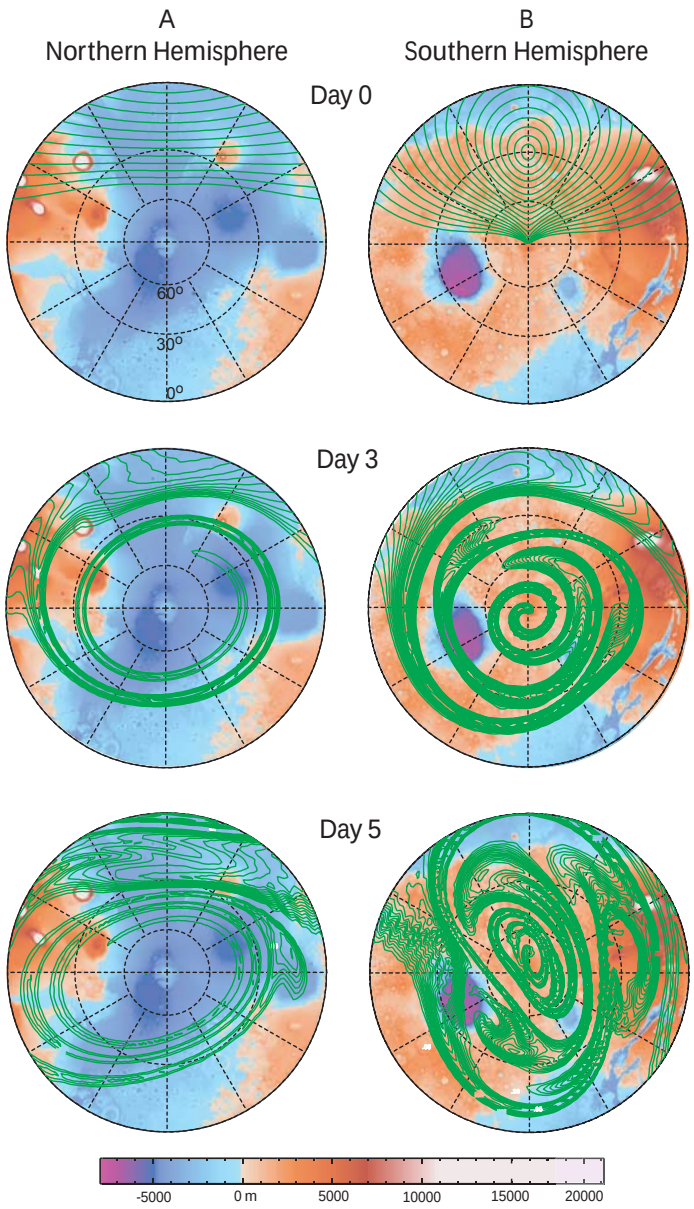

Figure 4. Basin-forming impact in southern hemisphere. The initial plume radius is 5000 km and initial shock radius is 12000 km. Particles are dispersed over both hemispheres within a few days.

WATER ON MARS: EVIDENCE FROM MINERALS AND MORPHOLOGY. P. R. Christensen[1] [1]Arizona State University, Department of Geological Sciences, Tempe, AZ 85287-6305; phil.christensen@asu.edu.

Introduction: A wealth of recent remote measurements of the mineralogy, elemental abundance, and morphology of the martian surface have greatly improved our view of the history of water on Mars. Mineralogic data from orbital spectroscopy reveal a volcanic planet that lacks extensive aqueous weathering or carbonate formation, but which has undergone significant localized aqueous mineralization. Mid- to high-latitude hydrogen abundances and unusual morphologies suggest extensive deposits of water ice with localized, recent melting to form gullies. The upper surface of Mars appears to have an extensive water inventory, but this water may have existed in a frozen state throughout much of martian history.

A Dry Mars: Global mineral mapping using Mars Global Surveyor Thermal Emission Spectrometer (TES) data has shown that Mars is dominated by volcanic minerals and volcanic rocks [1-3]. Rocks classified as basaltic on the basis of their mineralogy and inferred chemistry are found in the ancient cratered terrains of Mars and appear to be representative of the early martian crust. Detailed mapping using TES data has revealed the presence of olivine in abundances of 10-15% in basalts in isolated regions [4-6]. These rocks have been exposed to martian environmental conditions over long periods of time, yet show no unequivocal evidence for aqueous weathering products [1, 7].

Mars Odyssey Thermal Emission Imaging System (THEMIS) multi-spectral infrared data have revealed the presence of a layer of olivine-rich basalt exposed in the walls near the floor of Ganges Chasma [8]. This layer is 50-100 m thick, occurs beneath 4.5 km of overlying rocks, and extends over an area at least 30 by 100 km in size. The composition of the Ganges floor material determined from individual TES spectra is basaltic; the wall unit is similar but contains ~10-15% olivine with an Mg/(Mg+Fe) ratio of 68 (Fo68) [8]. The olivine-rich layer could have been; (1) emplaced as an olivine-enriched lava flow, followed by deposition of 4.5 km of overlying units; (2) injected as sill; (3) formed as a cumulate layer in layered intrusive body; or (4) deposited as a sedimentary layer in which olivine was enriched during transport or deposition. In any case, this ancient layer was once buried to a depth of at least 4.5 km and subsequently exposed at the surface. The preservation of olivine, which is unstable in aqueous conditions, indicates that (1) significant weathering did not occur deep beneath the surface in this particular region, and (2) significant surface weathering has not occurred since this layer was exposed.

Carbonates in the regolith have long been proposed to play an important role in the CO_2 exchange cycle, acting as a reservoir for sequestering large amounts of CO_2 from the ancient martian atmosphere [e.g. 9, 10-12]. Thus, the presence, or absence, of carbonates has important implications for the evolution of the martian atmosphere, placing constraints on the abundances, reaction chemistry, and history of H_2O and CO_2. To date, neither TES nor THEMIS data have revealed any evidence for carbonate rock units on Mars, and it is possible to conclude that large-scale (>10's km sized) carbonate deposits are not currently exposed at the surface of Mars [1]. It remains possible that carbonate deposits are buried by younger deposits or UV dissociated to calcium oxide [13]. However, the detection of unusual, and presumably rare, mineralized hematite units shows that either carbonates are less common than mineralized hematite, or the processes by which they remain "hidden" are more efficient.

Recent analysis of the spectra of Mars bright regions in which the atmospheric contributions have been rigorously removed [14] have detected the occurrence of minor (<5%) abundances of carbonates in the fine-grained dust of Mars [15, 16]. The low carbonate abundance and its occurrence on dust-covered surfaces with high surface-area-to-volume ratios are consistent with carbonate formation by interaction between the current Mars atmospheric CO_2 and water vapor and surface mineral grains as proposed by Booth and Kieffer [9, 15]. While it is possible that these carbonates formed by erosion and dissemination of extensive carbonate rock units, a more likely scenario is their formation *in situ* in the current atmosphere [15, 16]. Thus, the detection of carbonates, rather than suggesting an ancient period of a warm, wet Mars, instead argues for minor carbonate formation in a cold, dry Mars. Furthermore, the detection of carbonates by TES argues against UV dissociation or difficulties in detecting carbonates from thermal IR spectra as the explanation for the lack of detection of widespread carbonate units. It appears that carbonate rock layers may never have formed, and Mars may never have experienced a period of extensive interaction between large amounts of liquid water and a thick CO_2 atmosphere.

A Wet Mars: While much of the mineral evidence from TES, THEMIS, and other spectroscopic observations argues against extensive, global aqueous miner-

alization, there are examples of localized deposits that are suggested to have formed through aqueous processes. The TES data have revealed unique deposits of crystalline gray hematite exposed at the martian surface in Sinus Meridiani, Aram Chaos, and in scattered locations throughout Valles Marineris. The Sinus Meridiani material is an in-place, rock-stratigraphic sedimentary unit characterized by smooth, friable layers composed primarily of basaltic sediments with ~10-15% crystalline gray hematite. This unit has outliers to the north that appear to have formed by stripping and removal. The hematite within Aram Chaos occurs in a sedimentary layer within a closed basin that was likely post-dates the formation of associated chaos and outflow terrains. This unit appears to be exposed by erosion and may be more extensive beneath the surface. The Valles Marineris occurrences are closely associated with the interior layered deposits, and may be in place within the layers or eroded sediments. Overall, crystalline gray hematite is extremely uncommon at the surface, yet in all observed locations it is closely associated with layered, sedimentary units.

Formation modes for gray hematite detected by TES have been grouped into two classes: (1) chemical precipitation and (2) thermal oxidation of magnetite-rich lavas [17, 18]. Chemical precipitation models include (1a) low-temperature precipitation of Fe oxides/ oxyhydroxides from standing, oxygenated, Fe-rich water, followed by subsequent alteration to gray hematite, (1b) low-temperature leaching of iron-bearing silicates and other materials to leave a Fe-rich residue (laterite-style weathering) which is subsequently altered to gray hematite, (1c) direct precipitation of gray hematite from Fe-rich circulating fluids of hydrothermal or other origin, and (1d) formation of gray hematitic surface coatings during weathering [17, 18]. Models (1a) and (1b) require an oxidative alteration process (e.g., burial metamorphism) to convert Fe-oxide/oxide assemblages (e.g., red hematite, goethite, ferrihydrite, goethite, and siderite) to coarse-grained (>10 μm), gray hematite.

Although none of these models can currently be excluded, the geologic setting of the martian hematite deposits suggest they formed by chemical precipitation from aqueous fluids, under either ambient or hydrothermal conditions [18, 19]. All three hematite sites are sedimentary environments, and the hematite-bearing units in Aram and Valles Marineris occur in closed sedimentary basins consistent with deposition in water. Sub-surface water was clearly present in Aram Chaos as evidenced by collapse and outflow features, and the hematite-bearing unit in Ophir/Candor is associated with layered, friable deposits that may be of aqueous origin [20-22]. The primary argument against thermal oxidation of magnetite-rich lavas (model 2) is the absence of distinct morphological evidence for lava flows or constructs, and the presence of evidence for material more friable than primary lava in the Sinus Meridiani hematitic unit [18, 23].

Thus, the TES mineralogic data provide evidence that liquid water was stable near the surface, probably for extensive periods of time, in specific locations on early Mars.

An Icy Mars: Mars Odyssey Gamma Ray and Neutron Spectrometer observations have shown that water ice is abundant at latitudes poleward of ~50° in both hemispheres [24-26]. It has also been suggested that extensive deposits of unusual materials that mantle the martian mid-latitudes are ice-rich deposits [27-29]. A model has been proposed in which the recent martian gullies that are found in the mid-latitudes are related to these mid-latitude, ice-rich mantles, and that the gullies were eroded recently through melting of these overlying deposits [30]. In this model: (1) Water is transported from the poles to mid-latitudes during periods of high obliquity, forming a water-rich snow layer [31-34]. (2) Melting occurs as mid-latitude temperatures increase, producing liquid water that is stable beneath an insulating layer of overlying snow; (3) Gullies form on snow-covered slopes through erosion by meltwater or as a result of meltwater seeping into the loose slope materials and destabilizing them; (4) Gullies incised into the substrate are observed where the snow layer has been completely removed; (5) Patches of snow remain today where they are protected against sublimation by a layer of desiccated dust/sediment [27]; and (6) Melting could be occurring at the present time in favorable locations in these snowpacks [30].

While melting snow provides an interesting possible explanation for the formation of recent gullies, the more important outcome of this model is the evidence that the gullies provide that the mid-latitude mantles are not simply volatile rich, but must be primarily water ice. Ice that enters the regolith and fills the pores through vapor exchange during periods when the mid-latitude temperatures are relatively low [27, 35], will most likely exit in the same manner when the climate warms. Therefore, it is unlikely that ice-rich soils will produce the melting necessary to erode gullies. On the other hand, snow deposits are capable of producing meltwater due to the solid-state greenhouse effect of ice that contains minor amounts (~1,000 parts per million, mass) of dust [36]. Thus, the formation of gullies by melting snow provides evidence that the mid-latitude deposits are dirty ice, rather than icy dirt.

This model suggests that at least some mid-latitude mantles were deposited directly on the surface with

(very) high ice-to-soil ratios. The high (>50% volume) water-ice abundances inferred in the upper few meters at high-latitudes from Odyssey Neutron and Gamma-Ray Spectrometer data [24-26], suggest that the ice in these regions was also deposited on the surface rather than in pores. A common surface texture found from 30-50° latitude in both hemispheres has been interpreted to be the result of devolatilization and erosion of ice-cemented soils that are up to several meters thick [27]. Mustard et al, [27] suggested that the ice was recently emplaced through vapor diffusion into the pore space [27, 37]. However, these eroded mantles transition poleward into continuous mantles, and the boundary of this transition corresponds to the sharp increase observed in near-surface ice abundance [38]. This correlation suggests that the equatorward portion of this mantle may be the same ice-rich material whose upper few meters have been thoroughly desiccated [30]. In this case the high-latitude ice-rich materials observed by the Odyssey Neutron/Gamma-Ray spectrometers, the poleward continuous mantles, the dissected mid-latitude mantles, and the gully-forming snow deposits may all have been formed by deposition of atmospheric condensates onto the surface, and may all have high (70-100%) water-ice abundances. If this model is correct, then these surface mantles would have substantially more water than previously suggested [27].

Summary: The available remote measurements of martian mineralogy and morphology suggest a complex and diverse set of states of martian water. Near-surface water ice appears to be more abundant than previously considered. Aqueous processes have occurred locally to produce hematite mineralization in isolated regions. However, the lack of extensive carbonates (and clays?) and the presence of ancient olivine suggests that liquid water has been rare at or near the surface over time. Together these observations suggest a relatively water-rich surface layer in which water is primarily in a frozen state expect for isolated, and very interesting, events.

References:

[1] Christensen, P.R., et al. (2001), *J. Geophys. Res., 106*. 23,823-23,871. [2] Bandfield, J.L., et al. (2000), *Science, 287*. 1626-1630. [3] Hamilton, V.E., et al. (2001), *J. Geophys. Res., 106*. 14,733-14,747. [4] Clark, R.N. and T. Hoefen (2000), *Bull. Am. Astron. Soc., 32(3)*. 1118. [5] Hoefen, T.M. and R.N. Clark (2001), *Lunar and Planetary Science Conference, XXXII*. abstract #2049 (CD-ROM). [6] Hamilton, V.E., et al. (submitted), *Meteoritics and Planetary Science*. [7] Bandfield, J.L. (2002), *J. Geophys. Res., 107*. 10.1029/2001JE001510. [8] Christensen, P.R., et al. (submitted), *Science*. [9] Booth, M.C. and H.H. Kieffer (1978), *J. Geophys. Res., 83*. 1809-1815. [10] Fanale, F.P. and B.M. Jakosky (1982), *Planet. Space Sci., 30*. 819-831. [11] Kahn, R. (1985), *Icarus, 62*. 175-190. [12] Fanale, F.P., et al., *Epochal climte change and volatile history*, in *Mars*, H.H. Kieffer, et al., Editors. 1992, University of Arizona Press: Tucson, AZ. [13] Mukhin, L.M., et al. (1996), *Nature, 379*. 141-143. [14] Bandfield, J.L. and M.D. Smith (2003), *Icarus, 161*. 47-65. [15] Bandfield, J.L., et al. (2003), *Lunar and Planet. Sci., XXXIV*. Abstract #1723 (CD-ROM). [16] Bandfield, J.L., et al. (submitted), *Science*. [17] Christensen, P.R., et al. (2000), *J. Geophys. Res., 105*. 9623-9642. [18] Christensen, P.R., et al. (2001), *J. Geophys. Res., 106*. 23,873-23,885. [19] Hynek, B.M., et al. (2002), *, J. Geophys. Res., 107*. 5088, doi:10.1029/2002E001891. [20] McCauley, J.F., *Geologic Map of the Coprates Quandrangle of Mars, scale 1:5,000,000.* 1978, U.S. Geol. Surv. Misc. Inv. Series Map I-897. [21] Lucchitta, B.K. (1982), *Reports of Planetary Geology Program, NASA TM-85127*. 233-234. [22] Nedell, S.S., et al. (1987), *Icarus, 70*. 409-441. [23] Arvidson, R.E., et al. (in press), *J. Geophys. Res.* [24] Boynton, W.V., et al. (2002), *Science, 297*. 81-85. [25] Feldman, W.C., et al. (2002), *Science, 297*. 75-78. [26] Mitrofanov, I., et al. (2002), *Science, 297*. 78-81. [27] Mustard, J.F., et al. (2001), *Nature, 412*. 411-414. [28] Malin, M.C. and K.S. Edgett (2001), *J. Geophys. Res., 106*. 23,429-23,570. [29] Carr, M.H. (2001), *J. Geophys. Res., 106*. 23,571-23,595. [30] Christensen, P.R. (2003), *Nature, 422*. 45-48; doi:10.1038/nature01436. [31] Toon, O.B., et al. (1980), *Icarus, 44*. 552-607. [32] Jakosky, B.M. and M.A. Carr (1985), *Nature, 315*. 559-561. [33] Jakosky, B.M., et al. (1995), *J. Geophys. Res., 100*. 1579-1584. [34] Haberle, R.M., et al. (2001), *J. Geophys. Res., 106*. 23,317-23,326. [35] Costard, F., et al. (2002), *Science, 295*. 110-113. [36] Clow, G.D. (1987), *Icarus, 72*. 95-127. [37] Mellon, M.T. and B.M. Jakosky (1995), *J. Geophys. Res., 100*. 11,781-11,799. [38] Tokar, R.L., et al. (2002), *J. Geophys. Res., 29*. 1904, doi:1029/2002GL015691.

VERTICAL DISTRIBUTIONS OF DUST OPTICAL DEPTH DURING THE 2001 PLANET ENCIRCLING STORM FROM A SPHERICAL RADIATIVE TRANSFER ANALYSIS OF MOC LIMB IMAGES. R. T. Clancy[1], M. J. Wolff[1], B. A. Whitney[1], and B. A. Cantor[2], [1]Space Science Institute (P.O. Box 3075, Bald Head Island, NC 28461, clancyr@colorado.edu) for first author, [2]Malin Space Science Systems.

Introduction: The Mariner 9 IRIS thermal profile analysis of Conrath [1] and Viking limb analysis of Jaquin et al. [2] form the basis for our current understanding of dust vertical profiles during major (planet-encircling) Mars dust storms. The June-Sept 2001 major dust storm provides the opportunity for a much more comprehensive study, based upon MGS MOC (Mars Orbital Camera [3]) limb imaging and TES (Thermal Emission Spectrometer [4]) limb scan observations of dust vertical profiles in a globally extended dust storm. The current analysis pertains to MOC blue wide angle (WA) images returned in late July during the peak phase of the 2001 dust storm (L_s=200-205°), and in September during the early clearing phase of the storm (L_s=236°). A broader study under development will incorporate coarser vertical resolution TES limb observations (15 km versus the 2 km MOC resolution) with thermal IR (7-45 μm) and solar band (λ_{eff} = 0.7 μm) spectral coverage. This will eventually allow us to derive specific information on the vertical distribution of aerosol particle sizes. Here, we limit analysis to the retrieval of dust optical depth versus altitude for the purpose of defining the vertical extension of dust lifting during a planet-encircling dust storm.

MOC Limb Images: We have analysed a subset of MOC WA blue (400-450 nm) images that obtained atmospheric limb coverage with optimum vertical (i.e., unbinned, ~1.3 km/pixel) resolution during the July-Sept period of the 2001 Mars dust storm. The calibration and flat fielding for the MOC blue WA remain preliminary, especially at the margins of the CCD where the atmospheric limb is imaged in these data. Consequently, we compare radiative transfer (RT) models and MOC limb brightnesses in a relative sense. In this presentation we emphasize an unusually extended MOC limb image, characterized by continuous coverage from 48S to 45N latitudes, centered on 240W longitude, for L_s=205°. Additional, much less extended (in latitude) MOC limb images are modeled for L_s of 199°, 202°, and 236°.

Monte Carlo RT Model: We employ the full spherical, multiple scattering Monte Carlo RT code developed by Barbara Whitney for astrophysical studies, which she has recently reconfigured for Mars RT applications [5]. This model currently provides both emission and scattering source functions which may be specified with full three dimensional distributions, although we employ purely scattering calculations with one dimensional dust distributions in the vertical for this study. Dust scattering properties (single scattering phase function and albedo) are represented by simple Henyey Greenstein expressions as well as full T-matrix ellipsoidal expansions, based upon analysis of multi-color HST images observed during 2001 dust storm [6].

Model-Data Comparisons: Figure 1 presents a typical limb brightness profile from the L_s=205° MOC image (asterisk sysmbols), at a latitude of 35S as indicated on the figure. Two model profiles are presented as solid and dashed lines, corresponding to a constant dust mixing ratio and a dust mixing ratio which

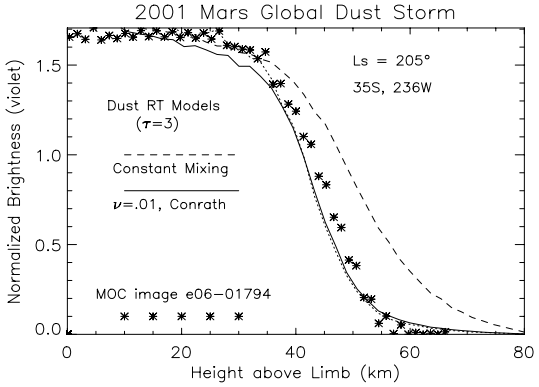

decreaes above 30 km according to the Conrath parameterization with ν=0.01, respectively. A dust vertical distribution in which particle settling velocities become significant relative to vertical lifting and mixing for altitudes above 30 km is implied by the observed MOC limb brightness. In general, this behavior typifies the vertical distribution of dust among the range of MOC limb profiles so far analyzed. However, the latitude range 5N to 20S for this particular image displays distinctly shallower dust vertical mixing. Furthermore, there are significant variations within the 30-50 km region and distinct "plateaus" of limb brightness at altitudes of 50-70 km which appear common during this dust storm. We will present these range of dust mixing profiles for a broader crossection of MOC imaging data, as well as preliminary TES solar band and thermal IR limb profiles.

References: [1] Conrath B. J. (1975) *Icarus*, 24, 36-46. [2] Jaquin F., P. Gierasch, and R. Kahn (1986) *Icarus, 68,* 442–461. [3] Malin M. C. et al. (1998) *Science, 279,* 1681-1685. [4] Christensen P. R. (1998)

Science, 279 1692–1697. [5] Whitney I. J., M. J. Wolff, and R. T. Clancy (1999), The Fifth International Conference on Mars, Abstract #6213. [6] Wolff M. J. , J. F. Bell, and J. Sohl-Dickstein, 2002, AGU Fall Meeting, Abstract #P72A-0494.

ACID SNOWBANK AS SOURCE, SINK AND ABODE. Benton C. Clark, Lockheed Martin, Space Exploration Systems, POB 179, Denver, CO 80201. benton.c.clark@LMCO.com

Introduction: Persistent deposits of water ice may exist at the surface, even in certain non-polar regions on Mars. Their origins can include: atmospheric precipitation (snow); surface adsorption; clathrate formation; upward percolation of H2O vapor or wicking of liquid created by subsurface heat sources; or deflation of overburden to expose buried ice or ice-rich permafrost (for purposes of expediency, such surface-exposed deposits will be referred to in this paper as "snowbanks", regardless of the source or mechanism of transport of H2O to the surface). Many of the characteristics discussed here are relevant to any exposed body of ice. Such deposits may have unique roles as a source of H2O, a sink of chemically active gases injected into the atmosphere, and through various favorable factors, providing a haven for growth and reproduction of biological organisms on Mars which would, on Earth, be considered extremeophiles.

Snowbank Interactions with the Atmosphere: Long-term survivabity of ice against sublimation is abetted by location on anti-solar slopes and/or covering by high albedo, low thermal inertia material. Location in a natural shaded cavity is a mechanism often observed in rugged mountainous terrain on Earth for the preservation of snow deposits well into summertime. Deposits can even summer-over, depending on shadowing, local weather, and climatological conditions. Winds and dust loads in the atmosphere provide varying inputs of new material, warm or moist atmosphere, shielding of solar insolation, and erosive forces.

The high degree of eolian activity on Mars maintains a source of atmospheric dust fallout, which coats the surface ice and may, especially if saltation is active at that site, admix with it to some depth, depending on the degree of snowbank porosity. Albedo is lowered, so that heat transfer from solar insolation is amplified, but a surface debris mantle, not unlike that hypothesized for the inactive portions of cometary surfaces, can develop and evolve. These concentrations of water ice can be in communication with the atmosphere to an extent that many other reservoirs, deep underground or at polar locations, are not.

Acidification of the Martian Snowbank: Gases in the martian atmosphere which are chemically reactive with H2O will be taken up and sequestered from their source. Such gases arise from all magmatic exhalations, whether explicit extrusive releases or seepage through vents, fumeroles, or sulfataras. Typical releases include the sulfur and chlorine-containing gases as well as water, and less reactive gases such as CO2 and CH4. Impacts by large bolides will also cause the release of S from the relatively S-rich igneous rocks (based on martian meteorites). Reduced compounds, such as H2S, S, SO, SO2, and CH4 will be quickly converted into their high oxidation state analogs by the plethora of oxidative species (atomic oxygen, OH radical, H2O2, superoxide ion, ozone) that reside in the martian atmosphere as a result of the intense UV-mediated photochemical environment. As a result, SO3 will be readily available from these transient events to combine with the H2O ice. These two molecules have an extremely high affinity for reacting together, and once they do the resulting solution is both hygroscopic and reactive with SO3.

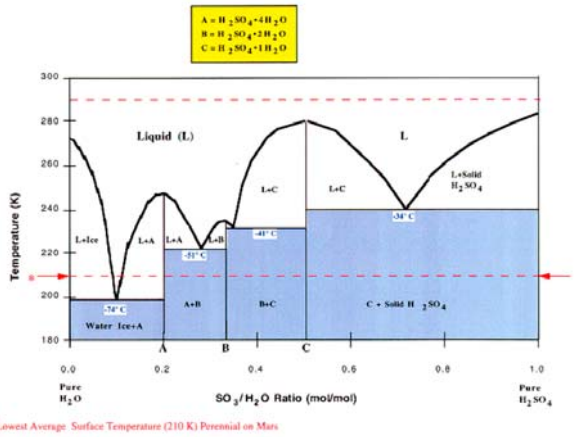

Consequences of the Acidic Snowbank: Liquefaction and Geological Processes: As seen in the accompanying phase diagram, several eutectics are formed, each with freezing points which are depressed relative to pure water or, for that matter, sulfuric acid "neat" (pure). These freezing points range from –34 to –74 ºC, well below the depressing capabilities of most salts and below peak and average temperatures, respectively, in non-polar regions on Mars (polar temperatures of –125 ºC cause freeze-up, slowing the process to one limited by solid-state diffusion). The first eutectic, which has the strongest depressant effect, requires only 1 molecule of SO3 per 10 molecules of H2O, and hence will form in the earliest stages of conversion of native ice to acidic ice. Liquefaction is therefore physically possible, without even accounting for supercooling effects. The proportion of material

which becomes liquid may be small since transformation to the solid phase can alter the composition of the residual liquor. Physical affects on the macroscale can vary from solid plasticity to slush to free liquid, depending on the exact chemical makeup and bulk temperature. Macro-movement is inevitable in response to gravitational forces, resulting in regimes encompassing sliding, creep and free flow. A premier example of intense current interest is the side-wall gullies found on crater walls at high latitudes. Many other less obvious manifestations should occur, however, from sapping to analogs of glacial activity.

Abode for Extremeophiles: On the microscale, liquefactions enable all the special benefits that render liquid H2O so beneficial to life forms on Earth (mobility for transport of nutrients and waste products, consumption as a chemical reactant; stabilization of macromolecular tertiary structure; as a diluent; as a catalyst; as a medium for organism motility). From the standpoint of microorganisms, this is perhaps the single most critical prerequisite to their ability to function metabolically. The acidic snowbank therefore provides an abode for these organisms which can survive the low pH of the environment. Acid-compatible extremeophiles are abundant on Earth, and encompass a variety of detailed lifestyles. However, the acidic habitats on our planet are almost always at high temperatures, the hydrothermal and sulfateric environments associated with magmatic centers of activity. Such environments are possible on Mars as well, but the overall aridity and very low pressure of the atmosphere mitigate against the longevity of hydrothermal regions, unless buried and isolated from communion with the surface.

Acidophiles on earth often are hyperthermophilic. Any putative martian organism in this environment must, rather, be a psychrophile as well as acidophile, and able to function at stressingly low levels of water activity, hence an osmophile. On the other hand, such organisms need not be as xerophilic (desiccation-loving) like their non-ice dwelling cousins in the surface regolith of Mars.

Energy metabolism may take advantage of a number of possibilities. Sunlight can penetrate ice and even "dirty" ice, which attenuates the lethal, short wave-length UV that penetrates the thin atmosphere to reach the surface of Mars. Hence, phototrophs may exist within this ecoenvironment. A number of chemolithotrophs are acidophiles, but their typical energy source is from the oxidation of reduced iron or sulfur compounds. It has been proposed that H2 is almost sufficiently abundant in the martian atmosphere to support sulfate reduction. The source of such sulfate could that thought to be in the ubiquitous soil, and the resulting sulfide could be recycled in a sufuretum ecology to produce sulfate again.

Nutrient availability is enhanced in many respects. Low pH solubilizes many ions, especially the metal cations (e.g., transition elements) that enable enzymes to have high specificity and catalytic kinetic effect. It is also now known that the shergottite martian meteorites can be extracted with acidic solution to yield abundant phosphate and other nutrients.

Persistence and Lifetime: Once acidified to even just a low degree, the equilibrium partial pressure of H2O is reduced over the H2O-H2SO4 solution. Thus, the acid snowbank can effectively "pump" H2O from a non-saturated atmosphere to not only prevent sublimation losses but to even grow. During neutral-atmosphere periods when the content of chemically active gases is extremely low, as in the present epoch, the compositional shift of the snowbank will be toward further dilution of the acidic mix. After a major meteoroidal impact or magmatic release of gases, SO3 uptake may dominate over H2O uptake, and the pH will drop as the snowbank evolves toward the H2SO4 end-member. Once SO3 is reduced sufficiently towards final depletion, the H2O uptake will again predominate. The stasis point for the acidified ice will depend, of course, on availability of these gases as well as the physical nature of the body – whether is is highly porous and equilibrated throughout, or exhibits rinds and layers reflecting "seasonal" effects.

Non-ice areas of martian regolith may also take up SO3 or any H2SO4 formed in the atmosphere, and react with it. Igneous minerals, and especially their glassy counterparts, are typically rich in cations (Ca, Mg, Na, Fe, even Al) which can react to form sulfites and sulfates. These tend to irreversibly bind up the S-containing molecules and remove them from the recyclable inventory. However, under desiccated, cold martian conditions, the reaction rates of these active molecules with minerals are suppressed, yet they will react rapidly with the snowbank ice. Thus, these objects serve as highly efficient sinks for the reactive gases. The apparently universal martian fines, which include the soils and dust grains, are very rich in S, most probably in the sulfate form, that their intrinsic reactivity may have already been used up, rendering them relatively inert with respect to the reactive gases injected into the atmosphere. Thus the snowbank ice

and dust serves the purpose of isolating ice from the igneous minerals which would otherwise serve as an irreversible loss mechanism for the reactive forms.

Exploration of Martian Snowbanks: If this thesis has merit, then acid snowbanks should be a high priority for astrobiological exploration. It extends "follow the water" to "find the liquid water and bioavailable nutrients." A major problem here is that the known gully topographies are extremely steep for safe spacecraft landing and operations, most likely aggravated by poor bearing strength of associated soils. It is not known how many gully systems actually arise from snowbank sources of liquid, but recent tantalizing evidence could be taken as a clue that it may be common.

How can acidic ice deposits on more accessible terrain be detected? There could be morphological clues, since snowbank or ice forms can evidence rounding and globular appearance. General examples are known, such as the gently ridged and featureless material in Newton crater. Acidity cannot be detected by remote sensing, and we still do not have substantive evidence of the pH of martian soil. Small hard lander or penetrator probes could easily make the required measurement, with a low cost instrument and in a matter of minutes or hours. However, the cost of the probe itself is, today, substantial, especially if targeting is required for what generally are small opjects on the scale of landing errors. Highly mobile landers, such as hoppers, might be a more cost-effective solution for reconnaissance to explore several identified targets within a general region of interest.

Conclusion: Deposits of snow or any other forms and origins of ice at the surface of Mars at moderate to low latitudes could be important as an abode for extremeophiles because their interaction with reactive atmospheric gases could result in acidic state with greatly suppressed freezing point. The resultant liquidity is favorable to life processes, as well as certain geological processes. Detection and exploration of such features will be challenging.

FROM GLOBAL RECONNAISSANCE TO SAMPLE RETURN: A PROPOSAL FOR A POST-2009 STRATEGY TO FOLLOW THE WATER ON MARS. S. M. Clifford[1], J. A. George[2], C. R. Stoker[3], and G. Briggs[3]. [1]Lunar and Planetary Institute, 3600 Bay Area Blvd, Houston, TX 77058, clifford@lpi.usra.edu. [2]NASA Johnson Space Center, Houston, TX 77058, jeff.george@jsc.nasa.gov. [3]NASA Ames Research Center, Moffet Field, CA 94035, cstoker@mail.arc.nasa.gov, gbriggs@mail.arc.nasa.gov.

Introduction. Since the mid-1990's, the stated strategy of the Mars Exploration Program has been to "Follow the Water". Although this strategy has been widely publicized, its degree of influence -- and the logic behind its current implementation (as reflected in mission planning, platform and instrument selection, and allocation of spacecraft resources) – remains unclear.

In response to this concern, we propose an integrated strategy for the post-2009 exploration of Mars that identifies the scientific objectives, rationale, sequence of missions, and specific investigations, that we believe provides the maximum possible science return by pursuing the most direct, cost-effective, and technically capable approach to "following the water". This strategy is based on the orbital identification, high-resolution surface investigation, and ultimate sampling of the highest priority targets: near-surface liquid water and massive ground ice (potentially associated with the discharge of the outlfow channels or the relic of a former ocean). The analysis of such samples, in conjunction with the data acquired by the necessary precursor investigations (to identify the locations and characterize the environments of the optimum sampling sites), is expected to address a majority of the goals and high priority science objectives identified by MEPAG.

Goals and Rationale. Since the inception of the Mars Surveyor Program of the mid-1990's, the search for water has been identified as the common thread of Mars research -- its abundance and distribution having important implications for understanding the geologic and climatic evolution of the planet; the potential origin and continued survival of life; and the accessibility of a critical in-situ resource for sustaining future human explorers. For these reasons, it was argued, a strategy to "follow the water" would necessarily benefit all of Mars research.

The unique role and importance of water was more recently affirmed by the identification and prioritization of scientific goals, objectives and measurements undertaken by the Mars Exploration Payload Analysis Group (MEPAG) [1], where the determination of the 3-dimensional distribution and state of H_2O was identified as the single highest-rated objective of the Mars Exploration Program (Table 1).

Of the planet's estimated 500 – 1000 m global inventory of H_2O [2], ~0.000001% is found in the atmosphere, while ~5-10% is thought to be stored as ice in the perennial polar caps and layered terrain. This leaves ~90-95% of the planetary inventory of H_2O that is unaccounted for, the vast bulk of which is believed to reside, as ground ice and groundwater, within the planet's crust.

Although the belief that Mars is water-rich is supported by a wide variety geologic evidence, our ignorance about the heterogeneous nature and thermal evolution of the planet's crust effectively precludes geomorphic or theoretical attempts to quantitatively assess the current geographic and subsurface vertical distribution of ground ice and groundwater [3]. For this reason, any exploration activity (such as drilling) whose

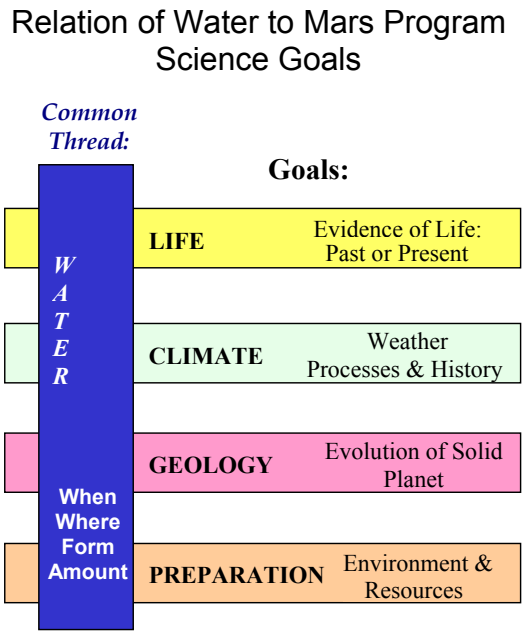

Figure 1. Rationale for the "Follow the Water" strategy.

success is contingent on the presence of subsurface water, must be preceded by a comprehensive high-resolution geophysical survey capable of assessing whether local reservoirs of water and ice actually exist. Terrestrial experience has demonstrated that the accurate identification of such targets is likely to require the application of multiple geophysical techniques [4] – investigations that are most effectively conducted on (or in close proximity to) the planet's surface.

Unfortunately, the relative fraction of the Martian surface that can be investigated by a single lander, rover, or even aerial platform, is extremely small, requiring a prohibitively large number of spacecraft to conduct a global reconnaissance on any time frame shorter than several human lifetimes. Therefore, given the significant uncertainties that exist in our knowledge of the distribution of subsurface H_2O, how do we most effectively employ the limited number of opportunities that we will have to address this issue following the last of the currently planned missions in 2009?

Because conducting a high-resolution 3-dimensional global survey of the distribution of subsurface water on Mars exceeds our present (and foreseeable) technical capabilities and resources, we propose that initial efforts be focused on a more efficient and achievable task – emphasizing the identification and location of the most important and accessible H_2O targets. Of the potential volatile targets identified by the Mars' planetary science, astrobiology, and human exploration communities, those of greatest interest are: liquid water, massive deposits of near-surface ground ice (associated with the ponded discharge of the outlfow channels or the relic of a former ocean), and the polar layered deposits [1].

Table 1 – *MEPAG priority and traceability of "Follow the Water" strategy.*

Goal	Investigation	Priority	Measurements
Life	Map the 3-D distribution of water in all its forms.	1	I.A.1.a.
Climate	Determine the processes controlling the present distribution of H2O, CO2 and dust.	1	II.A.1.d&c.
	Characterize the history of climate change recorded in the stratigraphy of the polar layered deposits and residual ice caps.	2	II.B.2
Geology	Determine the present state, distribution and cycling of water on Mars.	1	III.A.1.a,b,c&d.
Preparation	Understand the distribution of accessible water in soils, regolith, and Martian groundwater system.	3	IV.A.3.a&b.

With regard to the first two of these targets, an additional requirement is imposed by our desire to obtain samples for in-situ and Earth-based analysis. Thus, the geographic location and subsurface extent of a target must be known with sufficient resolution to guide the placement of a drill.

In this abstract we propose an integrated strategy and sequence of missions for the geophysical exploration of Mars that we believe represents the fastest, most cost-effect, and technically capable approach to identifying, investigating, and ultimately sampling the most probable occurrences of near-surface liquid water and massive ground ice. This strategy is based on a synthesis of input from a wide range of sources; however, it owes its greatest debt to the authors and participants of the Mars Program Office white paper "A Strategic Framework for the Exploration of the Martian Subsurface" by Beaty et al. [5], in which the basic elements of this strategy were first proposed.

Global vs. Local Investigations. One of the most critical issues for developing a coherent geophysical strategy to assess the distribution of subsurface water is the appropriate role and timing of global vs. local investigations. The principal attributes of local investigations (such as lander-based GPR) are their relative simplicity and their ability to "map" local variations in dielectric properties (that are potentially indicative of variations in lithology and volatile content) at high resolution. However, given the natural scale and variability of crustal properties, the structure, lithology, and distribution of H_2O, is likely to differ significantly from one location to another [3]. Therefore, to have any confidence in accessing a particular volatile target, drilling operations must necessarily be limited to those sites where local geophysical investigations have already been performed.

A strategy to search for water by proceeding directly to the use of high-resolution local surveys has a significant drawback – for while such surveys may help determine the local distribution of volatiles to high precision, they provide no global context. Thus, while a high-resolution investigation might suggest the presence of a specific volatile target at a depth of 500 m at one location, it could well miss the opportunity – located only 20 km away – where that same volatile target was present at a depth of 100 m. Differences of this magnitude could well be critical to the success or failure of any follow-on drilling effort.

The above argument suggests that local investigations aree most effectively employed following the completion of an initial global geophysical reconnaissance. Although such surveys may be unable to resolve the fine-scale distribution of ground ice and groundwater, they can aid in the identification of moderate- and regional-scale characteristics that can be used to identify the most promising local sites for further study. In this way, global investigations can be used to target local surveys (conducted by local surface networks, rovers, and other techniques) that can verify and map the distribution of potential volatile targets at a resolution sufficient to direct the placement and operation of both shallow- and deep-subsurface drills.

Proposed Strategy. Based on the above reasoning, we propose a two-phase approach to the search for subsurface water on Mars. The first consists of missions devoted to characterizing the large-scale global distribution of liquid water and massive ground ice within the crust. Currently, the most promising candidates for such a reconnaissance are: (i) a polar-orbiting synthetic aperture radar/sounder, and (ii) a 20+-station global geophysical and meteorological network A second "high-resolution" phase would then follow this initial global reconnaissance with more focused investigations of the most promising local (<10 km^2 in area) sites identified from the global data.

Polar-Orbiting Synthetic Aperture Radar/Sounder. An orbital radar sounder has a distinct advantage over other water-detecting geophysical methods in that, given an optimal design, such a sounder has the potential to provide global coverage at moderate resolution using a single spacecraft – a potential that no other technique comes close to approaching.

The first attempt at such an investigation will be made by the 2003 Mars Express mission, which will include a multi-frequency radar sounder called MARSIS. Given ideal conditions, MARSIS is designed to detect the presence of liquid water at depths as great as several km. In 2005, MARSIS will be followed by another orbital sounder called SHARAD, that will fly aboard the Mars Reconnaissance Orbiter. SHARAD will operate at higher frequencies in an effort to improve its resolution of potential water-related targets at shallower depth. Unfortunately, because both Mars Express and the Mars Reconnaissance Orbiter include a number of other high-level investigations, MARSIS and SHARAD have been forced to accept some compromises in mission and spacecraft design that have limited their potential capabili-

ties.

A dedicated orbital SAR/Sounder mission would offer opportunities for a number of significant technical and operational improvements – not the least of which would be absence of resource and compatibility issues associated with the need accommodate other instruments. Among the most significant potential enhancements would be (1) the adoption of a low altitude, slowly migrating polar orbit – thus insuring global coverage with overlapping footprints that will permit data from adjacent orbits to be processed coherently to improve cross-track resolution and enhance clutter rejection., (2) increased power to improve signal-to-noise -- ideally ~10 kW (supplied by an RTG) vs. the 60 W available to MARSIS, and (3) optimized antenna design (i.e., increased size and better geometry) for both the SAR and Sounder.

Other desired enhancements include improvements in the number and range of operational frequencies, bandwidth, receiver sensitivity, utilization of alternate signal waveform designs and the use of two (or more) receivers – either boom-mounted on the same orbiter or achieved by simultaneous operation with compatible radars on other polar-orbiting spacecraft. This potential for orbital interferometry could greatly aid the 3-dimensional characterization of the crust – helping to discriminate between structural, lithologic and volatile signatures in both the near- and deep-subsurface.

A polar orbiting radar Sounder offers a unique ability to carry out such tasks by investigating and mapping the observed and derived electromagnetic properties of the subsurface on a global basis -- information that may provide significant insights about the vertical structure and evolution of the crust. This is particularly true over the polar layered deposits, whose combination of favorable location (due to the high density of orbital ground tracks) and expected low-loss attenuation characteristics may permit a Sounder to obtain a detailed look at the deposits' stratigraphy and basal topography – providing invaluable information relevant to understanding their climatic and deformational history.

Although the unambiguous identification of crustal H_2O may be difficult or impossible using orbital sounding alone, the geometry and contrast associated with those targets of greatest scientific interest (i.e., near-surface liquid water and massive lenses of ground ice) are expected to be sufficient that, under favorable observing conditions (and with the additional interpretive context provided by the analysis of other remote sensing data), the best examples can be identified and mapped with reasonable confidence. At a minimum, an orbital Sounder will provide information on local subsurface properties that can be used to identify the most promising sites for further study (e.g., by subsequent higher-resolution surface and airborne investigations), as well as assist in ruling out those areas whose local characteristics are either inconsistent with the presence of subsurface water or preclude its detection.

Additional scientific and mission synergy would result from the inclusion of the SAR a synthetic aperture radar on the same polar orbiting spacecraft. The addition of the SAR radar would allow investigations of the shallow subsurface, mapping the potential occurrence of buried channels, craters , and other features that could provide important insights into the nature and evolution of the Martian landscape.

Global Geophysical and Meteorological Network. The most logical follow-up to the flight of an advanced orbital SAR/Sounder is a global Geophysical and Meteorological Network consisting of at least 20-stations. Although this number will not provide sufficient spatial coverage to verify in detail the global interpretations derived from the flight of an advanced orbital Sounder, they will provide an opportunity for surface-based seismic and electromagnetic observations that can be used to independently test the large-scale volatile distribution, stratigraphy, and structure of the crust.

When distributed in clusters of 3-5, such stations are also capable of providing the more localized studies needed to investigate and further refine our understanding of the true nature of the most promising volatile sites identified by the orbital SAR/Sounder. The ability of such a Network to discriminate between lithologic and volatile units would be greatly enhanced by the inclusion of multiple geophysical investigations onboard each station, such as magnetotelluric and permitivity instruments, active and passive seismometers, and ground penetrating radar (GPR). Such a mission might also include the acquisition of local compositional and thermophysical data that could assist in interpreting the geophysical sounding results and help characterize the global range of material properties that might be encountered by subsequent drilling efforts.

A logical compliment to the geophysical investigations conducted by such a Network, would be the inclusion of meteorological instruments to provide global and regional measurements of atmospheric pressure, temperature, and wind speed – data that would prove invaluable to the further refinement of general circulation and climate models. A key requirement for both types investigations would be that the individual stations be long-lived (>4 years), providing a sufficient baseline to assess interannual variations in weather as well as the frequency of large-scale seismic events.

Such a Geophysical and Meteorological Network could be emplaced in a single mission (with penetrator-style stations dispersed from a polar-orbiting bus) or be built up incrementally, over two or more successive launch opportunities. In 2009, the four-station NetLander mission will provide an important demonstration of the potential return from network science – effectively doubling (in a single mission) the number of surface locations visited on the planet since the flight of Pathfinder in 1996.

High-Resolution Characterization and Sampling of Local Sites. An expected result of the first phase of global reconnaissance will be the identification and prioritization of the most probable sites for the occurrence of near-surface liquid water and massive ground ice as a prelude to sending more focused investigations. The most logical progression of follow-on missions would be: (1) a high-resolution ground-based survey to verify the nature and extent of the most promising site(s) for the occurrence of near-surface liquid water or massive ground ice, (2) a drill to investigate and sample this target, and (3) a vehicle to return these samples to Earth for further study.

Hi-Resolution Site Survey & Sample Acquisition Rover. While a number of potential platforms could be employed to carry out a high-resolution geophysical and environmental site survey, the one that provides the greatest mission flexi-

bility is an MSL-class Rover. Equipped with high-frequency GPR, an active seismic investigation (including a large array of deployable geophones), and other geophysical instruments, the Rover's principal task would be to conduct the most technically capable investigations possible to verify the true nature of the local target, determine its spatial extent (at a sufficiently high resolution to guide the placement and successful acquisition of samples by a drill), and assess the geology and surface properties of the surrounding area to provide an understanding of the target's context and identify any potential landing hazard's to a follow-on drill and sample return vehicle.

A useful enhancement of this mission would be the ability for the Rover to collect surface samples (including, perhaps, shallow – 1-2 m – drill cores) from the surveyed area, perform preliminary in-situ analyses, and cache the samples in an onboard canister that could be transferred to a future sample return vehicle.

50-100 m-Capable Drill. Once the location and nature of a high-priority volatile target has been verified (to as high a probability as is possible by geophysical methods), the next obvious mission would be to send a Drill capable of reaching, investigating (w/downhole instruments), and acquiring samples for eventual return to Earth. Samples of liquid water or massive ground ice would provide the very highest probability of finding evidence of extant (or at least geologically recent) life, as well as insights into the aqueous geochemistry and isotopic evolution of the Martian crust and groundwater. When combined with selected samples of intervening regolith and rock cored by the drill, and the data obtained during the precursor Rover site survey, such a mission would provide an enormously detailed environmental and stratigraphic record for sample interpretation.

To minimize complexity and enhance stability, the preferred platform for a 50-100 m drill would be a stationary lander – guided to its optimum sampling location by terminal guidance and a beacon deployed by the precursor Rover.

Sample Return Vehicle. As with the targeting of the Drill, the landing of a Sample Return Vehicle would be aided by the radio beacon deployed by the precursor Rover. Cached drill cores, and surface samples obtained by the Rover during its site characterization survey, could then be transferred to the Sample Return Vehicle by the Rover for return to Earth. Another alternative, that would simplify surface operations, would be to incorporate the return vehicle on the drilling platform itself.

Summary. Knowledge of the distribution and state of subsurface water is of fundamental importance to astrobiology, human exploration, and to our understanding of how Mars has evolved as a planet. We believe that the "Follow the Water" strategy and mission sequence outlined here represents the most direct and cost effective approach for addressing the goals and high priority science objectives identified by MEPAG.

References: [1] MEPAG Science Goals Document, 2000; [2] Carr, M. H., Icarus, 68, 187-216, 1986; [3] Clifford, S.M., *Lunar Planet. Sci Conf. XXVIII*, 1998; [4] Stoker, C. *Mars Deep Water Sounding Workshop Summary*, http://astro-biology.arc.nasa.gov/worshops/1998/marswater/index.html, 1998; [5] Beaty, D. et al., *Analysis of the Potential of a Mars Orbital Ground-Penetrating Radar Instrument in 2005*, Mars Program Office White Paper, 2001.

Post Impact Mars Climate Simulations using a GCM. A. Colaprete[1], R. M. Haberle[2], T. L. Segura[3], O. B. Toon[3], K. Zahnle [1]SETI (NASA Ames Research Center, Moffett Field, MS 245-3, Mountain View,CA 94035, tonyc@freeze.arc.nasa.gov, [2]NASA Ames Research Center (NASA Ames Research Center, Moffett Field, MS 245-3, Mountain View,CA 94035),[3]Program in Atmospheric and Oceanic Sciences, Laboratory for Atmospheric and Space Physics, University of Colorado, Campus Box 392, Boulder, CO, 80309.

Introduction: The first images returned by the Mariner 7 spacecraft of the Martian surface showed a landscape heavily scared by impacts. Mariner 9 imaging revealed geomorphic features including valley networks and outflow channels that suggest liquid water once flowed at the surface of Mars. Further evidence for water erosion and surface modification has come from the Viking Spacecraft, Mars Pathfinder and Mars Global Surveyor's (MGS) Mars Obiter Camera (MOC). This evidence includes apparent paleolake beds, fluvial fans and sedimentary layers (Cabrol and Grinn, 1999; Heberle et al., 2001). There is evidence for subsurface water as well. Rampart crates suggest an abundance of water in the near surface regolith (Mouginis-Mark, 1986). The estimated erosion rates necessary to explain the observed surface morphologies (Golombek and Bridges, 2000) present a conundrum. The rates of erosion appear to be highest when the early sun was fainter and only 75% as luminous as it is today. Furthermore the rates of erosion appear to correlate with the rate at which Mars was impacted (Carr and Waenke, 1992). All of this evidence suggests to a very different climate than what exists on Mars today.

The most popular paradigm for the formation of the valley networks is that Mars had at one time a warm ($T_{average} > 273$), stable and wetter climate. Possible warming mechanisms have included increased surface pressures (Pollack et al, 1987), carbon dioxide clouds (Forget and Pierrehumbert, 1997) and trace greenhouse gasses. Yet to date climate models have not been able to produce a continuously warm and wet early Mars (Haberle, 1998). An alternate possibility is transient warm and wet conditions initiated by large impacts.

It is widely accepted that even relatively small impacts (~10 km) have altered the past climate of Earth to such an extent as to cause mass extinctions (Toon et al., 1997). Mars has been impacted with a similar distribution of objects. The impact record at Mars is preserved in the abundance of observable craters on it surface. Impact induced climate change must have occurred on Mars.

Background

Large Impacts: The impacts of asteroids and comets larger than 100 km in diameter have left more than thirty craters on Mars (Kieffer et al. 1992). Collisions of such large, energetic objects result in the production of meters thick debris layers that are global in extent (Melosh 1989; Sleep and Zahnle, 1997). Figure 1 shows a sequence of events associated with the impact of a large object. At impact (Figure 2a) the object and a portion of the target material is melted, vaporized or pulverized. A thermally expanding debris plume transports the melt/vapor portion, about 20% of the total debris mass, globally on ballistic trajectories (Figure 2b). As melt/vapor rains back onto the planet with temperature in excess of 1600 K (Figure 2c) it radiates to the surface increasing the surface and atmospheric temperature rapidly. The remaining 80% of the total debris mass is composed of pulverized rock with temperatures of about 400 K and is confined to within a few crater diameters of the impact center. A 100 km impact will result in a global melt/vapor debris layer approximately 10 cm thick and a local pulverized debris layer several meters thick (Figure 2d).

In addition to the heat introduced by the impact, a substantial amount of vaporized water, both from the impactor itself and from the target material is injected into the atmosphere. A large impact may release an equivalent global surface water layer meters or more in depth. Water vapor is an excellent greenhouse gas and works to trap the impact generated heat within the atmosphere. The hot rock debris layer and the additional water greenhouse may keep surface temperatures above the freezing point of water for as long as several decades (Segura et al., 2002). As the atmosphere cools water injected into the atmosphere will condense and precipitate to the surface. Following the impact, the thermal pulse that travels downward into the regolith may release additional water from subsurface reservoirs adding to the total liquid water amount at the surface. In principle, depending on the composition of the impactor and the target material, large impacts could inject enough water to explain some of the geomorphic evidence for liquid water at the Martian surface.

The environmental effects of 100 and 200 km diameter objects on the Martian surface have been explored with a 1D (height) model (Segura et al., 2002). This model includes a radiative transfer code to calculate the evolution of the atmospheric temperature

following the impact and a model of the regolith to calculate the evolution of the ground temperature. In all simulations Segura et al. (2002) assumed a surface pressure of 150 mbar (CO_2 + water vapor) and a 1% water fraction in the impactor and target material. It was found that the planet can be kept above freezing for years (decades) following the impact of a 100 (200) km diameter object, and that a half a meter (few meters) of water may precipitate from the atmosphere and melt from the subsurface as a result of this warming. Larger impacts kept the planet above freezing for centuries, and released larger amounts of water. These 1D calculations suggest that large impacts have the potential to drastically alter the climate for many years and provide a source of surface water. At a minimum, large impacts would have worked to redistribute water globally as injected water is transported and condenses out. Multiple impacts over time may have worked to globally fractionate Martian subsurface water through a process of release and transport.

GCM Simulations: The obvious limitation of these 1D calculations is the absence of dynamics. An accurate assessment of the effects of impacts on the climate will need to include the transport of both heat and water vapor. Reported here are the initial results of post impact climate simulations using the Ames Mars General Circulation Model (MGCM). A hydrological cycle has been incorporated into the Ames MGCM that includes the formation of clouds, precipitation and surface reservoirs. In these simulations, an initial warm and wet atmosphere, like that which would immediately follow an impact, is allowed to evolve back to a steady state.

As an example, the results of one of these simulations is shown in Figure 2. In this specific simulation the global atmosphere was initialized isothermally at 300 K, a subsurface soil layer 2 m thick was initialized at 350 K, and approximately 5 pr. cm of water vapor was uniformly mixed everywhere. Figure 2 shows the total accumulated liquid rainfall for the first 100 days of the simulation. Also shown in Figure 2 is the MOLA topography (black contours), the location of outflow channels (black speckles), and the location of network channels (red speckles). The location of the region of observed hematite and Gusav Crater are also indicated. Maximum rainfall accumulation is greater than 400 cm. Locations of high rain fall amounts appear to be controlled by large scale topography. In general there is good correlation between areas of highest rainfall and the location of outflow channels. The correlation is not as good for areas of highest rainfall and the location of outflow channels, however. In particular, this simulation predicts dry conditions on the eastern and southern sides of Tharsis.

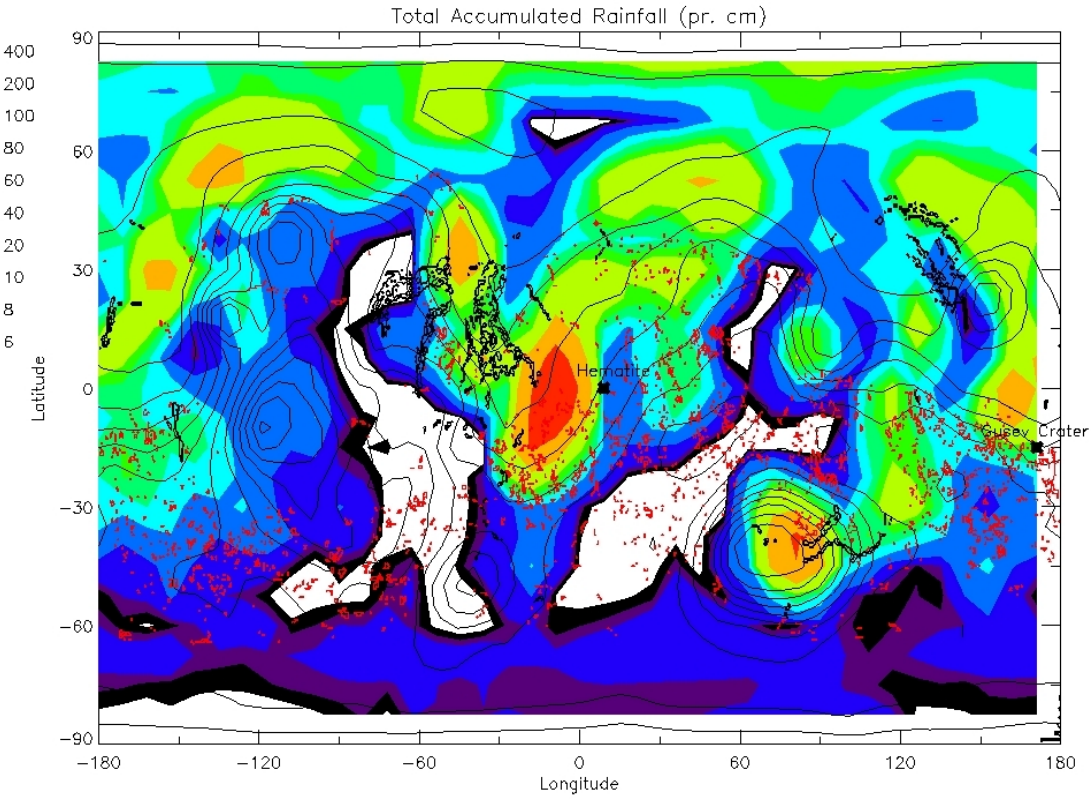

Figure 1.

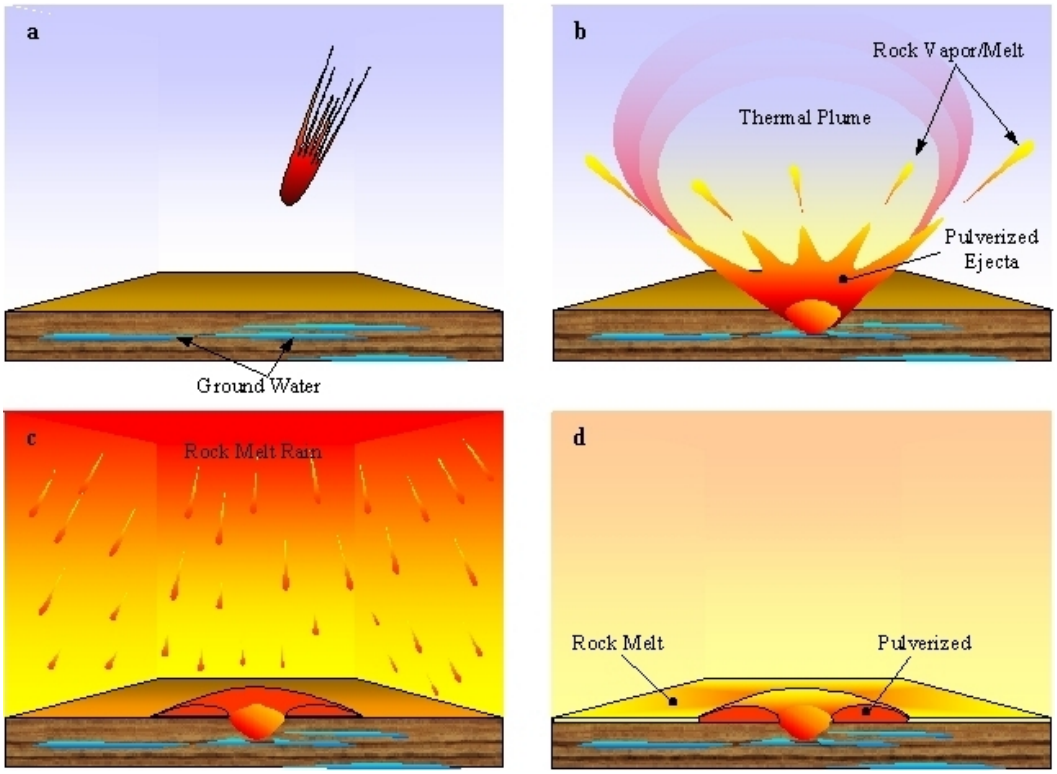

Figure 2.

High Channels on Mars Indicate Hesperian Recharge at Low Latitudes. N. M. Coleman[1], C. L. Dinwiddie[2], and K. Casteel[3], [1]Member, American Geophysical Union (nmc@nrc.gov), [2]Southwest Research Institute (cdinwiddie@swri.edu), [3]Member, American Geophysical Union (252 Johnston Ln., Mercersburg, PA 17236).

Abstract: A special class of Martian outflow channels discharged from enormous fracture zones. These channels were sourced by groundwater, not surface water, and when observed on high-standing plateaus they provide paleo-indicators of climax groundwater levels. We identify two outflow channels of Hesperian age that issued from a 750-km-long fault zone extending from Candor Chasma to Ganges Chasma. One channel source stands ~2600 m above the datum, too high to be explained by discharge from a global aquifer. The indicated groundwater levels require regional sources of recharge and provide evidence that a high-standing, ice-covered lake probably existed in eastern Candor Chasma.

Introduction: The transition from the Noachian to the Hesperian era represents a significant shift in surface conditions on Mars. The crust formed during the Noachian, and the planet was heavily bombarded by planetesimals. It is likely that the atmosphere was thickest and the water inventory highest during this time because isotopic evidence shows that the planet has lost large fractions of water and other volatile inventories over geologic time [1]. Extensive valley networks developed in the cratered highlands [2] and lakes possibly formed in many craters [3]. Noachian erosion rates are estimated to have been ~1000 times greater than during later eras [4]. By Hesperian time, which began 3.5–4.3 Gyr ago [4], the atmosphere had thinned and a thick, planet-wide cryosphere may have evolved [5]. Immense shield volcanos began forming in Tharsis, and flood basalts inundated large areas. The Hesperian was also the peak of outflow channel activity [6], when enormous channels were carved and large water bodies may have collected in the northern lowlands [7,8]. But how did water accumulate in the floodwater source areas?

Polar Recharge: Extensive groundwater recharge is inconsistent with the idea of a thick planet-wide cryosphere on Mars, which would inhibit the migration of water from the surface to underground aquifers. To resolve this dilemma, it has been suggested [8,9] that Hesperian recharge occurred at the base of the polar layered deposits and migrated to low latitudes in a globally connected aquifer system. Carr [10] tested this polar recharge model using the MOLA database of surface elevations obtained by Mars Global Surveyor. He identified 1500 m as a soft upper limit for the elevation at which recharge can efficiently occur by melting beneath the south polar layered terrains. Carr [10] concluded that major discharges of groundwater onto the surface at elevations >1500 m are unlikely to have the South Pole as a source. Examples of high-standing water-carved features include valleys on the flanks of Alba Patera and Ceraunius Tholus. These valleys could readily be explained by local processes, such as erosion by discharges from hydrothermal springs [2].

Outflow Channels Near Ganges Chasma: We have studied two specific channels that reveal new insights about Hesperian paleohydrology. They provide evidence that regional groundwater recharge occurred at low latitudes during one or more intervals of Hesperian time. Elaver Vallis begins at the eastern rim of a large, 80-km-wide Noachian crater located south of Ganges Chasma (Figure 1A). A pit more than 5000 m deep resides inside the southern part of this crater. We interpret this pit as being undermined and excavated by the eruption of confined groundwater, forming a Hesperian lake in the surrounding crater. The crater floor is exceptionally flat and smooth. A profile 40 km long from west to east across the center of the crater shows that elevation varies less than ~30 m [11]. This smooth crater floor morphology is consistent with lacustrine deposition. Lake levels rose so high that the eastern crater wall was breached, leading to catastrophic release of ponded waters and the carving of the Elaver Vallis channel complex. The flooding apparently occurred during the mid- to late-Hesperian because the channel eroded lower Hesperian strata (unit Hpl_3) of the Plateau Sequence [12].

West of Elaver Vallis is Allegheny Vallis (name provisionally approved by the IAU), a channel that emerges from an elongated pit (Figure 1, A to C). This channel was nearly imperceptible in Viking imagery, but MOLA data confirm that it is a continuous valley 250 km long that terminates at the western rim of Ganges Chasma. At first glance, the channel looks like a typical valley network, but in fact it is a true outflow channel. The waters that carved Allegheny Vallis erupted from the surface at an elevation of ~2600 m, far above the 1500 m threshold [10] for contributions from polar basal recharge. Could the channel elevation

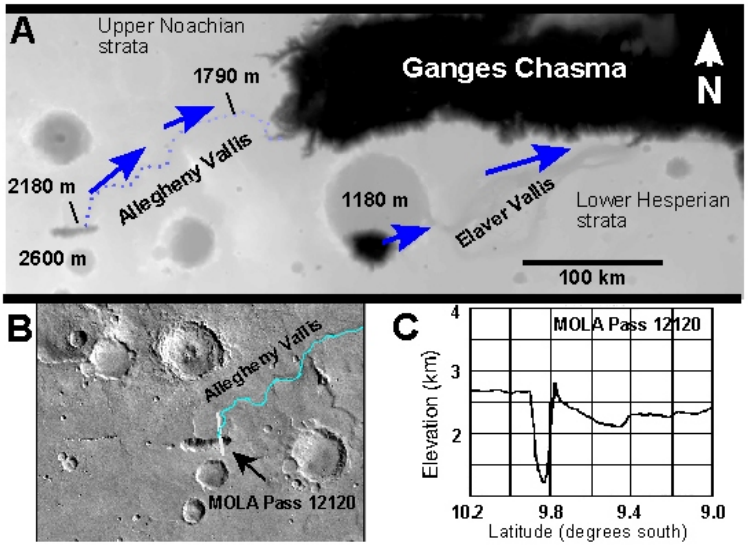

Fig. 1. (A) Source areas for Elaver Vallis and Allegheny Vallis. MOLA image at 1/128th degree resolution, available at http://wufs.wustl.edu/missions/mgs/mola/megdr2.html. (B) Viking image of the source area for Allegheny Vallis. Frame is 240 km across. The channel emerges from a deep pit at 10.0°S, 54.5°W. Note the chain of pits parallel to and west of the elongated pit, suggesting that these features were produced by common geologic structures. (C) MOLA profile across the channel source. Pit is ~1500 m deep. The discharge erupted from terrain at ~2600 m. Data for MOLA pass 12120 available at http://wufs.wustl.edu/missions/mgs/mola/.

have changed over time? Extensional tectonics in the Valles Marineris seem more likely to have lowered the channel than to have raised it. Therefore, if the channel source elevation has not changed appreciably, or has been lowered since Hesperian time, or if relative elevation differences have been preserved, then the outflows must have derived from regional recharge at higher elevations. Allegheny Vallis cut upper Noachian strata [12], but it also embays Ganges Chasma, which mainly formed during the Hesperian. The discharge probably occurred in mid- to late-Hesperian time, concurrent with the flows in Elaver Vallis.

The discharges that carved Allegheny and Elaver Valles erupted from depressions in a long chain of pits (Figure 2) that extends 750 km from eastern Candor Chasma to western Ganges Chasma. We interpret the pit chain as the surface manifestation of a mega-fracture zone or an incipient graben system that was part of the Valles Marineris structural complex. This fault system would likely have created highly anisotropic conditions in the aquifer system, greatly enhancing the easterly flow of groundwater. The idea that both channels were carved by aqueous flows from the same mega-fracture zone suggests that the flows were concurrent. More discharge over a longer time could have occurred in Elaver Vallis because its outflow zone is lower in elevation than is the source of Allegheny Vallis.

We can now add Allegheny and Elaver Valles to a special class of Martian channels: those that were carved by flows emerging from immense fault zones. Such channels include Athabasca Vallis, which emanated from the Cerberus Fossae [13], and Mangala Valles [14], which discharged from the Memnonia Fossae west of Tharsis. The fact that some large Martian channels debouched from fault zones supports a groundwater source and aqueous flood origin, and contradicts speculative mechanisms for outflow channel formation, such as carving by wind [15] or erosion by gas-supported debris flows [16]. Carbon dioxide-based models, which re-cently seemed plausible [16,17], face theoretical difficulties that now appear insurmountable [18,19].

Hesperian Recharge Zones: Where do we find potential recharge areas for Allegheny and Elaver Valles, and for most of the large outflow channels that

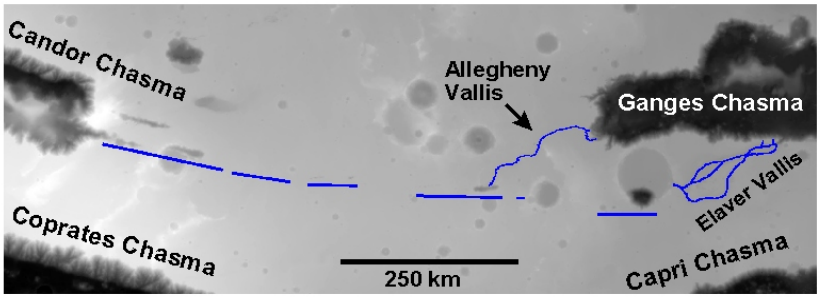

Fig. 2. Trends of aligned pits that extend ~750 km from eastern Candor Chasma to the vicinity of Ganges Chasma. Allegheny and Elaver Valles are shown in relation to this interpreted mega-fracture zone. Average land surface elevations decrease from the rim of Candor Chasma toward Ganges Chasma. This regional slope would have favored easterly migration of groundwater along structurally-enhanced flowpaths. MOLA image is at 1/128th degree resolution, available at http://wufs.wustl.edu/missions/mgs/mola/megdr2.html.

emptied into Chryse Planitia? Large regions near the Valles Marineris stand higher than 2500 m (Figure 3), including the elevated terrain of the Tharsis plateau, Olympus Mons, and Alba Patera. Other high-standing terrain includes the Hesperian plains of Syria Planum, Sinai Planum, and Solis Planum. We estimate that over 80 percent of the high ground is covered by Amazonian and Hesperian units [12]. We infer that Hesperian strata occur beneath most of the Amazonian units because geologic mapping [12] shows only a few unconformities where Amazonian deposits directly contact Noachian units. The occurrence of widespread Hesperian volcanism over most of the potential recharge areas for Allegheny and Elaver Valles suggests causal relationships between long-lived volcanism, large-scale genesis of liquid water, and channel formation. We note that Hesperian water-carved features may have existed in some areas now veneered with Amazonian strata.

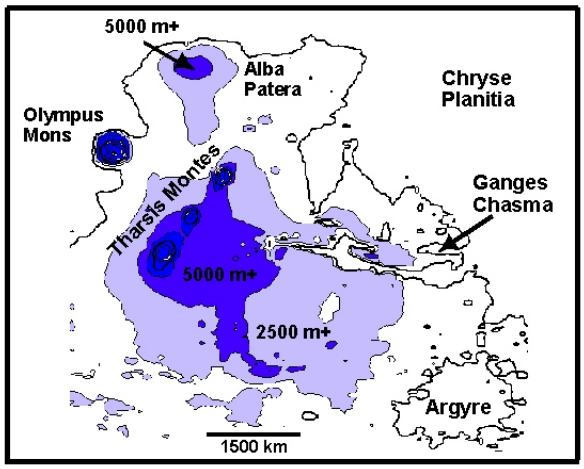

Fig. 3 Topography for the region south and west of Chryse Planitia. Terrain shown in light blue exceeds 2500 m above the global datum. Dark blue terrain stands higher than 5000 m. The terrain east and south of Tharsis Montes that exceeds 2500 m covers an area greater than 1×10^7 km^2. Map contoured using MOLA data grid at 1/4 deg. resolution available at: http://wufs.wustl.edu/missions/mgs/mola/iegdr.html.

Canyon Lakes: Groundwater generated west and north of the aligned volcanos of Tharsis Montes would have flowed westward into Amazonis or into the northern lowlands. Groundwater east of Tharsis Montes and south of the Valles Marineris would have flowed generally toward the canyons, supporting ice-covered lakes in the basins. Water could readily have been stored in canyon lakes beneath ice covers, even at the equator. Thin (~1 m) deposits of dust or ash on ice covers would stabilize sublimation rates at ~10^{-5} cm yr^{-1} [4]. The current topographic configuration would not permit deep lakes in the canyons because water would drain eastward to ultimately discharge in Chryse Planitia. Present-day topography shows that portions of canyon floors in Melas and Coprates Chasmas are deeper than the canyon floors to the east. It would be possible for water bodies deeper than 1000 m to collect within them if water were released. However, these water bodies would be limited in height by overflow elevations of -3600 m to -3900 m in the eastern canyons. During the Hesperian, if the juncture between Coprates and Capri Chasmas had been closed, lake levels to the west would still have been limited by the ~1720 m overflow elevation of the canyon rim at 16.08°S, 56.33°W. Much higher lakes would have been possible in ancestral western canyons with higher rims (e.g., Candor, Ophir, and Melas chasmata) if they had been fully enclosed, similar to Hebes Chasma today. Landform evolution in the canyons provides a possible explanation for former high lake levels and the ~2600 m outflow elevation of Allegheny Vallis.

We interpret the geomorphic evidence described above to propose that one or more ice-covered lakes existed in eastern Candor Chasma (and perhaps also in Melas Chasma and western Coprates Chasma) when Allegheny Vallis was carved. The ice-covered lake surfaces would have been in equilibrium with regional groundwater levels. Groundwater would have preferentially drained eastward toward Ganges Chasma, which may also have contained an ice-covered lake [19]. The aquifers east of Candor would likely have been confined beneath a cryosphere. Eventually, the potentiometric surface in these confined aquifers rose above the land surface, creating conditions for groundwater breakout. High groundwater levels would have helped to lubricate fault zones, increasing the potential for tectonic activity. A major fault movement may have occurred, causing groundwater breakouts to form the pits at the source locations of Allegheny and Elaver Valles. Heat from igneous intrusive events may also have contributed to fluid breakouts [20].

Water Ice Reservoirs: During the Hesperian, it appears that large volumes of liquid water were periodically produced near the Martian surface. The amounts were sufficient to partially fill a proto-Candor Chasma to >2600 m and to supply an active groundwater system. If the ancestral canyons had been smaller and more poorly connected than their modern counterparts, the water volumes needed to fill the ancient canyon lakes would have been much smaller than the canyon volumes we observe today. A likely source for liquid water was volcano-ice interaction [4]. We suggest that

atmospheric conditions in mid- to late-Hesperian, proximal to major volcanic eruptions, permitted precipitation of snow onto elevated terrain of the Tharsis plateau and other high terrain east of Tharsis. The plateau may have served, in effect, as a third "pole" of ice accretion. Precipitation would have been catalytically aided by gaseous and particulate emissions from Tharsis volcanism. Ice may also have deposited directly as frost during the adiabatic cooling of air masses rising onto and traversing Tharsis. Even under the present atmosphere, orographic formation of water ice clouds is common over the Tharsis rise [21]. Ice blankets layered with aeolian dust and volcanic ash could have accumulated at rates that outstripped sublimation. Fan-shaped landforms in Tharsis have been interpreted as the deposits and remnants of cold-based mountain glaciers [22]. More extensive former deposits would have provided substantial reservoirs of water ice that were susceptible to catastrophic melting. Eruption of flood basalts could have periodically melted these reservoirs and provided large volumes of water for surface runoff and infiltration. Highly permeable basalt aquifers would efficiently transport meltwaters eastward from recharge areas to the ancestral Valles Marineris canyons. The Hesperian structural complex of Noctis Labyrinthus (10°S, 100°W) provided a network of surface and underground pathways that would have enhanced drainage from elevated terrain in central Tharsis. The underlying structural complex is probably larger than mapping indicates [12] because Amazonian and upper Hesperian units appear to have overlapped and concealed a large part of its surface expression.

Conclusions: The polar basal recharge model [8,9] may indeed be a viable mechanism to create groundwater recharge on Mars. However, we have found water-carved features at low latitudes that cannot be explained by polar recharge and seem to require regional recharge sources on and east of the Tharsis plateau. Our results are consistent with the conclusions of researchers [3] who found that paleolake activity in Martian impact craters began in the Noachian era, but continued through the Hesperian and into the Amazonian era. Mars appears to have experienced periods of hydrologic quiescence with intermittent and pronounced hydrologic activity that brought about dramatic evolution of landforms during post-Noachian time. The evidence for high-altitude recharge at low latitudes, along with inferences about ice-covered lakes in the ancestral canyons, can be used to calibrate models of a volcanic-hydrologic climax during Hesperian time.

Implications for Life: Deep lakes and aquifers would have been ideal refuges for any extant life forms that could have evolved earlier in the Noachian. These environs would have protected organisms from the harsh conditions at the present-day surface. The evidence that a Hesperian lake formerly existed in a large, level-floored crater at 10°S, 51°W provides a potential target for landed science missions. Sediments deposited in the crater may preserve chemical traces of life forms, microfossils, or even spores. As experiments on Earth have shown, spore-forming bacteria as much as 250 million years old can be isolated and cultivated [23]. Therefore, the possibility of recovering evidence of life, or rejuvenating ancient Martian life remains an intriguing possibility for future Mars missions.

References: [1] Jakosky B. M. and Phillips R. J (2001) *Nature*, 412, 237–244. [2] Carr M. H. and Chuang F. C. (1997) *JGR*, 102, 9145–9152. [3] Cabrol N. A. and Grin E. A. (1999) *Icarus*, 142, 160–172. [4] Carr M. H. (1986) *Water on Mars*, Oxford Univ. Press. [5] Clifford, S. M. (1993) *JGR*, 98, 10973. [6] Tanaka K. L. (1986) *JGR*, 91, E139–E158. [7] Baker V. R. (2001) *Nature*, 412, 228–236. [8] Clifford S. M. and Parker T. J. (2001) *Icarus*, 154, 40–79. [9] Clifford S. M. (1987) *JGR*, 92, 9135–9152. [10] Carr M. H. (2002) *JGR*, 107, doi:10.1029/2002JE001845. [11] Elevation data at 1/32nd degree resolution available from the Mars MER 2003 website at: http://marsoweb.nas.nasa.gov/dataViz/. [12] Scott D. H. and Tanaka K. L. (1986) *US Geol. Survey Geol. Invest. Series Map I-1802-A*. [13] Burr D. M. et al. (2002) *GRL*, 29, doi:10.1029/2001GL013345. [14] Tanaka K. L. and Chapman M. G. (1990), *JGR*, 95, 14,315–14323. [15] Whitney M. I. (1979) *GSA Bull.*, 90, 1111–1127. [16] Hoffman N. (2000) *Icarus*, 146, 326–342. [17] O'Hanlon L. (2001) *Nature*, 413, 664–666. [18] Stewart S. T. and Nimmo F. (2002) *JGR*, 107, 5069, doi:10.1029/2000JE001465. [19] Coleman N. M. (2003 in press) *JGR*, 108, doi:10.1029/ 2002JE001940. [20] Wilson L. and Head J. W. (2002) *JGR*, 107, doi: 10.1029/2001JE001593. [21] Pearl J. C. et al. (2001) *JGR*, 106, 12325-12338. [22] Head J. W. and Marchant D. R. (2003) *Mars Atm. Modeling and Observations Workshop*, see abstract at http://www.mars.Lmd.jussieu.fr /granada2003/abstract/abstract.html. [23] Vreeland R. et al. (2000) *Nature*, 407, 897–900.

DEVELOPMENT AND TESTING OF LASER-INDUCED BREAKDOWN SPECTROSCOPY FOR THE MARS ROVER PROGRAM: ELEMENTAL ANALYSES AT STAND-OFF DISTANCES. D.A. Cremers[1], R.C. Wiens[2], Z.A. Arp[3], R.D. Harris[3], S. Maurice[4], [1]C-ADI (MS J565), [2]NIS-1, [3]NMT-15, Los Alamos National Laboratory, Los Alamos, NM 87545; [4]Observatoire Midi Pyrenees, Laboratoire d'astrophysique de Toulouse, France.

Introduction: One of the most fundamental pieces of information about any planetary body is the elemental composition of its surface materials.

The Viking Martian landers employed XRF (x-ray fluorescence) and the MER rovers are carrying APXS (alpha-proton x-ray spectrometer) instruments upgraded from that used on the Pathfinder rover to supply elemental composition information for soils and rocks to which direct contact is possible. These in-situ analyses require that the lander or rover be in contact with the sample.

In addition to in-situ instrumentation, the present generation of rovers carry instruments that operate at stand-off distances. The Mini-TES is an example of a stand-off instrument on the MER rovers. Other examples for future missions include infrared point spectrometers and microscopic-imagers that can operate at a distance. The main advantage of such types of analyses is obvious: the sensing element does not need to be in contact or even adjacent to the target sample. This opens up new sensing capabilities. For example, targets that cannot be reached by a rover due to impassable terrain or targets positioned on a cliff face can now be accessed using stand-off analysis. In addition, the duty cycle of stand-off analysis can be much greater than that provided by in-situ measurements because the stand-off analysis probe can be aimed rapidly at different features of interest eliminating the need for the rover to actually move to the target.

Over the past five years we have been developing a stand-off method of elemental analysis based on atomic emission spectroscopy called laser-induced breakdown spectroscopy (LIBS). A laser-produced spark vaporizes and excites the target material, the elements of which emit at characteristic wavelengths. Using this method, material can be analyzed from within a radius of several tens of meters from the instrument platform. A relatively large area can therefore be sampled from a simple lander without requiring a rover or sampling arms. The placement of such an instrument on a rover would allow the sampling of locations distant from the landing site. Here we give a description of the LIBS method and its advantages. We discuss recent work on determining its characteristics for Mars exploration, including accuracy, detection limits, and suitability for determining the presence of water ice and hydrated minerals. We also give a description of prototype instruments we have tested in field settings.

LIBS Method: The LIBS method has been studied for many years and has recently seen a huge growth in applications [1-6]. The method is diagrammed in Fig. 1 for measurements at stand-off distances and a photo of a laser plasma formed on a cliff face at 18 meters distance is shown in Fig. 2.

In the LIBS method, powerful laser pulses are focused on the target sample to form a laser spark or plasma. Material within the spark is the result of vaporization/atomization of a small amount of target material. The spark light contains the emission spectra of the elements within the plasma. Collection of the plasma light, followed by spectral dispersion and detection, permit identification of the elements via their

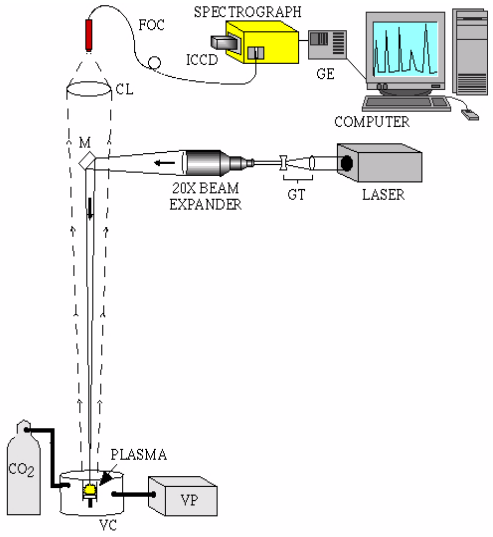

Fig. 1. Experimental set-up for analysis of geological samples at stand-off distances under Mars atmospheric conditions. GE=gating electronics; GT=Galilean telescope; FOC=fiber optic cable; CL=collection lens; M=mirror; VC=vacuum chamber; VP=vacuum pump.

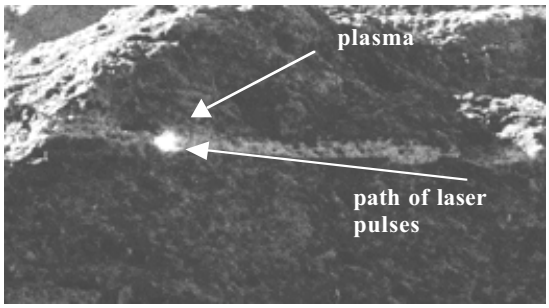

Fig. 2. Stand-off analysis of a cliff face at a distance of 18 meters. The horizontal white strip is the result of surface cleaning by moving the laser beam back and forth.

unique spectral signatures. When calibrated, concentrations can be determined. Advantages of the method compared to more conventional elemental analysis methods include: (1) rapid analysis (one measurement/pulse); (2) simultaneous multi-element detection; (3) ability to detect all elements (high and low z); (4) stand-off analysis capability [7]; (5) ability to remove surface dusts and weathered layers to permit analysis of underlying bulk materials. Stand-off analysis is possible because the laser pulses can be focused at a distance to generate the laser sparks on a solid. The distance that can be achieved depends on characteristics of the laser and the optics used to focus the pulses on the target. The use of LIBS for space applications has been discussed previously [8] but detailed studies for this application have only recently been carried out [9-11].

Experimental Apparatus: Using a laboratory "breadboard" LIBS system, a number of experiments have been carried out demonstrating the capabilities of LIBS for remote analysis. The breadboard system consists of an Nd:YAG laser (10 ns pulsewidth, 35-100 mJ/pulse, 1064 nm wavelength), a beam expander (x10 or x20) to expand and focus the pulses on the sample, a target chamber that can be adjusted to simulate the composition of the Martian atmosphere (5-8 Torr CO_2), a lens to collect the spark light and a spectrograph and optical array detector to process the spectra. Simulation of the Mars atmosphere is useful, as the plasma characteristics are affected by the partial pressure of the surrounding gas. Earlier results [9] showed that elemental emissions are significantly stronger at Mars atmospheric pressures than at Earth pressures due to increased ablation of surface material. Stand-off distances up to 19 meters between the target and the optics have been achieved [9].

Results:

Analytical Figures of Merit. Analytical figures of merit for LIBS soil analysis include detection limits, accuracy, and precision. A calibration curve for the detection of K (in 6 Torr CO_2) in a series of basalt samples is shown in Fig. 3. Each measurement involved averaging the spectra from 20 laser plasmas. The average accuracy for the samples with the five highest K concentrations (>0.42% K_2O) was 8.1%.

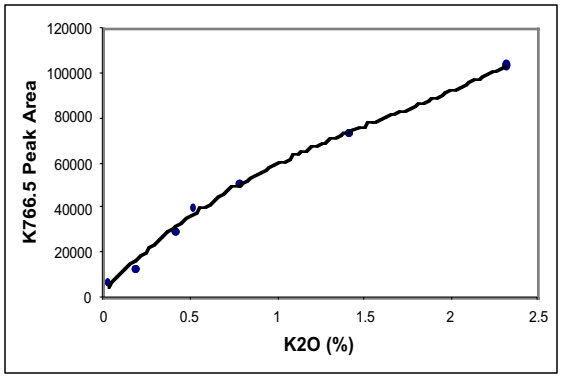

Fig. 3. Calibration curve for K (as K_2O) in basalt samples. Determination of K is being developed for use in K-Ar dating of Martian rocks.

Selected detection limits are presented in Table 1 for samples at a distance of 19 meters in an atmosphere of 5 Torr CO_2 and a laser energy of 100 mJ/pulse. These limits were determined by constructing a calibration curve for each element using synthetic silicate soil samples and then plotting the element signal versus concentration. Also listed in the Table is the average precision of the measurements designated as the %RSD (% relative standard deviation). Figure 4 shows the dependence of measurement precision on the number of LIBS spectra averaged. Clearly, precision increases with the number of measurements averaged.

Table 1. Detection limits (DL) for elements in synthetic soils at 19 meters.

element	DL(ppm)	%RSD
Ba	21	5.5
Cr	39	8.2
Cu	43	10
Hg	647	27
Li	20	8.8
Ni	224	14
Pb	95	13
Sn	84	14
Sr	1.9	6.3

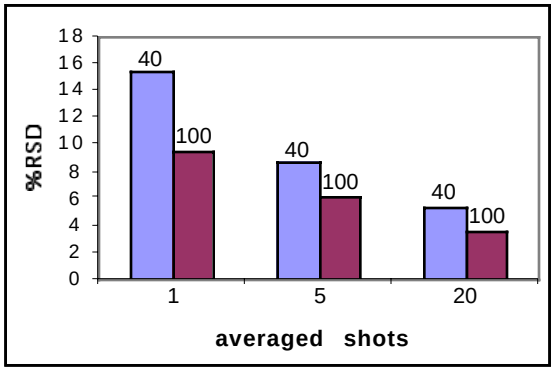

Fig. 4. Dependence of the percent relative standard deviation (%RSD) on the number of laser pulses averaged. Energies were 40 and 100 mJ.

Repetitive ablation for surface cleaning. Repetitive ablation at the same spot on the sample can be used to remove dusts and weathered surface layers. This is demonstrated in Fig. 5 illustrating the change in Mn and Si signals as a weathered granite surface is ablated. The ablation crater (depth ≈ 1mm) produced on jasperoid by repeated sampling (1000 shots) at the same spot is shown in Fig. 6.

Detection of water ice. For these experiments, water ice samples and water ice/soil mixtures were positioned on a cold finger chilled by liquid N_2 or by a eutectic mixture of ethanol/dry ice. The samples were

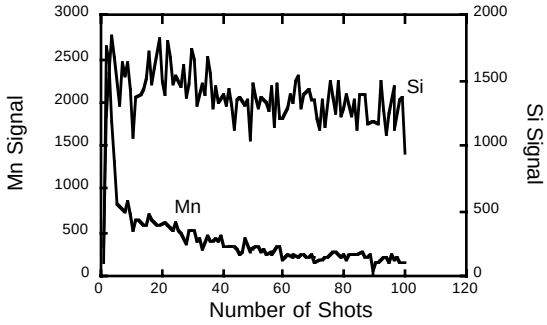

Fig. 5. Variation in Si and Mn signals upon repeated ablation of a granite sample.

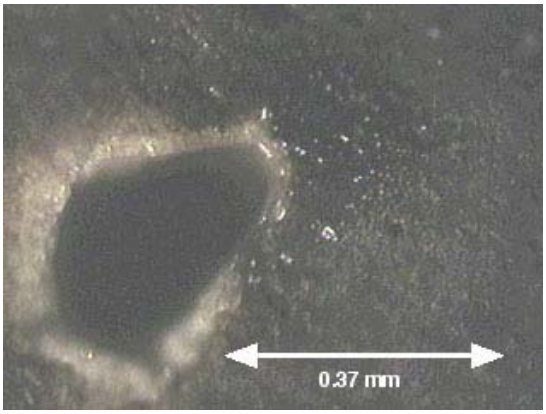

Fig. 6. Ablation crater produced by 1000 laser pulses directed at the same point on a sample of jasperoid. Crater depth is approximately 1 mm.

H	656.28, 486.13, 434.04 nm
O	777.19, 777.41, 777.53,725.41, 725.44, 700.19, 700.22, 822.18 nm

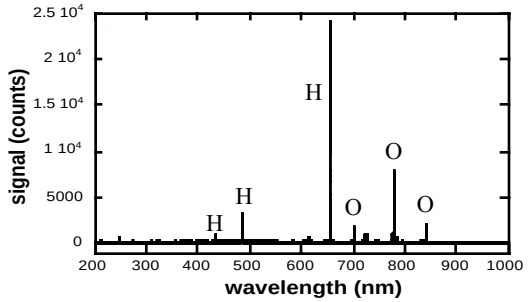

Fig. 7. LIBS spectrum of pure water ice in 7 Torr CO_2. The strongest emission features are listed in the table.

located in a sealed chamber containing CO_2 at 7 Torr. A spectrum of pure water ice is shown in Fig. 7 along with a list of the stronger emission lines observed. Figure 8 shows the strong emission at 306.4 nm due to OH emission indicative of water.

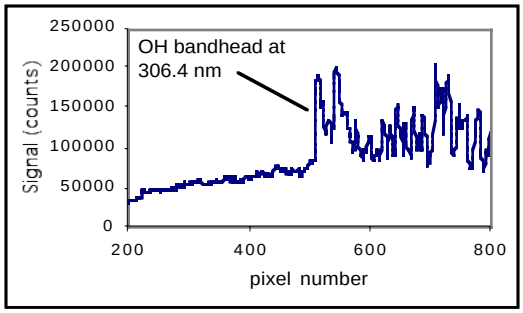

Fig. 8. OH bandhead indicative of water ice.

Prototype Development and Testing. A relatively simple prototype LIBS instrument was built and incorporated into the NASA Ames K9 rover testbed. The instrument and testing are described in [10]. Figure 9 shows the LIBS sensor head on the right side of the K9 mast head. The spectrograph, detector, and laser power supply were contained inside the rover body. The results were compared with VISIR spectra of the same rocks. The LIBS results demonstrated the importance of obtaining elemental compositions to complement passive spectroscopy, even if the results are somewhat qualitative in nature. The results also pointed to the importance of the depth profiling and surface cleaning capabilities of LIBS. Samples that showed IR signatures of alteration products were in

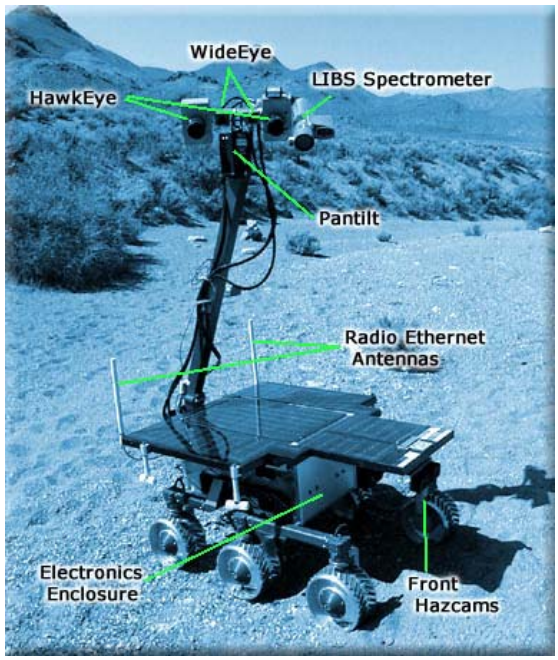

Figure 9. K9 rover during joint field tests, 2000, showing the LIBS prototype sensor head mounted on the mast. Photo courtesy of NASA Ames.

some cases shown by LIBS to carry thin layers of alteration covering the pristine rock composition. This surface cleaning capability is expected to be all the more useful on Mars, where dust coatings are ubiquitous and the nature of surface alteration is unknown.

Our present development work is focused on improving the spectrograph and detector system in anticipation of eventually building a flight instrument. The spectrograph used for the work described in [10] was not ideal in that it had a low spectral resolution of $\lambda/\Delta\lambda\sim500$ and a moveable grating with a range of ~80 nm at any given time. A resolution of at least $\lambda/\Delta\lambda\sim2000$ is desirable, and ideally the spectral range should cover all useful emission lines from 180 to 800 nm. In reality, alternate lines can be used on a number of elements, reducing the range actually needed. We are investigating both fixed-grating spectrographs and echelle spectrographs. Echelle spectrographs have the advantage of easily accommodating the full spectral range with sufficient resolution, but they are not optimized for size and optical throughput. A relatively compact echelle spectrograph (~11x14x29 cm) was used in field work at the FIDO rover site in 2001. A LIBS spectrum from this instrument is shown in Fig. 10. We are hoping to optimize the echelle design to the point where size, optical throughput, spectral resolution, and range are all suitable for a flight LIBS instrument.

Acknowledgments: This work was funded by the Laboratory Directed Research and Development program at Los Alamos National Laboratory and by NASA through the Mars Instrument Development Program.

References: [1] Cremers D.A. and Radziemski L.J. (1986) Laser Spectroscopy and Its Applications; Marcel Dekker: New York; Chapter 5. [2] Radziemski L.J. and Cremers D.A. (1989) Laser-Induced Plasmas and Application; Marcel Dekker: New York; Chapter 7. [3] Moenke-Blankenburg, L. (1989) Laser micro analysis; John Wiley: New York. [4] Rusak D.A., Castle B.C., Smith B.W., Winefordner J.D. (1997) *CRC Crit. Rev. Anal. Chem., 27*, 257-290. [5] Song K.; Lee, Y-I.; Sneddon J. (2002) *J. Appl. Spectrosc. Rev*., *37*, 89-117. [6] Tognoni E., Palleschi V., Corsi M., Cristoforetti G. (2002) *Spectrochim. Acta, B57*, 1115-1130. [7] Cremers D.A. (1987) *Appl. Spectrosc 41*, 1042. [8] Blacic J.D., Petit D.R., Cremers D.A., and Roessler N. (1992) *Proc. Intl. Symp. on Spectral Sensing Res*., 302-312, Maui, HI. [9] Knight A.K., N.L. Scherbarth, N.L., Cremers, D.A., Ferris M.J. (2000) *Appl. Spectrosc., 54*, 331-340. [10] Wiens R.C., et al. (2001) *JGR-Planets, 107*, E11. [11] Fabre C., Brennetot R., Fichet P., Vors, E., Lacour J.L., Dubessy J., Boiron M.-C., Rivoallan A., Maurice S., Cremers D., and Wiens, R. (2002) Technical Digest *Laser Induced Plasma Spectroscopy and Applications*, Sept. 25-28, 2002, Orlando, Fl, 96-98.

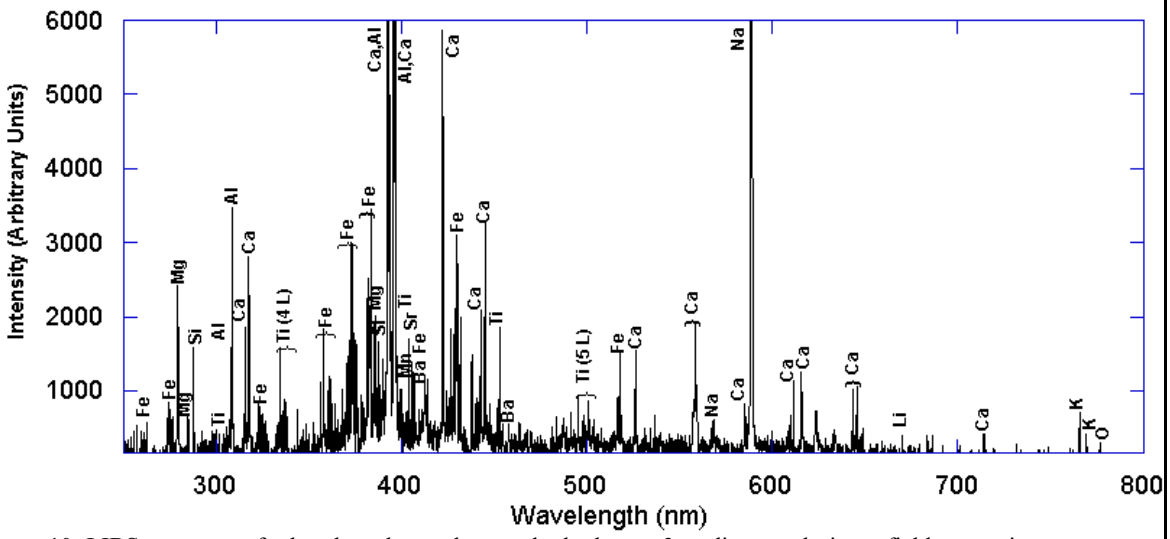

Figure 10. LIBS spectrum of a basalt rock powder standard taken at 3 m distance during a field test, using a compact echelle spectrograph.

FACTORS CONTROLLING THE POSITION OF THE MARTIAN MAGNETIC PILEUP BOUNDARY.

D. H. Crider[1], M. Acuña[2], D. Vignes[2], A. Krymskii[3*], T. Breus[4*], and N. Ness[5], [1] Catholic University of America Department of Physics, Washington, DC 20064 (dcrider@lepvax.gsfc.nasa.gov); [2]Code 695, NASA Goddard Space Flight Center, Greenbelt, MD 20771; [3]Rostov State University, Rostov-on-Don, Russia; [4]Space Research Institute, Russian Academy of Science, Moscow, Russia; [5]Bartol Research Institute, University of Delaware, Newark, DE. [*]currently visiting [(1)].

Introduction: The magnetic pileup boundary (MPB) at Mars is the position where the dominant ion of the plasma changes from solar wind protons to heavy ions of planetary origin [1]. As such, it is the obstacle to solar wind ions. We investigate the factors that influence the shape and position of the magnetic pileup boundary at Mars in order to better understand the Martian obstacle to the solar wind. Employing MGS data, we determine how the Martian MPB moves in response to factors including solar wind pressure and crustal magnetic fields. We also study the factors affecting the thickness of the MPB. Further, we compare the magnetic pileup boundary to the magnetic barrier at Venus. Direct comparison aids in our interpretation of the physics involved in the solar wind interaction with planets lacking a significant intrinsic magnetic field.

MPB variability: As external influences fluctuate and Mars rotates under the Sun, the MPB moves in and out. Its variability is obvious in Figure 1, which shows the position of the MPB as a function of solar zenith angle. The superposed line is the fit by Vignes et al. [2] to the MGS MPB crossings. The variability can be caused by a number of factors, including changing solar wind dynamic pressure, EUV flux, convection electric field, and position of crustal sources. The entire MPB does not have to move in response to local perturbations.

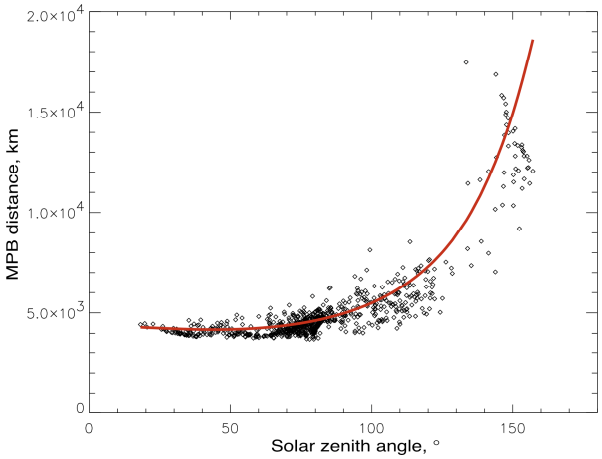

Fig. 1 Distance of observed MPB crossings as a function of solar zenith angle. The fit is that of Vignes et al. (2000).

The strong crustal fields have the effect of pushing the MPB position to greater altitudes [3]. Although there is no MPB crossing by MGS a high southern latitude, there is a trend that the MPB distance is greater and more variable in the southern hemisphere of Mars than in the northern hemisphere (Figure 2).

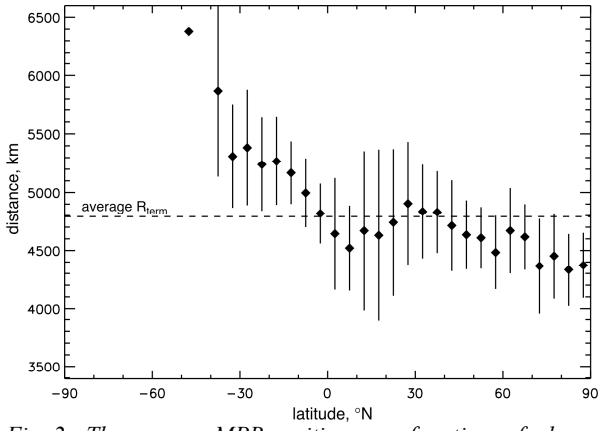

Fig. 2. The average MPB position as a function of planetary latitude. Each MPB position has been mapped to where it would occur in the terminator plane. A single horizontal line will no fit this data.

We have observed the compression of the MPB by strong incident solar wind ram pressure. Using a proxy for the solar wind pressure based on the magnetic pressure in the magnetic pileup region, we found that the MPB is 240 km closer to the planet on average when the solar wind pressure exceeds 1 nPa. (see Figure 3).

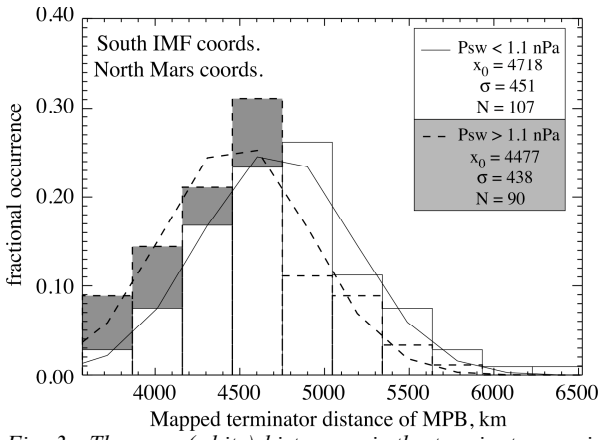

Fig. 3. The gray (white) histogram is the terminator position of the MPB for cases with P_{SW} > 1.1 nPa (P_{SW} < 1.1 nPa). To eliminate other sources of variability, we used only MPB crossings from the northern hemisphere that had southward electric field direction.

Our analysis has not revealed a dependence of the MPB position on the direction of the convection electric field. However, our method of determining the convection electric field direction yields high uncertainties. Our analyses cannot rule out the possibility that such an asymmetry exists.

MPB properties: The MPB is the position across which the dominant ion changes [1], the electrons cool [2], the magnetic field strength increases[4], magnetic field draping becomes well-defined[5], and wave activity decreases[6]. Generally at Mars, these changes occur abruptly. The average MPB thickness (i.e. the vertical distance over which the changes occur) is 300 km on the dayside.

In the southern hemisphere, the MPB thickness has a different distribution than in the northern hemisphere. The effect of the crustal fields is to make the MPB thicker on average (see Figure 4). This may be understood in terms of the diversion of the shocked solar wind flow around a mini-magnetosphere that protrudes into the flow. The increased flux to the sides of the crustal field will serve to thicken the MPB there. The MPB may be thinner directly above the crustal fields, however. Confirmation of this will have to await further data. It is difficult to deconvolve all of the known influences with the current data set.

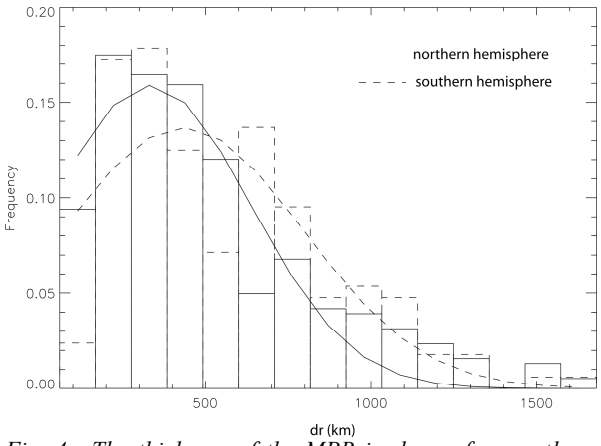

Fig. 4. The thickness of the MPB is shown for northern hemisphere crossings and southern hemisphere crossings. The distribution is broader and has a higher central value in the southern hemisphere.

Venus comparison: The magnetic barrier is a region in between the shocked solar wind and the ionosphere at Venus [7]. It comprises a mix of ionospheric and solar wind plasmas. This must be true because the IMF penetrates the barrier. Some plasma must carry it through. Magnetic pressure dominates in this region (83% of upstream solar wind pressure).

Breus et al. [8] called it the "topside ionopause." Photochemical processes produce the transition from solar wind to planetary plasmas. High P_{sw} modulates the region. On the other hand, Perez-de-Tejada[9] attributes the "intermediate transition" at Venus to an expansion of the plasma flow. Expansion is to compensate for losses to friction as the flow encounters the ionopause. Wave bursts at plasma frequency are located at the transition layer

The MPB (Mars) and the Magnetic Barrier (Venus) both are the obstacle in the gasdynamic description of the interaction [7]. The top altitude of the MPB is higher than the top of the magnetic barrier at Venus in terms of planetary radii. Both are depressed to lower altitudes and have higher peak magnetic fields with increasing solar wind pressure. A stronger asymmetry with electric field direction is observed at Venus than Mars.

The magnetic field strength builds over a short distance at Mars, and remains high over an extended distance before reaching the ionopause. There is a region of sustained high magnetic field that is sometimes up to 1000 km thick between the MPB and the ionosphere proper. In contrast, the magnetic field builds over an extended distance at Venus and achieves its maximum close to the ionopause.

Summary: Both Mars and Venus have a region in which magnetic pressure dominates that separates the planetary plasma from solar wind plasma. This boundary is the effective solar wind obstacle in the gasdynamic approximation. The MPR covers a larger part of the solar wind interaction region at Mars than at Venus.

The Martian MPB has variability of ±400 km at the terminator (or .12 R_{Mars}). We have verified that solar wind pressure and crustal fields modulate its postion. There is no evidence that electric field direction is important, although these results are not conclusive. Solar wind pressure plays a role at both Mars and Venus. Crustal magnetic fields play a role only at Mars.

The MPB thickness has a variability of ~300 km (or .09 R_{Mars}). The MPB is thicker on the nightside, under low solar wind pressure, and in the southern hemisphere.

References: [1] Lundin R. et al (1989) *Nature 341*, 609; [2] Vignes, D. et al. (2000) *Geophy. Res. Lett. 27*, 49; [3] Crider D. et al. (2002) *Geophys. Res. Lett. 29* 10.1029/2001GL01386; [4]Acuña M. et al. (1998) *Science 279*, 1676; [5] Bertucci, C. et al. (2003) *Geophys. Res Lett. 30*, 10.1029/2002GL01571; [6] Grard et al. (1989) *Nature 341*, 607; [7] Zhang, T. et al. (1991) *J. Geophys. Res. 96*, 11145; [8] Breus, T. et al. (1987) *J. Geophys. Res. 96*, 11165; [9] Perez-de-Tejada, H. (1998) *J. Geophys. Res. 103*, 31499; [10]

DEVELOPMENT OF A SURFACE-TO-EXOSPHERE MARS ATMOSPHERE MODEL. G. Crowley[1], M. A. Bullock[1], C. Freitas[1], Sidney Chocron[1], C. Hackert[1], D. Boice[1], L. Young[1], D. H. Grinspoon[1], R. Gladstone[1], W. Huebner[1], G. Wene[2] and M. Westerhoff[2] ([1]Southwest Research Institute, San Antonio, Texas, 78238-5166; 210-522-3475; gcrowley@swri.org,; [2]Department of Mathematics, University of Texas at San Antonio, 6900 North Loop1604 West, San Antonio, TX 78249-0616)

Introduction: Understanding of the diurnal, seasonal and epochal water transport and volatile loss on Mars is of major scientific interest. Volatile loss is a cornerstone of a number of important science questions because it must be understood to help explain the current atmospheric state and the relative lack of water on the planet. A new ground-to-exosphere GCM is needed which considers volatile loss processes and must include explicit ground interaction with the lower atmosphere, vertical transport of H_2O, and enough chemistry to reasonably represent the loss of H and H_2 (and heavier species) from the upper atmosphere and exosphere. Including these regions in a Mars GCM allows for the estimation of global escape fluxes for the present time, which can then be extrapolated backward in time to post-cast the atmospheric state at significantly earlier time periods with different orbital elements.

We are in the process of creating a new Mars GCM that will extend from the planetary surface to altitudes of about 500km, thus coupling the lower and upper atmospheres. It will explicitly include interactions between the ground and the atmosphere, such as gas phase and dust particle exchange between the two regions, and the effects of topography. Volatile transport will be simulated over both short (daily) and geological timescales to study the water distribution and to predict the D/H ratio of the present day atmosphere, thereby helping to constrain the history of water on the planet.

The new Mars GCM will include simulations of the transfer of water from the planetary regolith into the atmosphere through boundary layer processes. We will also explore the role that mesoscale dynamical processes play in lofting dust into the atmosphere. The role of the dust and clouds in the planetary heat budget will be included through the use of specific microphysical and radiative transfer modules. The Mars ionosphere will be simulated with a detailed suite of chemical reactions, and over the long-term, the evolution of the D/H ratio will be predicted.

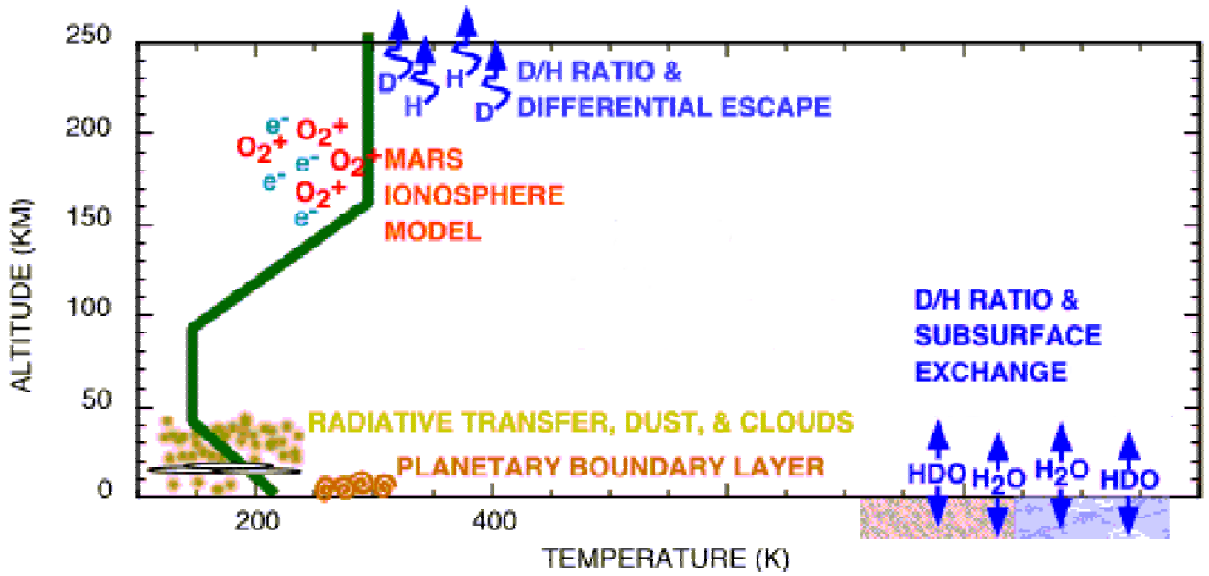

Figure 1. Major components of the new Mars GCM.

PHYSICAL CHARACTERISTICS, GEOLOGIC SETTING, AND POSSIBLE FORMATION PROCESSES OF SPRING DEPOSITS ON MARS BASED ON TERRESTRIAL ANALOGS.

L. S. Crumpler, New Mexico Museum of Natural History and Science, 1801 Mountain Road NW, Albuquerque, NM 87104; lcrumpler@nmmnh.state.nm.us.

Introduction. Spring formation is a predicted consequence of the interaction of former Martian aquifers with structures common to Mars, including basin margins, Tharsis structures, and other structural deformation characteristics. The arid environment and high abundance of water soluble compounds in the crust will have likewise encouraged spring deposit formation at spring sites. Such *spring deposits may be recognized from morphological criteria if the characteristics of formation and preservation are understood.*

An important first step in the current Mars exploration strategy [10] is the detection of sites where there is evidence for past or present near-surface water on Mars. This study evaluates the large-scale morphology of spring deposits and the physical processes of their formation, growth, and evolution in terms that relate to (1) their identification in image data, (2) their formation, evolution, and preservation in the environment of Mars, and (3) their potential as sites of long-term or late stage shallow groundwater emergence at the surface of Mars.

Purpose of this Research. The general geologic diversity of spring deposits and the factors controlling their formation and distribution are poorly constrained and incompletely documented. In addition, the relative importance of concentrated thermal sources (magmatic heat), water heated through deep groundwater circulation, and the mechanisms whereby water may circulate and emerge at the surface have been documented for limited settings. Systematic documentation of the range of spring deposit morphologies and their modes of formation is needed in order to search for spring deposits in the appropriate places on Mars and to be able to identify spring deposits given their wide range of characteristics. A survey of the large-scale morphologic characteristics and the geologic processes of spring deposits from the perspective of aerial identification, surgical processes, and general geologic association is needed in order to provide geologic context for biological, chemical, and *in situ* analyses and resource utilization studies.

Research on spring deposits has focused to date on obvious thermal springs consisting of combinations of carbonates, sulfides, related mineral species, and siliceous sinter, *yet the vast majority of springs are of non-thermal origin and are constructed from low-temperature minerals dissolved in deeply circulated ground water*. This second (low-temperature) type is likely to be important at many sites on Mars where groundwater emergence may be governed by hydrologic gradients more so than simple thermal convection. It is also likely to be more widespread given the limited occurrence of volcanic settings on Mars. The physical processes of mineral spring development, and the importance of an arid environment in preserving and controlling these processes, are not well studied. This study establishes (1) the characteristics by which they can be morphologically recognized to provide additional criteria for high science potential, and the details of spring deposit deposition, and (2) the structure that may relate to accurate identification and interpretation of outcrops at lander and rover scales of observation.

Spring Deposits on Earth. Deposits accumulated at the site of springs have been studied for their economic importance [*1*], and because their chemical and biological origins are significant to understanding both early hydrologic and biotic processes [*2*]. Although it is frequently assumed that spring mound formation is associated with warm ("hydrothermal") springs, many, and arguably most, examples arise from water emerging at or near ambient temperature (**Figure 1**). The observed temperature of most active spring discharges associated with spring mound formation is

Figure 1. Vioew of an ctive travertine spring deposit occurring along the western margin faults of the Rio Grande rift, New Mexico. The source springs are ambient temperature at the source. deposits that may be applicable.

Characteristics of Spring Deposits. Spring deposits may be as thick as 100 m and cover hundreds of square kilometers. They generally occur in one of five basic morphologies [*3*]: cascades, lake-fill, sloping mounds and fans, terraced mounds, and fissure ridges. In addition to these morphologies, a central vent-like (cratered cone) characteristic of non-thermal mineral springs occurs in a significant number of sites throughout the Southwest. Cratered cone spring morphologies appear similar to small volcanoes in that

they constitute distinct cones several hundred meters to over a kilometer in basal dimension that are frequently surmounted by a summit "crater" (**Figure 2**). The differing morphologies arise because the process of volume accumulation is constrained by the variable geometry and dynamics of a point source. The morphology may be sufficient for detection of spring

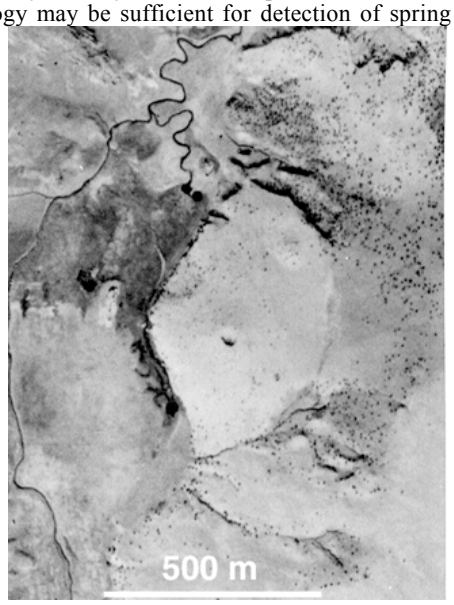

FIGURE 2. Air photo of a typical travertine mound, one of n such mounds consisting of freshwater carbonates associated the emergence of deeply circulated ground water along high-a fault lying down the hydrologic gradient from the Springer volcanic field [*11*].

sites from aerial and orbital image data when combined with knowledge of environments favorable for spring formation, their morphological variability, and factors influencing their morphology. Spring deposits are predicted to occur where there is evidence for long-term emergence of ground water at the surface or where emergence is predicted from considerations of potential groundwater hydrologic gradients.

Mineralogy of Spring Deposits. A significant part of most spring deposits terrestrially is travertine, a form of freshwater evaporite rock formed by both organic and inorganic processes [*3,4*]. $CaCO_3$ is the primary dissolved mineral in terrestrial spring deposits (Fig. 1), but H_2S is also significant in many springs and supports most of the bacterially precipitated deposits [*3*]. It is easy to envision that other water soluble minerals and elements, such as sulfur and sulfur-iron compounds, could be important where these are important constituents of host rocks.

Geologic Setting of Spring Deposits. Three conditions characterize spring deposits

- tectonism (high-angle faults)
- brine concentration (evaporation)
- water-soluble host rocks (mineral-source)

Throughout the southwestern U.S., spring deposits occur where a significant vertical discontinuity interrupts the subsurface flow and forces the groundwater to emerge at the surface. Many spring deposits are therefore associated with tectonic features such as high-angle faults and other prominent upper crustal discontinuities such as anticlines (Fig. 3) and monoclines.

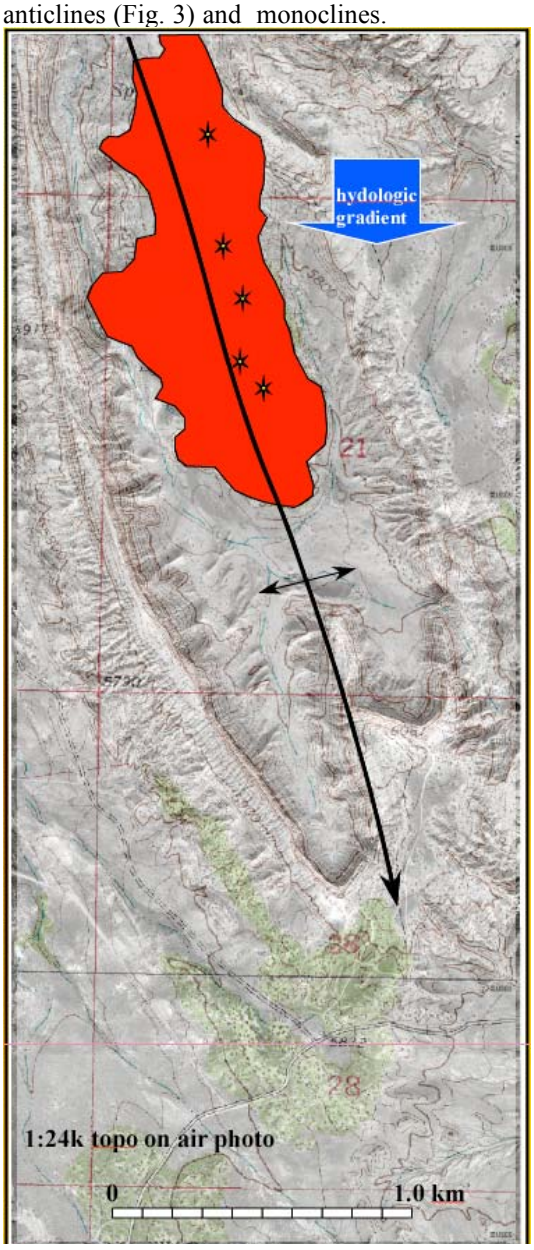

Figure 3. Example of travertine spring deposits (mapped in red) occurring along the axis of a large anticline. Active deposition of spring deposits in the form of conical mounds is occurring from water charged with CO2 and at ambient temperature in this area.

Spring deposits are particularly common in association with high-angle faults (Fig. 4), which act as high hydraulic conductivity conduits for aquifers confined by overlying aquitards and aquiludes. Faults on the margins of basins and other discontinuous structures, such as anticlines, where aqui-

fers are brought in contact with less permeable

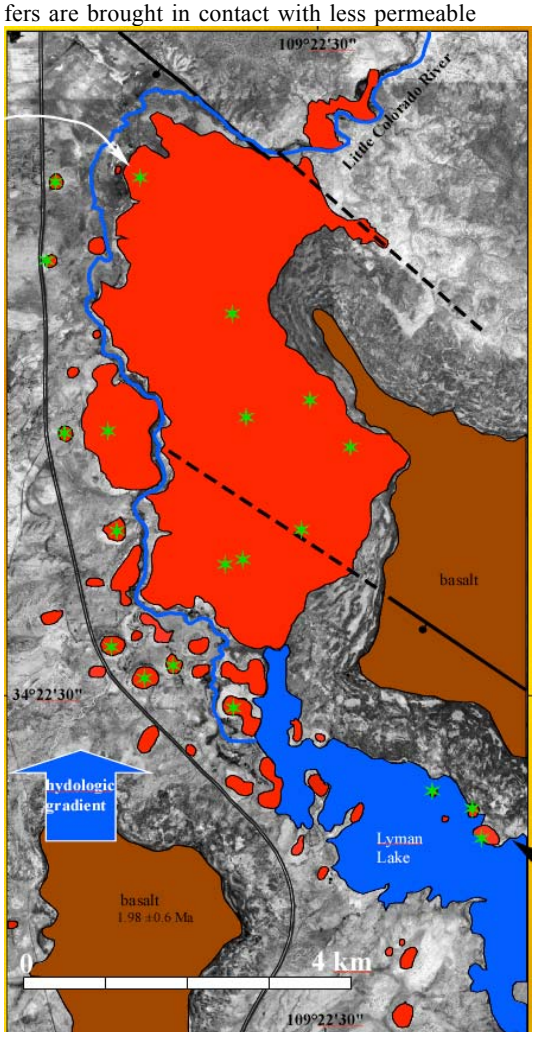

Figure 4a. Active sloping mound and conical mound spring deposits associated with forced convection (high angle fault).

rocks or where an aquifer is abruptly terminated within existing topographic slopes by recent faulting are common sites (Fig. 2, 3). Spring deposits are thus associated with many tectonically active and formerly active areas where evaporation rates and mineral content of spring water are high.

Conditions for Spring Deposit Formation. Based on the observed characteristics of spring deposits discussed above, not all spring deposits are associated with high groundwater thermal conditions. Any physical or chemical condition that results in dissolution of minerals in water and its deposition upon evaporation can result in significant deposits. The morphology of deposits is repeated in many deposits implying that a restricted set of characteristics is common to springs in a wide range of settings.

Results of this study indicate that three conditions are common to all spring deposits: (1) evaporation due to either (a) high temperature or (b) arid conditions; (2) circulation of water vertically

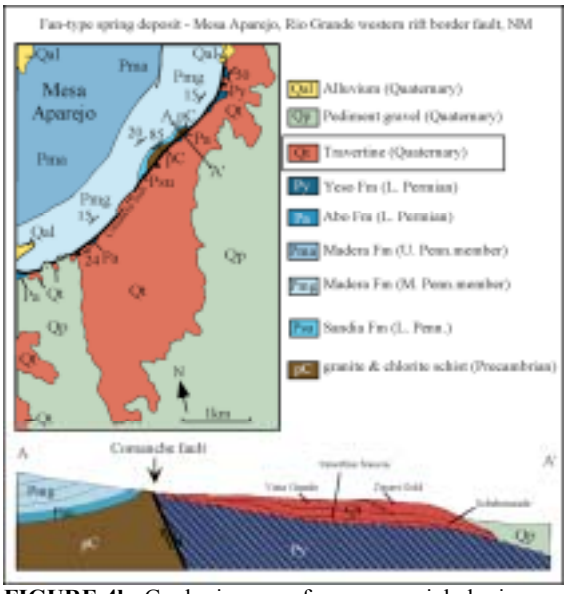

FIGURE 4b. Geologic map of a commercial sloping mound-and-fan type spring (travertine) deposit near Belen, New Mexico. Spring deposits at this site are one of many that are forming where de-watering of the elevated Colorado Plateau geologic section is occurring and water is emerging along one of the western boundary faults of the Rio Grande rift. Spring waters are relatively low-temperature and carbonate-charged. Active deposition is limited to relatively small areas that continually migrate leaving behind inactive deposits. Map after [*12, 13*].

within the near surface or upper crust either as a result of (a) free (hydrothermal) convection or (b) forced convection (emergence at a discontinuity); and (3) presence of significant abundances of dissolved minerals: crustal abundance of dissolvable minerals along the hydrologic pathway. On this basis it is suggested that two fundamental types of setting may be identified: (1) thermal type settings and (2) desert type settings.

Application to Mars. The upper few kilometers of the Martian crust are likely to be highly fractured [*5, 6*] and thus permeable to fluid flow and aquifer development [*7*]. If water is present in the subsurface as a fluid, it will accumulate within the permeable zone and, under the force of gravity, flow from topographically HIGH regions to regions of discharge at topographically low regions. At that point it is either discharged or accumulated in the subsurface. The gradient on the upper surface of the water-saturated region defines the top of the water table [*8, 9*]. The relief on the water table, or the potenti_ometric surface controls the flow, which is generally a subdued reflection of the surface topography. At the largest scales, we may expect that water in a Martian aquifer of regional extent will flow from high elevations, such as the highlands to lowlands or local basins.

An example setting would be on the margins of basins. Faults and other discontinuous structures, including antiformal and graben type structures, may be

common sites where aquifers are brought in contact with less permeable rocks, or where an aquifer is abruptly terminated within existing topographic slopes by faulting. Sulfur, sulfides, and related iron-rich materials may be important water-soluble materials that could constitute spring deposits on Mars. Given the deeply brecciated nature likely for the highlands and the widespread distribution of atmospherically transported volatiles and dust, including volcanic and impact-generated aerosols, the crust is likely to be liberally mixed with compounds that are unstable in water.

There are many physical features over the surface of Mars that are similar to the morphologies typical of terrestrial spring mounds. For example, large areas of pitted mounds, generally interpreted as hydro-magmatic (e.g., "pseudo-craters", *Frey et al., 1979)* or ice-related phenomena (pingos), bear many of the characteristics of summit-pitted spring mounds (**Fig. 5a**). Other anomalous mounds in non-volcanic terrain occur around basin margins (**Fig. 5 b**). these frequently occur in young basins or around the margins of basins.

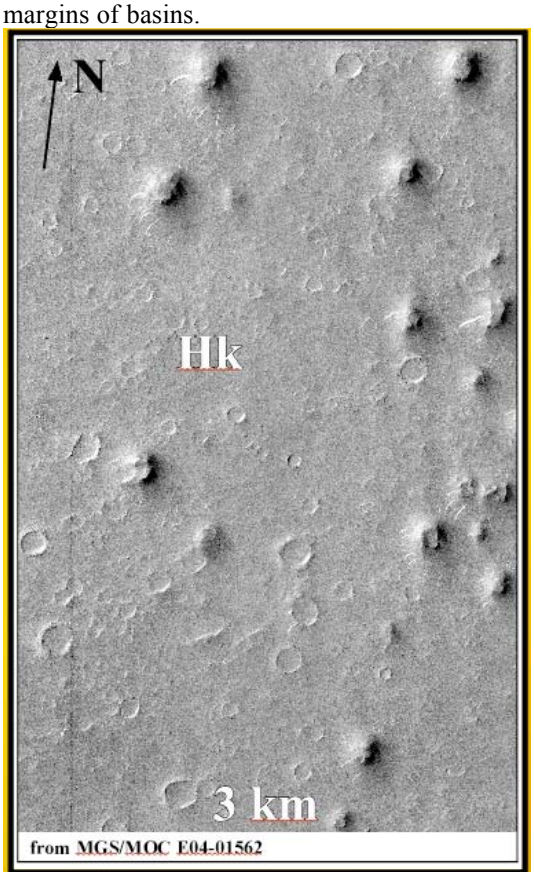

Figure 5a. Pitted mounds within the Isidis basin, long interpreted as possible volcanic conbes, may equally epresent the surface expression of volatile release from the subsurface analogous to spring deposits.

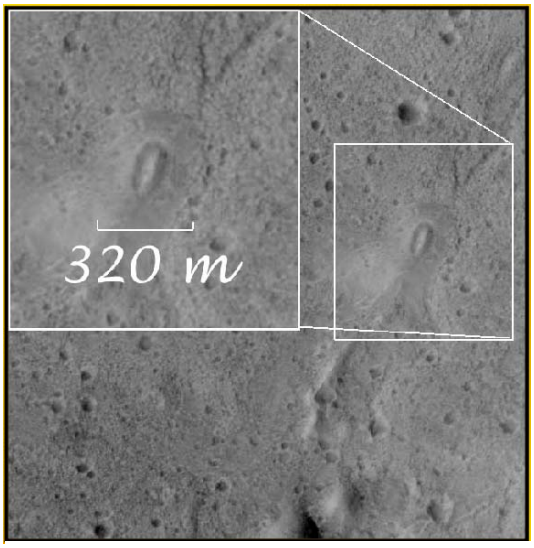

Figure 5b. Anomlous cone located on structure in an otherwise non-volcanic highland region.The area is down-gradient from significant valley network concentrations.

formed from carbonates appear relatively unlikely on Mars because there is as yet little evidence for extensive carbonate in the surface. Nonetheless many minerals are soluble in water and will respond similarly to dissolution, transportation, and deposition during desiccation. The abundant of dissolvable compounds in the Martian crust must be great. Given the deeply brecciated nature likely for the highlands and the widespread distribution of atmospherically transported volatiles and dust, including volcanic and impact-generated aerosols, the crust is likely to be liberally mixed with compounds that are unstable in water. Sulfur, sulfides, and related iron-rich materials may be important water-soluble materials that could constitute spring deposits.

This research is supported by the Mars Fundamental Research Program, NASA.

References. [1]Austin and Barker, . New Mexico Geology, New Mexico Bureau of Mines and Mineral Resources, **12**, 49-58, 1988; [2]Fisher, Unpublished M.S. thesis, New Mexico Institute of Mining and Technology, 152 pp, 1979; [3](Chafetz and Folk, . J. Sed. Petrology, **54**, 289-316, 1983; [4] Julia, Travertines. in Carbonate Depositional Environments, P. A. Scholle, D. G., Bebout, and C. H. Moore, eds., AAPG Memoir **33**, 63-72, 1983; [5]Fanale, Icarus, **28**, 179-202, 1976; [6] Carr, J. Geophys. Res., **84**, 2995-3007, 1979; [7]Clifford, . J. Geophys. Res., **98**, 10973-11016, 1993; [8] Hubbert, . Am Assoc. Petrol. Geol. Bulletin, **37**, 1954-2026,1953; [9]Freeze and Cherry, Groundwater. Prentice-Hall, Englewood Cliffs, New Jersey, 604p., 1979; [10] Mars Exploration Payload Group and Committee for Planetary Exploration, Science Planning for Exploring Mars, , Smithsonian Institution, Washington, D.C. JPL Publication 01-7, 2001; [11] Crumpler, New Mexico Geol. Soc. Field Conference Guidebook, 45th Field Conference, Mogollon Slope, 147-164, 1994; [12] Kelley and Wood, : *U. S. Geol. Survey, Oil and Gas Investigation, Prelim. Map* 47, scale 1:63,360. 1946; [12] Cooper, Unpublished Report to Ultra Marbles Inc., ALbuquerque, 66pp, 1964.